IMAGE-BASED FIELD METHODOLOGY TO DETERMINE FLUVIAL HYDROKINETIC ENERGY POTENTIAL

FELIPE RIBEIRO DE TOLEDO CAMARGO

DISSERTAÇÃO DE MESTRADO EM CIÊNCIAS MECÂNICAS - ENERGIA E AMBIENTE

DEPARTAMENTO DE ENGENHARIA MECÂNICA

FACULDADE DE TECNOLOGIA

UNIVERSIDADE DE BRASÍLIA

UNIVERSIDADE DE BRASÍLIA
FACULDADE DE TECNOLOGIA
DEPARTAMENTO DE ENGENHARIA MECÂNICA

IMAGE-BASED FIELD METHODOLOGY TO DETERMINE FLUVIAL HYDROKINETIC ENERGY POTENTIAL

METODOLOGIA DE CAMPO BASEADA EM IMAGENS PARA DETERMINAR O POTENCIAL HIDROCINÉTICO FLUVIAL.

FELIPE RIBEIRO DE TOLEDO CAMARGO

ORIENTADOR: PROF. DR. ANTONIO BRASIL JUNIOR

DISSERTAÇÃO DE MESTRADO EM CIÊNCIAS
MECÂNICAS - ENERGIA E AMBIENTE

PUBLICAÇÃO: PCMEC.TD-001/21

BRASÍLIA/DF: OUTUBRO - 2021

UNIVERSIDADE DE BRASÍLIA
FACULDADE DE TECNOLOGIA
DEPARTAMENTO DE ENGENHARIA MECÂNICA

IMAGE-BASED FIELD METHODOLOGY TO DETERMINE FLUVIAL HYDROKINETIC ENERGY POTENTIAL

FELIPE RIBEIRO DE TOLEDO CAMARGO

DISSERTAÇÃO DE MESTRADO SUBMETIDA AO DEPARTAMENTO DE ENGENHARIA MECÂNICA DA FACULDADE DE TECNOLOGIA DA UNIVERSIDADE DE BRASÍLIA COMO PARTE DOS REQUISITOS NECESSÁRIOS PARA A OBTENÇÃO DO GRAU DE MESTRE.

APROVADA POR:

_____

Prof. Antonio Brasil Junior, PhD. – ENM/Universidade de Brasília
Orientador

_____

Prof. Taygoara F. Oliveira, PhD. – ENM/Universidade de Brasília
Membro Interno

_____

Prof. Pierre Maruzewsky, PhD. – EDF/Hydro Lyon
Membro Externo

_____

Prof. Edgar Silveira, PhD. – ENM/Universidade de Brasília
Membro Suplente

BRASÍLIA, 05 DE OUTUBRO DE 2021.

FICHA CATALOGRÁFICA

CAMARGO, FELIPE
IMAGE-BASED FIELD METHODOLOGY TO DETERMINE FLUVIAL HYDROKINETIC ENERGY POTENTIAL [Distrito Federal] 2021.
xiv, 80p., 210 x 297 mm (ENM/FT/UnB, Mestre, Ciências Mecânicas - Energia e Ambiente, 2021).
Dissertação de Mestrado – Universidade de Brasília, Faculdade de Tecnologia.
Departamento de Engenharia Mecânica

1. LSPIV	2. ADCP
3. Potencial Hidrocinético	4. Drone
I. ENM/FT/UnB	II. Título (série)

REFERÊNCIA BIBLIOGRÁFICA

CAMARGO, F. (2021). IMAGE-BASED FIELD METHODOLOGY TO DETERMINE FLUVIAL HYDROKINETIC ENERGY POTENTIAL . Dissertação de Mestrado em Ciências Mecânicas - Energia e Ambiente, Publicação PCMEC.TD-001/21, Departamento de Engenharia Mecânica, Universidade de Brasília, Brasília, DF, 80p.

CESSÃO DE DIREITOS

AUTOR: Felipe Ribeiro de Toledo Camargo
TÍTULO: IMAGE-BASED FIELD METHODOLOGY TO DETERMINE FLUVIAL HYDROKINETIC ENERGY POTENTIAL .
GRAU: Mestre ANO: 2021

Felipe Ribeiro de Toledo Camargo

Departamento de Engenharia Mecânica (ENM) - FT
Universidade de Brasília (UnB)
Campus Darcy Ribeiro
CEP 70919-970 - Brasília - DF - Brasil

To my beloved parents, Ivan and Gisele

ACKNOWLEDGMENTS

I would like to thanks my father and mother for all the support given and for the incredible feedback and dinners that maintain me calm and happy in this challenging period of my life. Dad thanks for the example that you are in my life, for all the suggestions, lectures, conversation, and Flamengo games that we watch together. Mom, thank you for always believing in me, your discipline, and your courage to face the new challenges from life expire me to always do my best. To my sisters, Natalie and Laura, when I grow older I wanna be just like you. To both of their husband and my nephews that bring me joy and noise through the dissertation writing.

To my dear Flora, thank you very much for your company, patience, and hours trying to understand my dissertation theme, and always making my life lighter and beautiful.

To Professor Brasil, thank you for your trust and for guiding me through the two most learning years of my life. To my friends from the Energy and Environmental Lab, Rafael, Reginaldo, Guilherme these experiments and work could not be done without you guys. To all professors and friends that I have the pleasure to meet in the Master's degree, Prof. Taygoara, Prof Gurgel, Pedro, Arthur, Dario, Matheus and all the people from the PCMEC secretary, especially Rafael. To Gustavo Maia, Pedro Campelo, and Rafael Botelho that helped me and encouraged me to learn python and were always available to help me. To all my friends and family that in some way contributes to this work, all of you even if is not explicit cite here is a part of this and I'm very lucky to have you all in my life.

I would like to thank Serra do Facão Energia S.A. for providing financial support for the development of the project (ANEEL:P&D06899-2002/2020). Also to all the ADASA and SEFAC team that allowed and helped execute the experiments for this work.

Last but not least, thank you, God, that always in hard times, comforted and soothed me. I thought that achieving a master's degree would be a long and lonely road, thankfully for all these people, it was not. From all my heart, thank you!

RESUMO

Título: Metodologia de campo baseada em imagens para determinar o potencial hidrocinético fluvial.
Autor: Felipe Ribeiro de Toledo Camargo
Orientador: Prof. Dr. Antonio Brasil Junior
Programa de Pós-Graduação em Ciências Mecânicas - Energia e Ambiente
Brasília, 05 de outubro de 2021

Motivado pela necessidade global de expansão da matriz energética com baixa pegada de carbono. Este trabalho aplicou uma técnica para medir a velocidade superficial de rios que oferece uma metodologia não intrusiva, segura e simples para determinar o potencial hidrocinético de rios.

O trabalho tem o objetivo principal de poder medir a velocidade dos rios e o objetivo secundário de poder servir como um manual para coleta de dados de velocidade dos rios.

A Velocimetria de Imagens de Partículas em Grande Escala (LSPIV) é uma técnica derivada da famosa técnica de Velocimetria de Imagens de Partículas (PIV) amplamente usada na década de 1980 para experimentos envolvendo a mecânica dos fluidos. O LSPIV se destaca pelo avanço nas tecnologias que envolvem a gravação de vídeos e a capacidade de processamento do computador. Com o menor custo e a maior eficiência desses equipamentos, diversos experimentos envolvendo o LSPIV começaram a surgir pelo o mundo, no Japão, na França e nos Estados Unidos. Os experimentos foram normalmente realizados para estudar eventos de inundação em rios. Sucintamente, é uma técnica de correlação de padrão de frames.

Um equipamento ADCP (Acoustic Doppler Current Profiler) é utilizado como referência para as medições realizadas pela técnica LSPIV. Os vídeos gravados para a aplicação da técnica de correlação de frames foram feitos por um DJI Mavic Air 2 Drone, sempre voando sobre os rios ortogonalmente ao fluxo.

Três experimentos foram realizados. Dois no Distrito Federal, na região administrativa de Brazlândia, no rio Rodeador, e no Canal de Irrigação do Rodeador. O terceiro experimento foi realizado no rio São Marcos, que fica próximo à cidade de Catalão, no estado de Goiás. O rio está a jusante da barragem hidrelétrica SEFAC.

Uma lei de potência foi usada para comparar a velocidade superficial medida pelo LSPIV com a medida feita pelo equipamento ADCP. Além disso, o potencial hidrocinético foi estimado para ambas as metodologias. O trabalho atingiu seus objetivos e também serviu para indicar novos estudos e experimentos para aprimorar os resultados alcançados.

Palavras-chave: LSPIV, ADCP, Potencial Hidrocinético, Drone.

ABSTRACT

Title: IMAGE-BASED FIELD METHODOLOGY TO DETERMINE FLUVIAL HYDROKINETIC ENERGY POTENTIAL
Author: Felipe Ribeiro de Toledo Camargo
Supervisor: Prof. Dr. Antonio Brasil Junior
Graduate Program in Energy and Environmental
Brasília, October 05th, 2021

Motivated by the global need to expand the energy matrix with a low carbon footprint. This work applied a technique to measure the surface velocity of rivers that offers a non-intrusive, safe and simple methodology to determine the hydrokinetic potential of rivers.

The work has the main objective of being able to measure the speed of rivers and the secondary objective of being able to serve as a manual for data collection of speed in rivers.

Large Scale Particle Image Velocimetry (LSPIV) is a technique derived from the famous Particle Image Velocimetry (PIV) technique that was widely used in the 1980s for experiments involving fluid mechanics. LSPIV stands out with the advance in technologies involving image recording and computer processing capacity. With the lower cost and greater efficiency of this equipment, several experiments involving LSPIV are beginning to appear around the world, in Japan, France, and the United States. Experiments were typically carried out to study flood events in rivers. Succinctly, it is a frame pattern correlation technique.

An ADCP equipment (Acoustic Doppler Current Profiler) is used to serve as reference for the measurements performed by the LSPIV technique. The videos recorded for the application of the pattern correlation technique were made by a DJI Mavic Air 2 Drone, always flying over the rivers orthogonally to the flow.

Three experiments were carried out. Two in the Federal District, in the administrative region of Brazlândia on the Rodeador River, and the Rodeador Irrigation Channel. The third experiment was carried out in São Marcos River, which is close to the city of Catalão in the State of Goiás. The river is downstream of the SEFAC hydroelectric dam.

A power law was used to compare the superficial velocity measured by the LSPIV with the measure made by the ADCP equipment. Also the Kydrokinetic potential was estimate for both methodology. The work achieved its goals and also served to indicate new studies and experiments to improve the results achieved.

Keywords: LSPIV, ADCP, Hydrokinetic Potential, Drone.

SUMMARY

LIST OF FIGURES

LIST OF TABLES

LIST OF SYMBOLS

symbols

A	Is the quantity that expresses the extent of a two-dimensional region, shape, or planar lamina, in the plane.	$[\mathrm{m}^2]$
C_p	Machine Power Coefficient	
C	Sound Speed	
D	Change in frequency	
F	Frequency of the transducer	
N	Sample size	
x_p	Coordinates of a point in the distorted coordinate system	
y_d	Coordinates of a point in the undistorted coordinate system	
y_p	Coordinates of a point in the distorted coordinate system	
z_0	Bottom roughness height	$[\mathrm{m}]$
α_0	Skew Coefficient	
ccx	Image Center	
ccy	Image Center	
d_{50}	Diameter of the bed material	
Δt	Time between frames	$[\mathrm{s}]$
e_{hk}	Power Density of the flow	$[\mathrm{W/m}^2]$
k_s	Roughness height of Nikuradse	
k	Von-Kármen constant	
m	The base unit of length in the International System of Units (SI)	$[\mathrm{m}]$
ω	Rotor Speed	[RPM]
P_{hk}	Hydraulic Power	$[\mathrm{W}]$
ρ	The density of a substance is its mass per unit volume.	$[\mathrm{kg/m}^3]$
σ	Standard Deviation is a measure of the amount of variation or dispersion of a set of values.	
$\sum$	Is the addition of a sequence of any number types.	
τ_0	Shear stress limit	
θ	Angle of the acoustic beam in two adjacent density layer.	
u_*	Bottom shear Velocity	$[\mathrm{m/s}]$
u	Velocity	$[\mathrm{m/s}]$
$\bar{U}$	Velocity Mean	$[\mathrm{m/s}]$
W	Unit of power or radiant flux	$[\mathrm{W}]$
x_d	Coordinates of a point in the undistorted coordinate system	
y_0	Boundary distance of the wall	$[\mathrm{m}]$

LIST OF ACRONYMS AND ABBREVIATIONS

CO_2	Carbon dioxide molecules consist of a carbon atom covalently double bonded to two oxygen atoms. 1
ADASA	Federal District Water, Energy and Sanitation Regulatory Agency. 1
ADCP	Acoustic Doppler Current Profile. 1
ADV	Acoustic Doppler Velocimeter. 1
CAESB	Federal District Environmental Sanitation Company. 1
CETA	Center for water Research and Technology. 1
CLAHE	Contrast Limited Adaptive Histogram Equalization. 1
DCC	Direct Cross-Correlation. 1
DFT	Discrete Fourier Transformation. 1
GCP	Ground Control Point. 1
GUI	Graphical User Interfaces. 1
IBGE	Brazilian Institute of Geography and Statistics. 1
LSPIV	Large Scale Particle Image Velocimetry. 1
LSV	Laser Speckle velocimetry. 1
MHK	Marine and Hydrokinetic. 1
PCM	Power and Communication. 1
PIV	Particle Image Velocimetry. 1
PTV	Particle Tracer Velocimetry. 1
ROI	Region of Interest. 1
UVP	Ultrasonic Doppler Velocity Profiler. 1

1 INTRODUCTION

1.1 CONTEXTUALIZATION

Energy is definitively correlated to the life quality of human beings and all contemporary societies. The world is in a moment where developed countries are changing their electricity mix, adding more clean and renewable technologies of energy conversion from different sources. The global concerns with CO_2 emissions are the main reason that drives countries to rethink their way of producing electricity. On the other hand, the developing and under-developing countries have to expand their electricity generation to provide this important component for their development needs, and new innovative and sustainable solutions have been employed.

Approximately 51 billion tons of CO_2 are emitted per year and about 27% [9] come from how we generated electricity. Going to net-zero emissions is a really difficult mission because the energy that comes from fossil fuel is still much more affordable. Net-zero means huge declines in the use of coal, oil, and gas. Renewable energy has to become financially attractive to poor and developing countries so they can have access to cheap energy and can improve the lives of its citizens. If today we decide to change all our electricity mix to net-zero we would need to install the world's current largest solar park roughly every day until 2030 [10].

To achieve net-zero a lot of investment, estimate in $4 trillion per year [10], and good policymaking will need to be created to ensure that this decarbonization of the grid occurs. This will create millions of new jobs, significantly lift global economic growth, and achieve universal access to electricity and clean cooking worldwide by the end of the decade.

Brazil has a particular grid compared to the world. The Brazilian electricity mix is predominantly renewable, with most of the generation coming from hydropower, Figure 1.1. The low increase in energy supply in the country, Figure 1.2 (b), can demonstrates how the last few years have been bad for development.

Approximately there are 237 locations in Brazil, most parts located in the north region, that doesn't have access to the electricity grid. According to data from the last demographic census of the Brazilian Institute of Geography and Statistics (IBGE), the population considered without access to energy exceeded two million Brazilians [11]. Most of them riverside or low-income population. They are citizens who, due to the lack of electricity, do not also

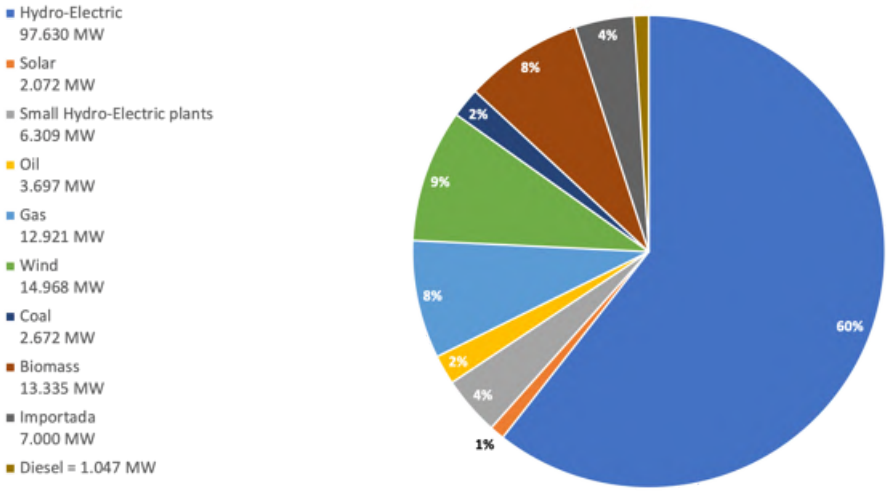

Figure 1.1 – Brazil Electricity Mix adapt from [1]

have access to communication, quality education, and improvement in their agro-extractive production. They are forced to travel to the place where they buy the fuel, return to their communities and use the fuel in fossil engines. To have electricity for a few hours a day, they emit much more greenhouse gases than a citizen connected 24 hours a day to the conventional grid. That is, there is a triple cost. In addition, the disposal of used fuel is not done correctly, being dumped, generally, in rivers or the land near the houses.

Motivated by this global demand to expand the supply of clean and renewable energy, Figure 1.3. Also to expand the electricity generation options to isolate communities. That needs a clean, renewable and continual source to improve their life quality. In conjunction with knowing that Brazil will need more energy to improve the development of the country. This work will apply and review a technique to determine the hydrokinetic potential from rivers.

Hydrokinetic Energy (HE) is the kinetic energy of a current of water. There are three main types of natural HE resources: inland currents (rivers), tidal driven currents (estuaries and channels), and ocean currents. Although natural occurring water flows are more usual, hydrokinetic energy in artificial channels is also a potential HE source. The ultimate origin of the HE is the water cycle, such that HE classifies as a renewable energy resource. This water mass movement in water currents provides potential relevant energy, which can be used for conversion into electricity utilizing suitable electromechanical devices. In this sense, this bias of energy restraint has been the object of an important development axis of technologies over the last decade [12] [13].

A brief explanation how the conversion technology on the quantification of energy in an aquatic current is necessary. Be therefore the power density associated with the kinetic

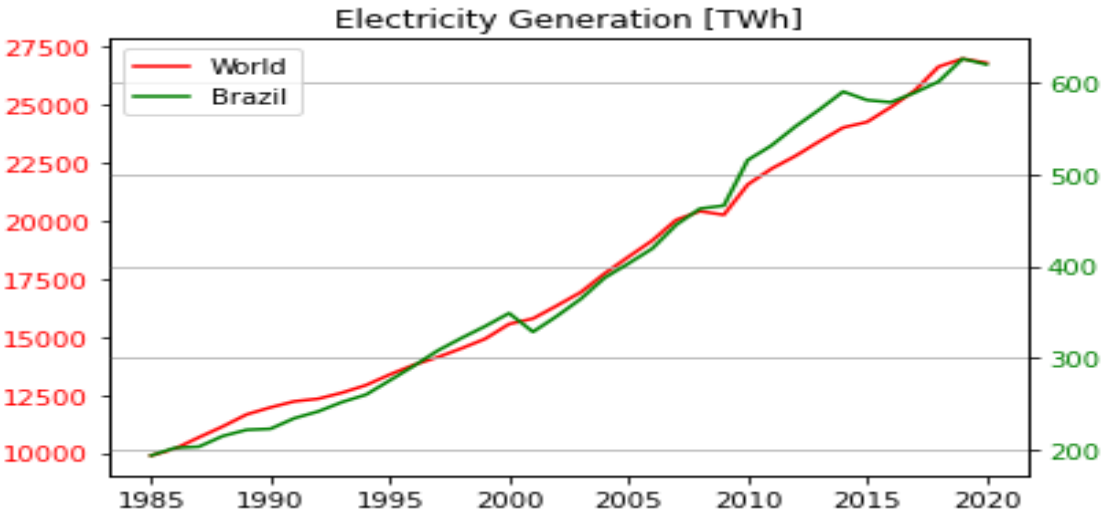

(a)

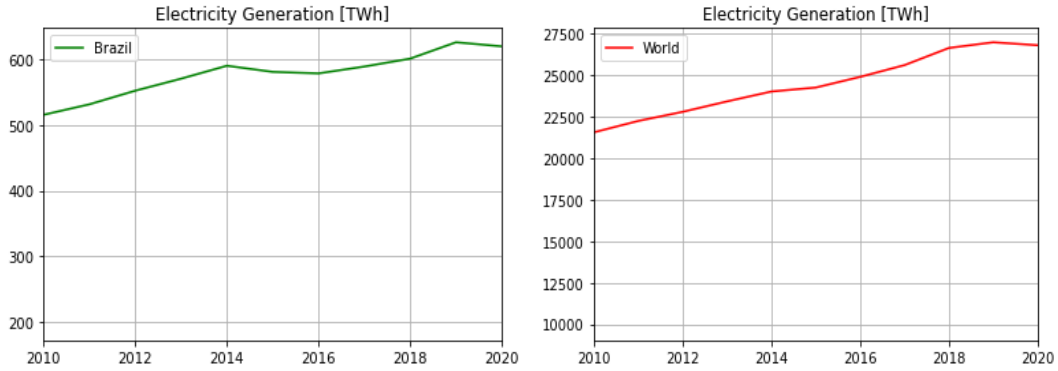

(b) (c)

Figure 1.2 – Electricity Generation [TWh] adapt from [2]. (a) Electricity Generation World × Brazil. (b) Brazil last 10 years Electricity Generation. (c) World last 10 years Electricity Generation.

energy of the flow of water (expressed in W/m²), which crosses a cross-sectional area A, which can be quantified by (1.1):

$$e_{hk} = \frac{1}{2}\rho V^3 \tag{1.1}$$

where ρ is the specific mass of water and V is the free flow velocity, see Figure 1.5.

From this energy availability, the hydraulic power that is converted by a turbine is generally quantified by (1.2)

$$P_{hk} = \frac{1}{2}C_p\rho A V^3, \tag{1.2}$$

In Equation 1.2, is introduce C_p, which is the machine‘s power coefficient. This dimensionless coefficient, typical of a given turbine, represents the hydrodynamic performance method of converting hydrokinetic energy into axis power.

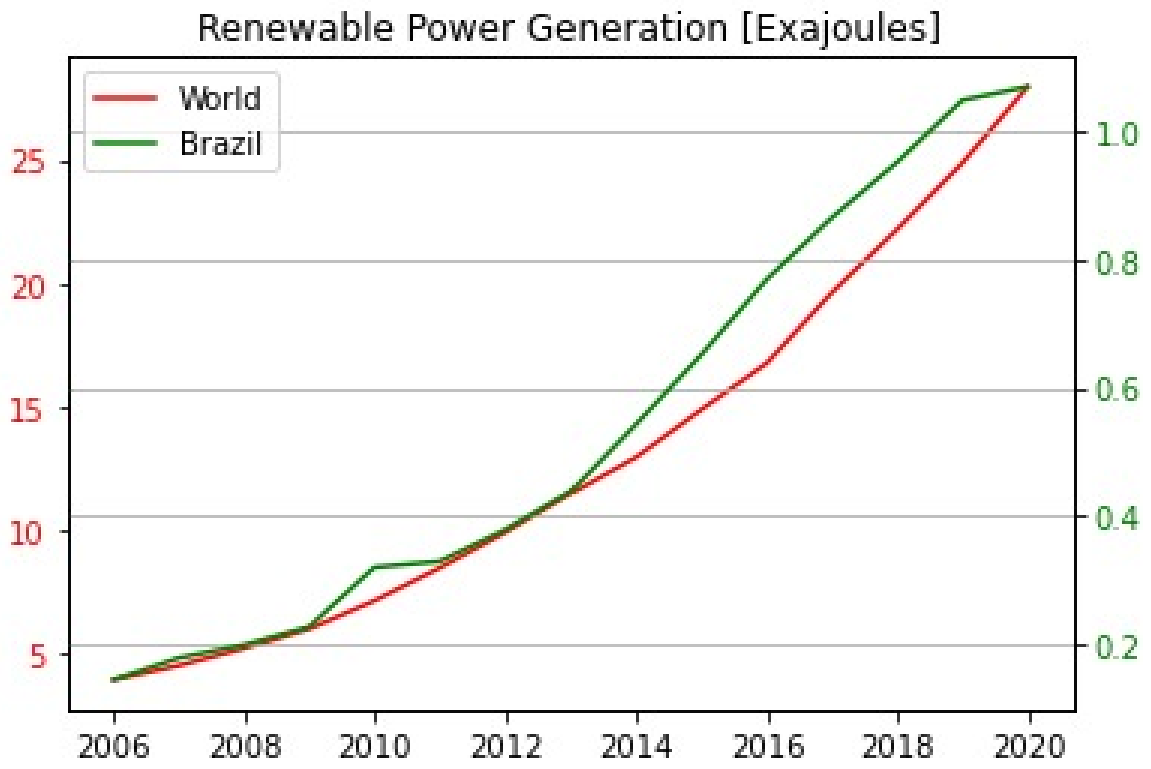

Figure 1.3 – Increase of Renewable Power Generation from world and Brazil adapt from [2]

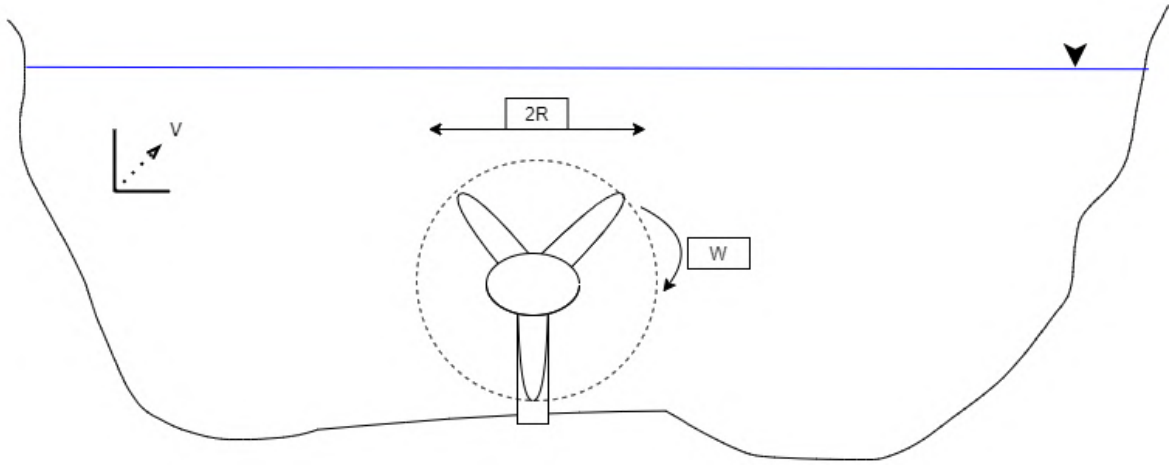

Figure 1.4 – Hydrokinetic Energy Conversion

The present technology envisages some contemporary challenges for its development: environmental impacts, accessibility and dispatchability, overall energy cost reduction, and the need to survey energy resources. As mentioned it‘s intended to present a methodology that can provide identification of priority areas in rivers. The feasibility of sites for installing systems provides a real window of opportunity for investments in technology. See Figure 1.5.

Hydrokinetic potential depends on some variables measurement, see table 1.1. Typical measurement techniques to collect these variables. The bathymetric survey can be done us-

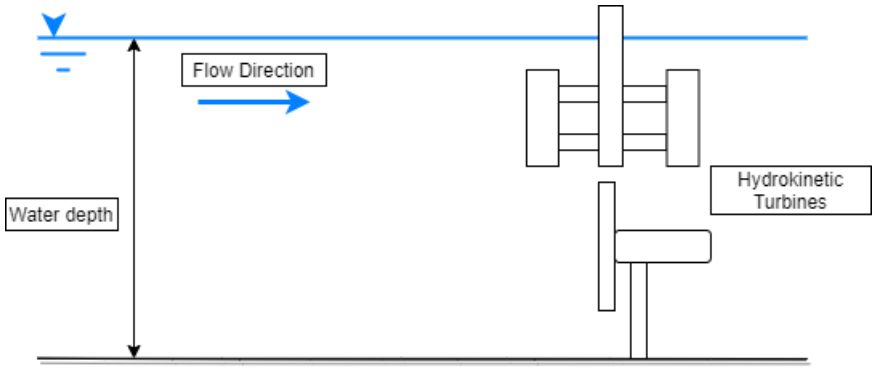

Figure 1.5 – Simplified sketch of turbines setup at river environment

ing direct methods: rulers or plumbs, or indirect methods: bathymetric probes with sonar or satellite images. In general, the depth of the water body is topographically raised along transverse lines, transects, so that later bathymetric charts and digital relief models background are built.

Discharge and current velocity are commonly calculated by Acoustic Doppler Current Profiler (ADCP) types of equipment. The ADCP works by transmitting "pings" of sound at a constant frequency into the water. As the sound waves travel, they ricochet off particles suspended in the moving water and reflect into the instrument.

Morphological Variables	
Bathymetry	Characterization of the bottom relief relative to the Reduction Level
Bottom roughness	Characterization of the water body bed
Physical Variables	
Temperature Water	Temperature record
Salinity	Characterization of local salinity
Turbidity	Water turbidity record
Hydrological Variables	
Discharge	Time series of characteristic flows tributary to water bodies
Quota	Same for quota time series
Hydrokinetic potential variables	
Current Velocity	Velocity measurement or model
Current direction	Alignment of the water current
Wave height	Wave height above average level

Table 1.1 – Variables used for hydrokinetic potential mapping

Predominantly the techniques of flow and velocity measurement are intrusive equipment that requires an operator near or inside the river. For this work, a non-intrusive, faster, and cheaper methodology is purposed to measure a hydrokinetic potential variable, the current velocity.

The technique is called LSPIV, Large Scale Particle Image Velocimetry, and this exper-

iment is being conduct broadly to measure flood events around the world [14], [15], [16], [17]. The method derives from the PIV (Particle Image Velocimetry) method, which was typically adopted to study fluids mechanics problems in the early eighties. PIV found great acceptability of the scientific community for being a cheap and efficient method and at that time were expected that with technologies advances this method becomes even more efficient, cheaper and reliable [18].

The LSPIV technique is applied to measure the surface velocity vector field of water bodies and compared it with measurements performed by an ADCP equipment. The idea is to apply the image velocimetry analyses to images recorded by an Unmanned Aerial Vehicle (UAV) flying over the rivers and compare them with velocities measured by the ADCP. Also using the bathymetric analysis collected by the ADCP equipment compared the flow calculated by the LSPIV technique and by the ADCP. An evaluation of adding a natural tracer to the river improves the results from the LSPIV are also performed.

1.2 LARGE SCALE PARTICLE IMAGE VELOCIMETRY - LSPIV

The LSPIV method is a experimental technique derived originally from the standard Particle Image Velocimetry (PIV) method. Historically, the investigation of flow through image dates back to the time of Leonardo da Vinci's sketches. If the human eye can perceive important qualitative aspects of the flow of a water body, transfiguring these visual impressions into quantitative information about the flow has recently become possible [19]. The beginning of this quantitative transfiguration can be given to researchers Barker and Fourney (1977) who used Lazer Speckle's method, which was originally a method used for solid mechanics but they have proven its applicability in measuring velocity fields in fluids.

Using a camera and a speckle laser they were able to map the line at constant velocity along a stream. In a method they named the "scattered-light speckle photographic method" which consisted of a plane of interest within the flux field being illuminated with a thin sheet of light from a double-pulsed laser, see Fig 1.6. A double exposure photograph is recorded of the resulting pattern of granular light spots (hence the name speckle). Knowing the time between each triggered leisure pulse and the camera angle concerning the illuminated flux field, it is possible to determine the velocity of this field [3].

In 1983, in Belgium, Meynart(1980) stood out among the researches regarding the use of the Lazer Speckle method, demonstrating that the method could be used both in laminar flow and in turbulent flow of liquids and gases. Meynart classified his work as "Laser speckle velocimetry" (LSV,) but when analyzing the images of his work it was common to find images of individual particles instead of grainy particles [21]. Adrian (1984) and Pickering and Halliwell (1984) are the first authors to mention the real importance of the particle image

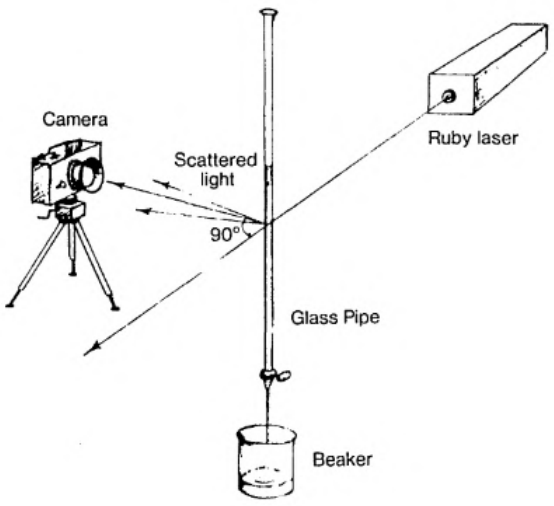

Figure 1.6 – Particle Image Velocimetry Setup by [3]

technique and the name Particle Image Velocimetry (PIV) appears to distinguish it from the method using the “Laser speckle velocimetry”.

A simple criterion was used to distinguish the LSV method from the PIV method, which was the creation of a dimensionless number called source density. This number indicates the average number of particles in a given volume. If the test is done for a fluid that presents a very high source density, the PIV method will be used [21]. Thus, the standard PIV method was characterized as a system consisting of pulse leisure that illuminates micrometer diameter particles in gases and tens of micrometers in liquids.

An excellent definition for PIV is given by Adrian (2005), it is the precise quantitative measurement of velocity vectors of a fluid in a very large number of points simultaneously. A great advance for the PIV method happened with the use of digital cameras to record images. Without the need for double exposure photographs and the problems caused in developing photos, the digital camera brought the ability to store a photo and then take another, a fact that greatly improved the cross-correlation operation needed to estimate the speed of particles registered in the images.

The implementation of digital cameras was perhaps the biggest advance in the PIV method, this type of camera brought three important improvements: it allowed the application of cross-correlation in images recorded separately; allowed the direction of flow to be automatically determined by the order of exposure, and eliminated small displacements of image overlapping [21]. In addition to the advances of the digital camera, the advancement of technology in recent decades has been extraordinary, enabling discoveries and uses for the PIV method.

With the advancement of technology, in the early 1990s, scientists started to apply the PIV method in large-scale measurements [24]. The first tests of this new model were carried

out in Japanese rivers, by Fujita and Komura (1994), and Aya (1995). From these works, surges the name LSPIV (Large Scale Particle Image Velocimetry) for the application of the PIV method on a large scale.

The image processing algorithm of the PIV method is very similar to the LSPIV method. However, special treatment must be given to flow illumination, flow tracking, and the removal of distortions in recorded images due to the camera lens and its oblique angles [27].

Fujita (1998) evaluated three experiments with the LSPIV method: the first a study of a hydraulic model to analyze aeration processes downstream of a power dam spillway and its relationship with changes in the spillway design and operation conditions, the second application was in a laboratory to study the movement of ice concerning rivers and the third to measure the velocity of the Yodo River in Japan, in full scale, during a flood. All experiments were performed in situations that traditional velocity measurement methods would take a long time to perform or would not be possible to perform with such methods.

Creutin (2003) performed measurements using the LSPIV method in the Iowa River in the United States of America and obtained results similar to those collected by the key river curve. The experiment also pointed out difficulties with the processing of images that appeared shaded in the registered images.

Fujita and Hino (2003) used images recorded from a helicopter during a flood on the Shin River in Japan to apply the LSPIV method and reached important conclusions: the need for control points to be able to orthorectify the collected images; and the turbidity of the river to identify natural tracers in image processing. Jodeau (2008) used the method to measure the velocity of a river downstream of a dam after the opening of the floodgates, highlighting the importance of the LSPIV method, which is unique among the traditional ones, such as measurements by a Doppler device, which does not place operator or equipment at risk during data collection.

Kantoush (2008) replicated the LSPIV assay in a laboratory and compared the result with the UVP method (Ultrasonic Doppler Velocity Profiler) reaching very close values for both measurements.

Several river velocity measurements have been carried out around the world as in Sun et al (2010), Le Coz et al (2010), Muste et al (2011), Dramais et al (2011), Kantoush et al (2011) and Gunawan et al (2012). All highlighting the importance of lighting, tracers in the water body, and orthorectification of the images obtained to achieve good results for river surface speed.

With the advancement of technology and the cheapening of several types of equipment, it became accessible to obtain a camera with an excellent resolution and the use of drones to capture images for the LSPIV method. Tauro et al (2015) built a drone and used it to measure a watercourse at Prospect Park in Brooklyn, evaluating the stability of the drone and how this

would affect the images recorded by it in the LSPIV method.

Bechle et al (2012) and Huang et al (2018) developed an automated surface velocity measurement system using the LSPIV method. The software developed to apply the method became so sophisticated that even movies recorded on youtube began to be used for studies. Le Boursicaud (2016) used recordings of flood situations and applied the method to calculate the surface velocity during these extreme events. Images from public cameras that recorded a flood event on the streets of Asunción, Paraguay were used by Guillén et al (2017) to determine surface velocity and locate risky sections that the flood could carry adults or children.

The LSPIV method is proving to be efficient, of low financial value, and simple to use. The difficulties presented by this method, analyzing several works, are usually in the lighting, the tracers, and the camera angle that obtains the images.

1.3 ACOUSTIC DOPPLER CURRENT PROFILER - ADCP

Acoustic and optical non-intrusive instruments using the Doppler effect have become increasingly popular in the engineering community for velocity measurements in laboratory and field conditions [15]. Among these instruments, the Acoustic Doppler Current Profiler (ADCP) has become extensively used for discharge measurements in field conditions, capitalizing on operational efficiency and rugged configuration.

The first generation of ADCPs, using narrow-bandwidth, single-pulsed acoustic systems has been initially applied to ocean and estuary current measurements. There is a vast literature describing ADCP‘measurements in oceanography to study two dimensional current structure from moving ships [40].

ADCPs that are used to measure discharge in a river are similar to those used on an oceanographic research ship except that oceanographers normally require measurements to greater depths. While deep-sea measurements are often made with the bottom well out of range, the bottom of a river will normally be within the range of an ADCP [41].

Currently, the most often conducted ADCP measurements from moving vessels in rivers are used for estimation of discharge [4]. Discharges in the measured areas are determined using the raw fluid velocity in the water column, boat velocity relative to the bed, depth, and time, see Figure 1.7. Despite the scattering of the measurements of the velocities and depths in single or multiple pings, the accuracy of the estimated discharges is relatively good compared to alternative conventional measurement procedures [4].

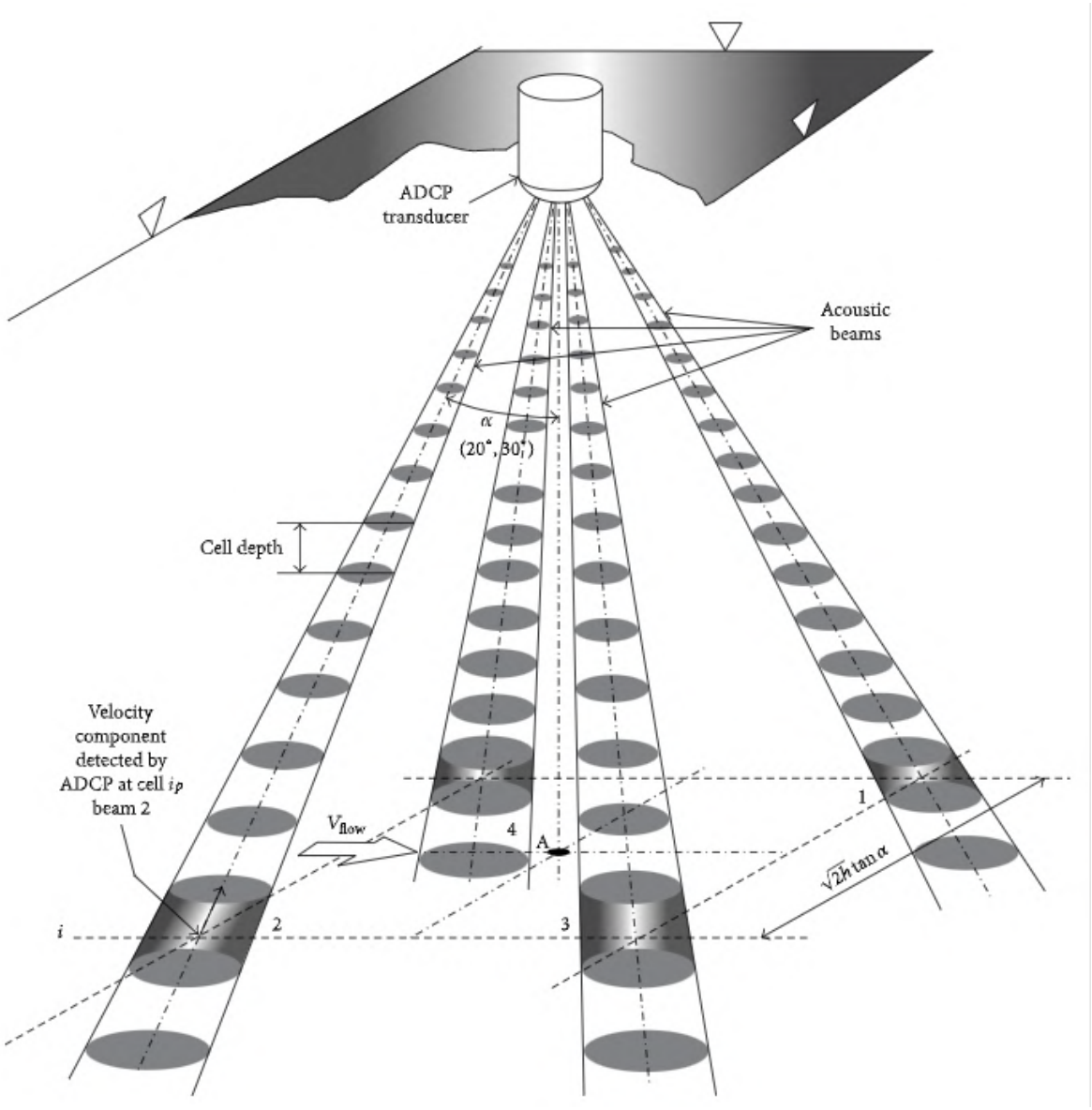

Figure 1.7 – ADCP measurement diagram by [4]

There continues to be a critical need for further analysis of the ADCP measurements conducted from moving and stationary vessels to fully assess the relationship between the flow and ADCP operational parameters to accurately capture mean and turbulence characteristics in a riverine environment. On table 1.2, are present the main sources of errors in ADCP measurements adapt from Muste (2004).

Error Source & Error type and dependencies	
Instrument (intrinsic)	Noise = F(frequency, transmit pulse length, lag distance, transmit power, echo intensity variation); Beam pattern and spread = F(transducer type and size, beam divergence, frequency); Beam-pointing angle = F(beam number, orientation, and assemblage); Speed of sound (affects vertical velocity component) = F(temperature and/or salinity change); Transducer ringing = F(receiver electronics, transducer and/or electronic housing, boat hull material and design); Side-lobe interference = F(beam geometry, depth; Heading/pitch/roll = F(sensor type, positioning, boat velocity)
Operator (external)	Mounting = F(transducer draft, relative position to the boat); Software setup = F(item setting in the communication, calibration, planning, and acquisition modules); Software application = F(pre-measurement checkups, data acquisition monitoring); Sampling time = F(turbulence intensity, flow regime); Site selection = F(geometry, flow non-uniformity and unsteadiness)
Environment (external)	Moving river bed = F(operation mode, sediment concentration); Noise = F(scatterer quantity and quality, water absorption coefficient, turbulence intensity, velocity gradient and magnitude, depth); Heading/pitch/roll = F(magnetic field, acceleration, waves

Table 1.2 – Source of errors in ADCP measurements adapt from Muste (2004)

1.4 OBJECTIVE

The main objective of this work is to study and review the LSPIV method to perform measurements and define the superficial velocity from rivers and channels. To achieve this, an UAV DJI Mavic Air 2 Drone was used to record the rivers flow. Additionally the secondaries objectives are:

- Compared the hydrokinetic potential calculate with the velocities measured from the LSPIV and ADCP techniques;
- Perform measurements in different conditions for rivers and channels;
- Analyse of if the addition of a natural tracer improves the LSPIV technique;
- A detailed explanation of the LSPIV methodology trusting that it can be replicated;

This work is divided into four chapters. The first one is an introduction to the subject with a briefly contextualization of the global scenario and the main techniques applied, follow by

motivations and finally the main and secondaries objectives of the work. Then the second with a detailed explanation of the methodology used in the field measurements. The third is about the results obtained in the field with a discussion and evaluation from it. Finally, the last chapter has a conclusion with a recommendation and summary of all the work.

2 METHODOLOGY

2.1 METHODOLOGY

Two field methodologies were performed in this work, LSPIV, and ADCP, and in this section, both will be discussed and explained in detail, see Figure 2.1. Even if they are two completely different techniques, they share a similar path to collect the data. First measurement in the field and then analysis and evaluation using a specific program or software. First, the LSPIV technique will be explained, how data was collected, and how it was handled, then the ADCP equipment. In this chapter, the procedures, and specifications of each method will be covered. Also, a simplified explanation of hydrokinetic potential will be present and how both field methodologies are connected with it.

Figure 2.1 – Field setup with the ADCP and the Drone at the Rodeador Channel

2.2 LARGE SCALE PARTICLE IMAGE VELOCIMETRY

Large Scale Particle Image Velocimetry has become popular with the advancement, development, and modernization of digital cameras. After the pioneering work of Fujita and Komura (1994), several works applied LSPIV to measure discharge in rivers across the world are: Yodo River [27], Kino River [42] and Uono River [14] in Japan; the Iowa River [15] in the USA; the Arc River [16] and Arde‘che River [30] in France, and River Blackwater [17]

(a) Open propellers (b) Close propellers

Figure 2.2 – Mavic air 2

in the UK.

Basically, is possible to make an LSPIV analysis, with any camera recording the flow of a river. In this methodology the camera used was from the DJI Mavic Air 2, see Figure 2.2, a drone manufactured by the DJI company. A part of the specification from the drone used is present at table 2.1. All the specification from the drone can be accessed from it website [8].

Mavic Air 2 Specification	
Weight	570g
Dimension Unfold (LengthxThicknessxHeight)	183x253x77 mm
Maximum duration stationary flight (no wind)	33 minutes
Maximum flight distance	18.5 km
Precision range in stationary flight	
Vertical (with visual positioning)	± 0.1 m
Vertical (with GPS positioning)	± 0.5 m
Horizontal (with visual positioning)	± 0.1 m
Horizontal (with GPS positioning)	± 1.5 m
Camera resolution	
Maximum resolutions of photo	48 MP 8000x6000 pixels
Video resolution and frame rate	
4K Ultra HD	3840x2160 24/25/30/48/50/60 fps
2.7K	2688×1512 24/25/30/48/50/60 fps
FHD	1920×1080 24/25/30/48/50/60/120/240 fps

Table 2.1 – Dji Mavic Air 2 Specifications adapt from [8]

The benefits of using a drone to record the video from the river flow are abounding. It

makes possible to access river location that would be dangerous or difficult to access with a traditional ADCP equipment. It's much lighter than traditionally ADCP equipment. Also allows extracting different data from the site location, like a digital model of the terrain [43].

Taking the proper precautions to take off and fly over the area of interest, the drone is reliable, easy to operate, and cheap equipment to use. The ideal is to take off the drone on a flat surface at least 1 meter away from any object or vegetation.

The Drone is positioned stationary above the river flow, see Figure 2.3. Another benefit of the Drone is that it has a gimbal that permits the controller to have a controllable range from the camera. So it's possible to set the camera orthogonal to the river.

The drone must be flying at a specific altitude above the river, so the wind created from the helices drones does not affect the river motion. Because that would cause interference in our measurement. As mentioned before the four main components for the LSPIV techniques are flow visualization, illumination, image recording, and image processing.

Define and inspect the site location is a very important task to perform at any river characterization. Flow visualization for the LSPIV procedure is crucial. Is necessary to know if it's possible to record the flowing of the river with the camera. Also if there is not too much vegetation around that can prejudice the footage. To improve flow visualization is common to add some type of natural tracer to the river. This natural tracer is added upstream to the region of interest where the analysis will occur. In all experiments conduct the tracer was sawdust, which is a biodegradable tracer that will not bring environmental harm to the site. In chapter 3 some results comparing if the addition of a natural tracer improves LSPIV measurement is presented, see Figure 2.4.

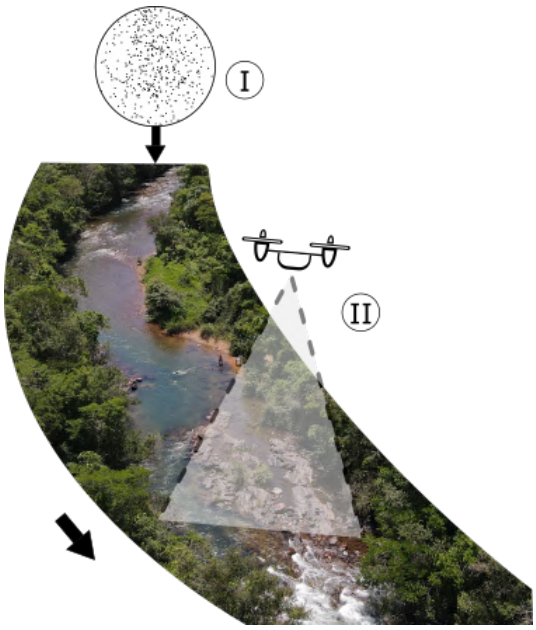

Figure 2.4 – LSPIV methodology adding a natural tracer

Figure 2.3 – Drone flying stationary above the Rodeador Channel

In traditionally PIV experiments the illumination is generated by a laser or an artificial at the laboratory. In LSPIV experiments even though it has some example using artificial light in laboratory sites, the standard illumination device is sunlight, so is extremely important that the measured day is performed at a day of homogeneous sunlight, basically a clear day, or a cloudy day, avoiding peaks of lights in the area recorded .

Deciding the site location, the recording device, paying special attention to the natural condition around the flow, and also to the illumination that is present at the site summarize the field procedure required for applying LSPIV. See figure 2.5.

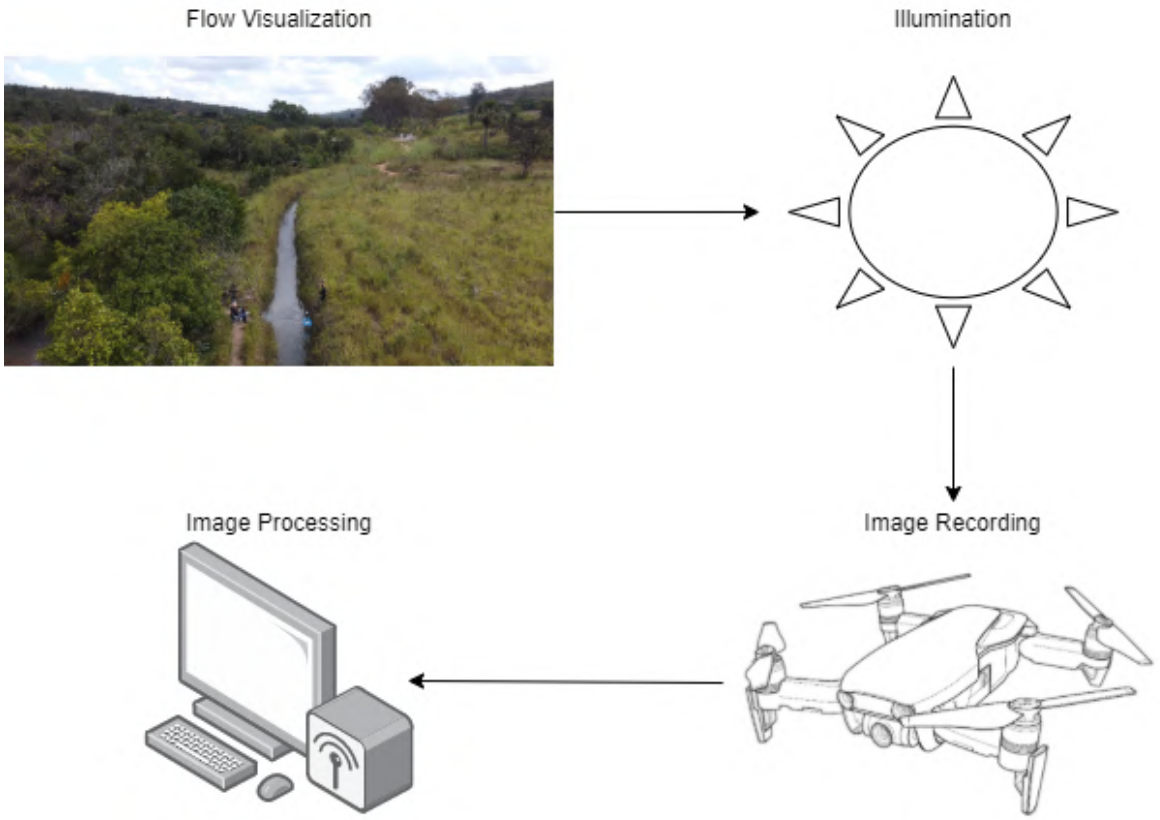

Figure 2.5 – Traditional flowchart of LSPIV

Before the image processing phase began is necessary to highlight an important step to guarantee a good execution of the technique. It's inside the image processing phase but is has to be adjust at the field location. The velocimetry analyse is made comparing pair of frames from images recorded at the field, the output of that analyses is in unit of measurement of $frames/time$, so is indispensable to know a physical measurement from the field that appears in the record to be possible to calibrate the analyses and obtain the velocity in a traditional measurement system, like $meters/second$.

This measure can be anything in the recorded that is possible to know precisely its size. Usually, some ground control points (GCP) are added to the field, so they can be used as an object to calibrate the procedure. The GCP has another important factor in LSPIV. When

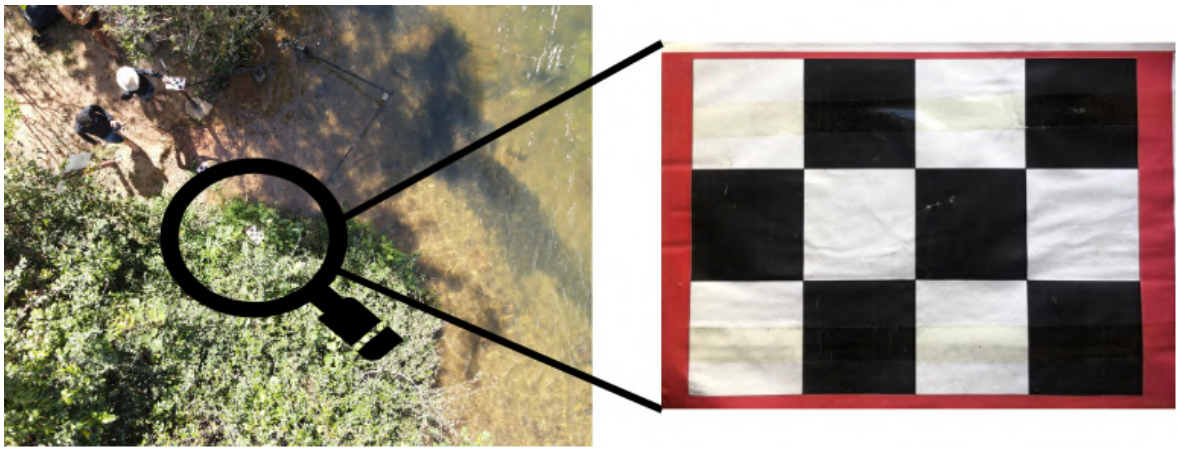

Figure 2.6 – Example of a Ground Control Point

cameras are not orthogonally positioned to the river. It needs to perform an extra step in the image processing step, called orthorectification. Orthogonal camera views require an accurate geometric rectification of the images, or velocity results, to overcome the appreciable distortions produced by the viewing angle of the camera [44]. In a fixed camera at least 4 GCP and their distance between each other is needed to orthorectify the image, see figure 2.6.

After registering the images of the desired river the image processing phase start. Numerous free computational tools have been developed during the last years for PIV analysis for example, OpenPIV, PIVlab and RIVeR.

For this work, two Graphical User Interfaces (GUI) were used and will be explained in this chapter. The first one is called RIVeR and is a standalone application developed in the Center for Water Research and Technology (CETA) at the National University of Cordoba, Argentina, beginning in 2013. RIVeR has been developed to provide an efficient experimental large scale water surface characterization (for example, flow velocities and trajectories) and flow discharge estimation in rivers, artificial channels (for example, irrigation, treatment plant, and others.), or large scale hydraulic physical models [44].

The second one is called PIVlab and it's an open-source tool for digital particle image velocimetry in MATLAB. The tool takes advantage of several built-in MATLAB features and eases subsequent data processing by providing a close link to the popular MATLAB user interface [5]. A simplified sequence of the image processing step is presented at Figure2.7.

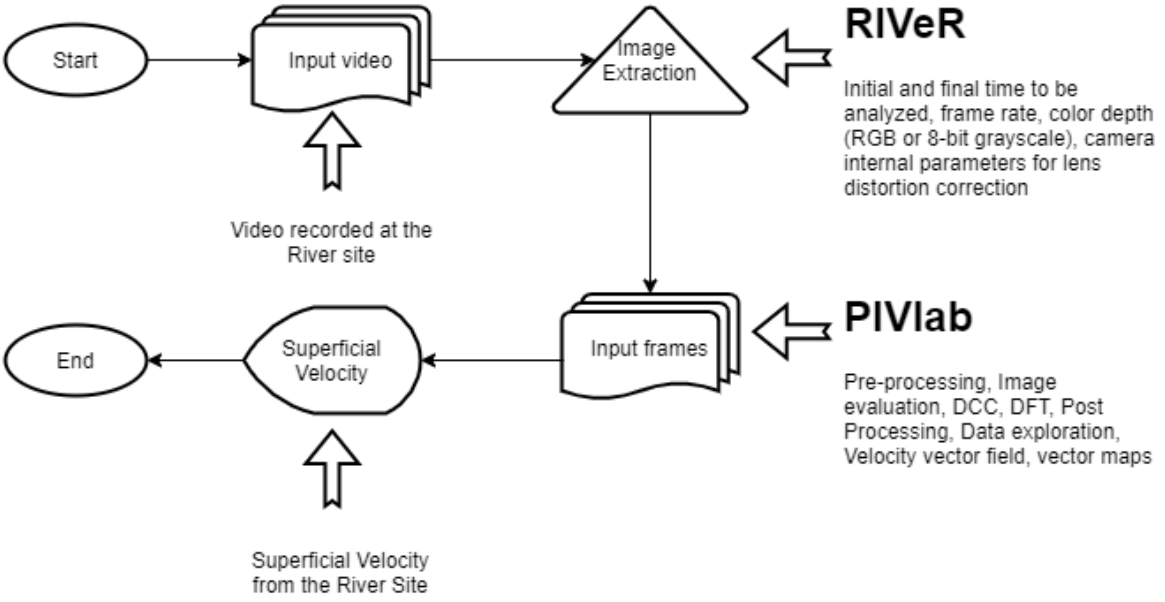

Figure 2.7 – Simplified flowchart of the image processing phase

Following the sequence presented in Figure 2.7. The first step is to input the video recorded into RIVeR program. Then a toolbox with the option to extract the frames will be presented, see Figure 2.8. The duration of the film is show and the ratio that was recorded. The time between frames, Δt, is given and is important to register this value. Velocity is displacement over time, so knowing how much time passed between frames is a piece of crucial information to calculate the superficial velocity of this method.

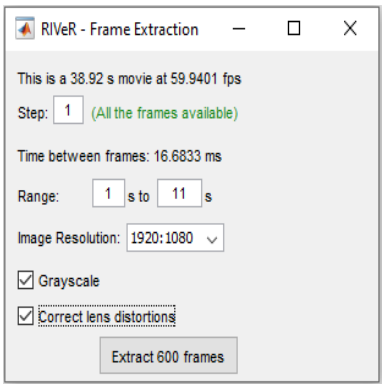

Figure 2.8 – Frame extraction with RIVeR program

The toolbox gives the option to extract the frames in grayscale and to perform a correction in lens distortions. Both options are marked because in the following steps of the processing phase, having the frames in grayscale and a lens distortion correction improves the quality of the processing. The distortion model is a Matlab® based subroutine that also is presented in the work done by Taborda and Silva (2012). The subroutine can be described as the following:

$$\begin{bmatrix} X_p \\ Y_p \\ 1 \end{bmatrix} = KK \begin{bmatrix} X_d \\ Y_d \\ 1 \end{bmatrix}, where KK = \begin{bmatrix} fcx & \alpha_0 * fcx & ccx \\ 0 & fcy & ccy \\ 0 & 0 & 1 \end{bmatrix} \tag{2.1}$$

Where X_d, Y_d, and X_p, Y_p represent the coordinates of a point in the distorted and undistorted coordinate system, respectively, fcx and fcy are the focal lengths in x and y directions, respectively, ccx and ccy are the image center, and α_0 is the skew coefficient defining the angle between the x and y pixel axes. KK is obtained from multiple views of a chessboard of known dimensions with the Camera Calibration Toolbox [44]. Although the lens correction fix distortion that occurs there is another problem with the images collected by a non-fixed camera.

This work uses a non-fixed camera to register the river flow. The drone that is flying above the river in stationary flight can still change its fixed position due to wind or from it on flying mode. In table 1.2 is present the range that in stationary flight the drone stays. So an additional step is performed to guarantee that the frames that are being analyzed are from the same position. The RIVeR program has an option to unshaken the video recorded drawing a mask where is desire to implement the LSPIV, see Figure 2.9.

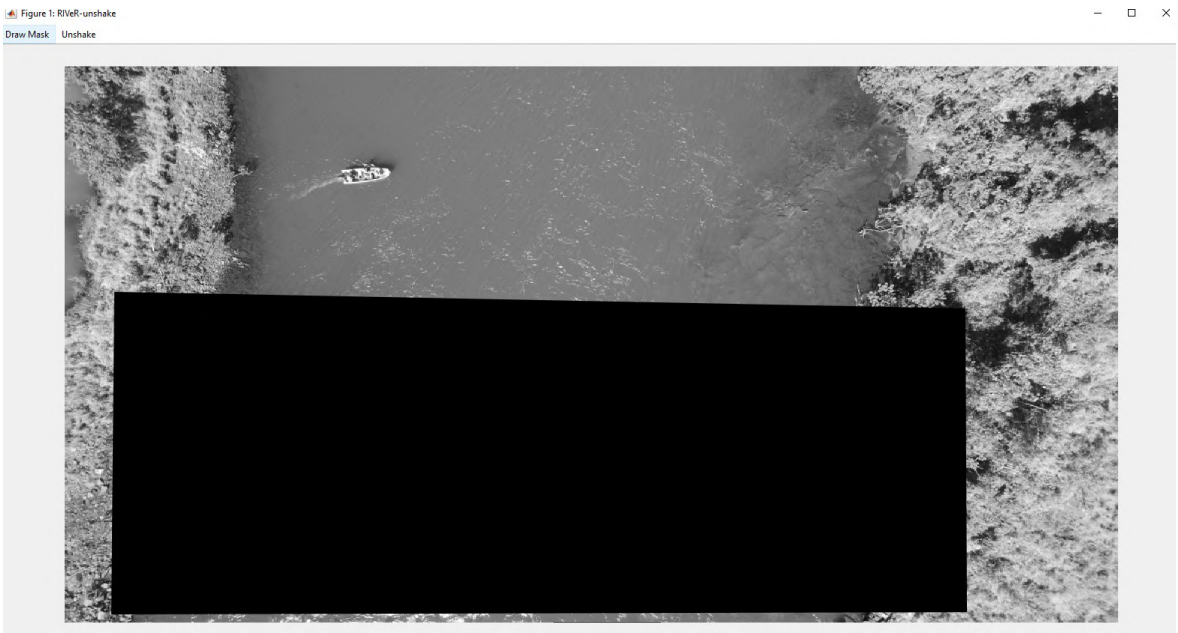

Figure 2.9 – Masked area to applied the unshake processment from RIVeR

After the extraction is complete, it obtains 600 frames in grayscale with the distortion from the camera fixed. Through several trials, a value of 10 seconds was established for extracting the frames that guaranteed the convergence of the mean and standard deviation of the velocity vectors. So from each video it was select only 10 seconds from the total

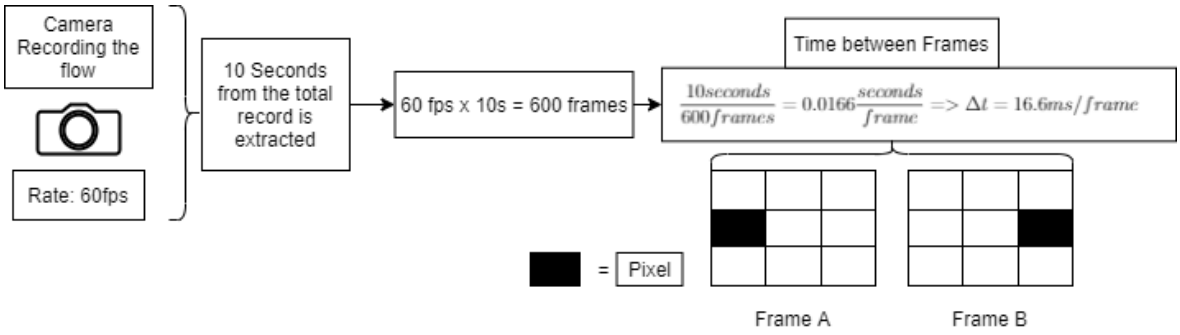

Figure 2.10 – Time between each frame: Δt

recorded. The camera has a rate of $60 fps$. Thereby with 10 seconds recorded, a total of 600 frames were extract and the Δt between each frame is $16.6ms$, see Figure 2.10. Now with the time between frames calculate, is needed to measure the distance that each pixel travels from one frame to another. Having the space and the time calculate the velocity is simple to determine.

Importing all the frames to the PIVLab program, see Figure 2.11 is chosen the option to compare each frame in sequence instead of pair of frames in sequence. So the first frame will be analyzed with the second, then the second with the third, and so on.

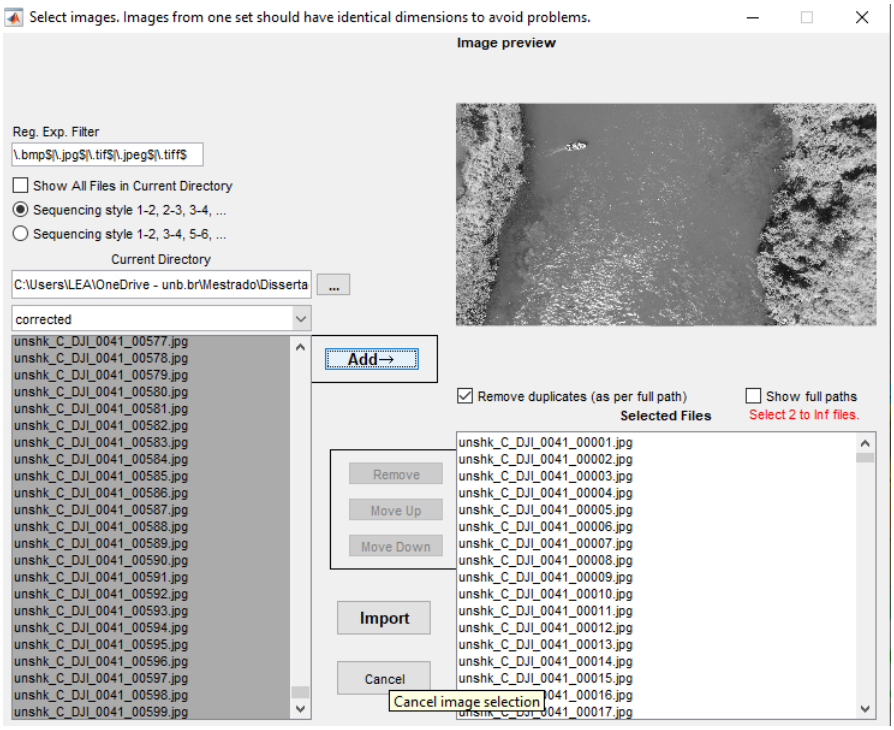

Figure 2.11 – Loading frames to PIVLab

PIVLab can perform either PIV or PTV analysis for the image series will depend on the desired information and the number and type of tracers used at the water surface. Determining the mean velocity field is the primary purpose of the analysis, and the tracers are

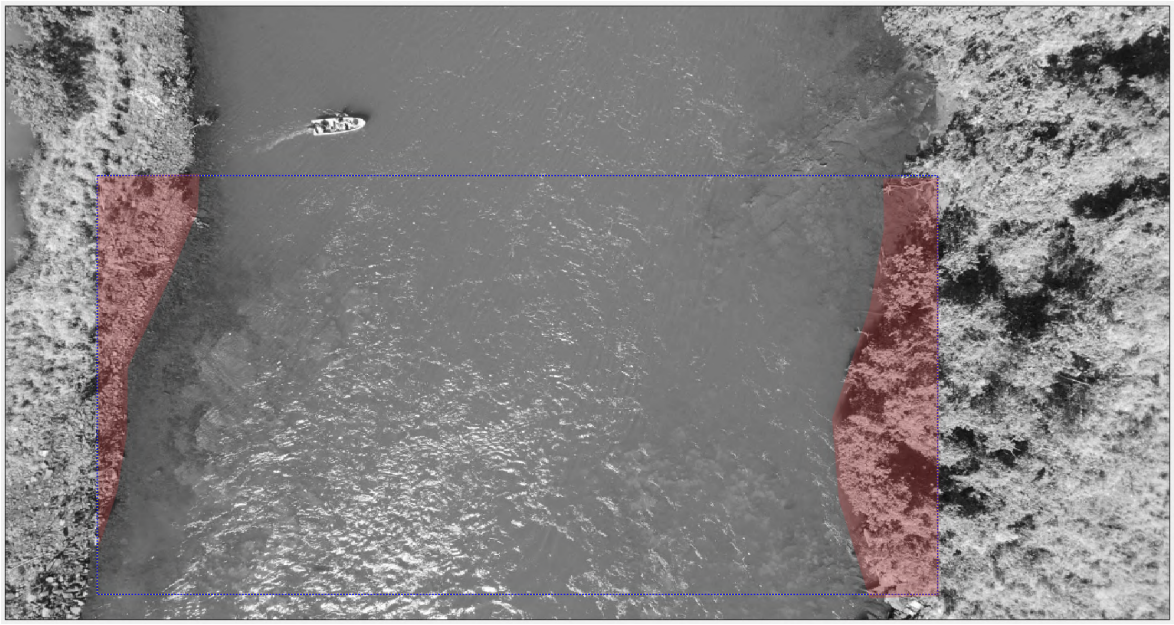

Figure 2.12 – Example of a ROI and a Mask draw in a LSPIV analyses

homogeneously and densely distributed over the water surface. Afterward, the images should be analyzed in an Eulerian framework with PIV. Otherwise, if the tracer density is sparse and individual trajectories are required, for example, for flow velocity field characterization near hydraulic structures then PTV should be used in a Lagrangian framework of analysis [44].

With all the frames imported, the next step is to decide the Region Of Interest (ROI), that is the region where the velocity field vector will be calculated. The program offers the options to draw a mask in the ROI to no perform a velocity analysis in this part, see Figure 2.12. The blue dashed rectangle is an example of an ROI and the red spots in the figure are the masks. The ROI and the mask are defined at the first frame extracted from the video. Then it expands this selection to all the other frames.

Previously when the importance of performing the lens correction and the unshake option in the RIVeR program was mentioned it's just for when it came the time to define the ROI and the mask, all frames were within the same ROI, and the mask was positioned in the same place. To ensure that all the frame sequences were processed equally. Figure 2.13 is a good example of how much a mask can dislocate from one frame to another, in this example no lens correction and no unshake option were performed so the mask that should be on the top of the rock dislocate to the left from the first frame to the final frame.

Moving on with the processing phase. With all the frames imported and with the ROI and mask establish, see Figure 2.14 (a), there is multiple filter disposal at PIVLab to improve the image analysis. The enhancement of images before the actual image correlation takes place improves the quality of the measurement. The pre-processing techniques that are accessible in PIVLab are:

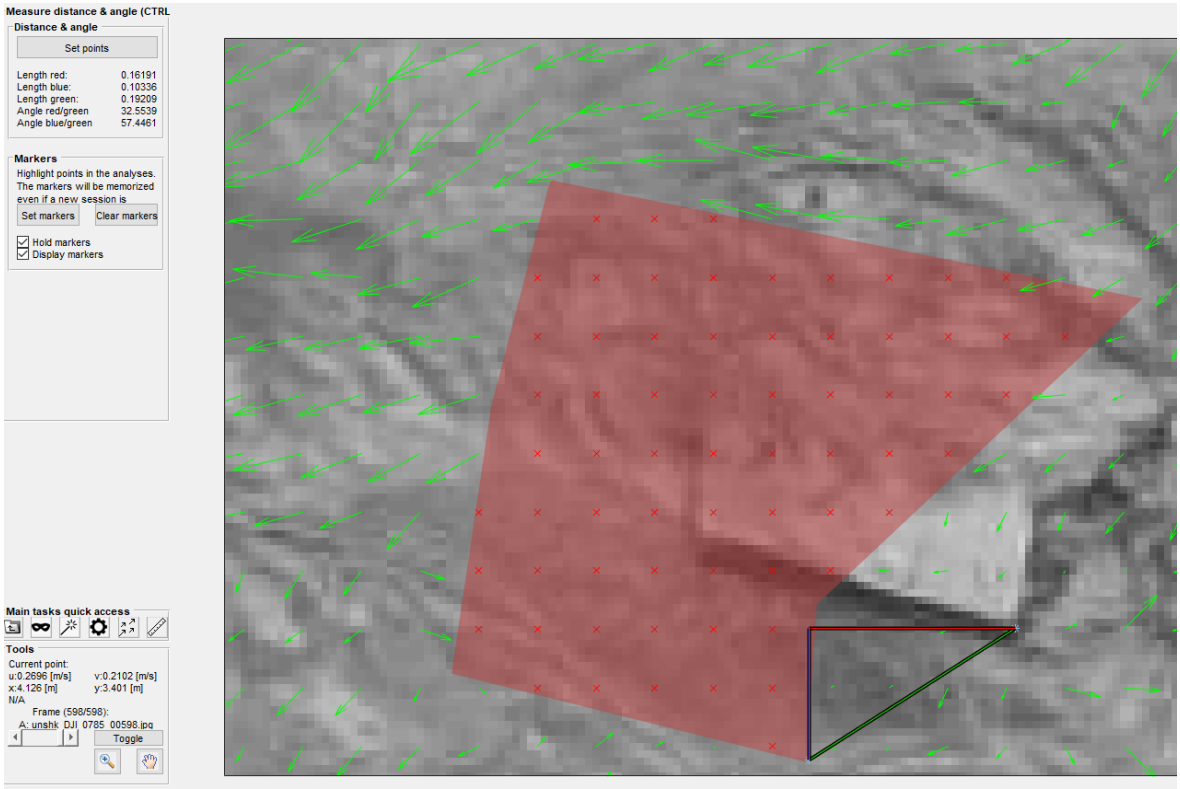

Figure 2.13 – Dislocation from the mask caused from drone flight instability

- CLAHE: Contrast limited adaptive histogram equalization, see Figure 2.14(b). CLAHE operates on small regions (tiles) of the image: In every tile, the most frequent intensities of the image histogram are spread out to the full range of the data (from 0 to 255 in 8-bit images). Regions with low exposure and regions with high exposure are therefore optimized independently. CLAHE significantly improves the probability of detecting valid vectors in experimental images by 4.7 ± 3.2% [5].

- Highpass: Inhomogeneous lighting can cause low frequency background information which can be removed by applying a high-pass filter that mostly conserves the high frequency information from the particle illumination. The filter emphasizes the particle information in the image, and suppresses any low frequency information in the images, see Figure 2.14(c).

- Capping: Bright particles or bright spots within the area will contribute statistically more to the correlation signal, which may bias the result in non-uniform flows. The intensity capping filter, see Figure 2.14(d) circumvents this problem. An upper limit of the greyscale intensity is selected, and all pixels that exceed the threshold are replaced by this upper limit. Therefore, unlike CLAHE, only a small amount of the pixel intensity information is adjusted, limiting the potential negative impact of image modifications [9]. Intensity capping improves the probability of detecting valid vectors in experimental images by 5.2 ± 2.5% [5].

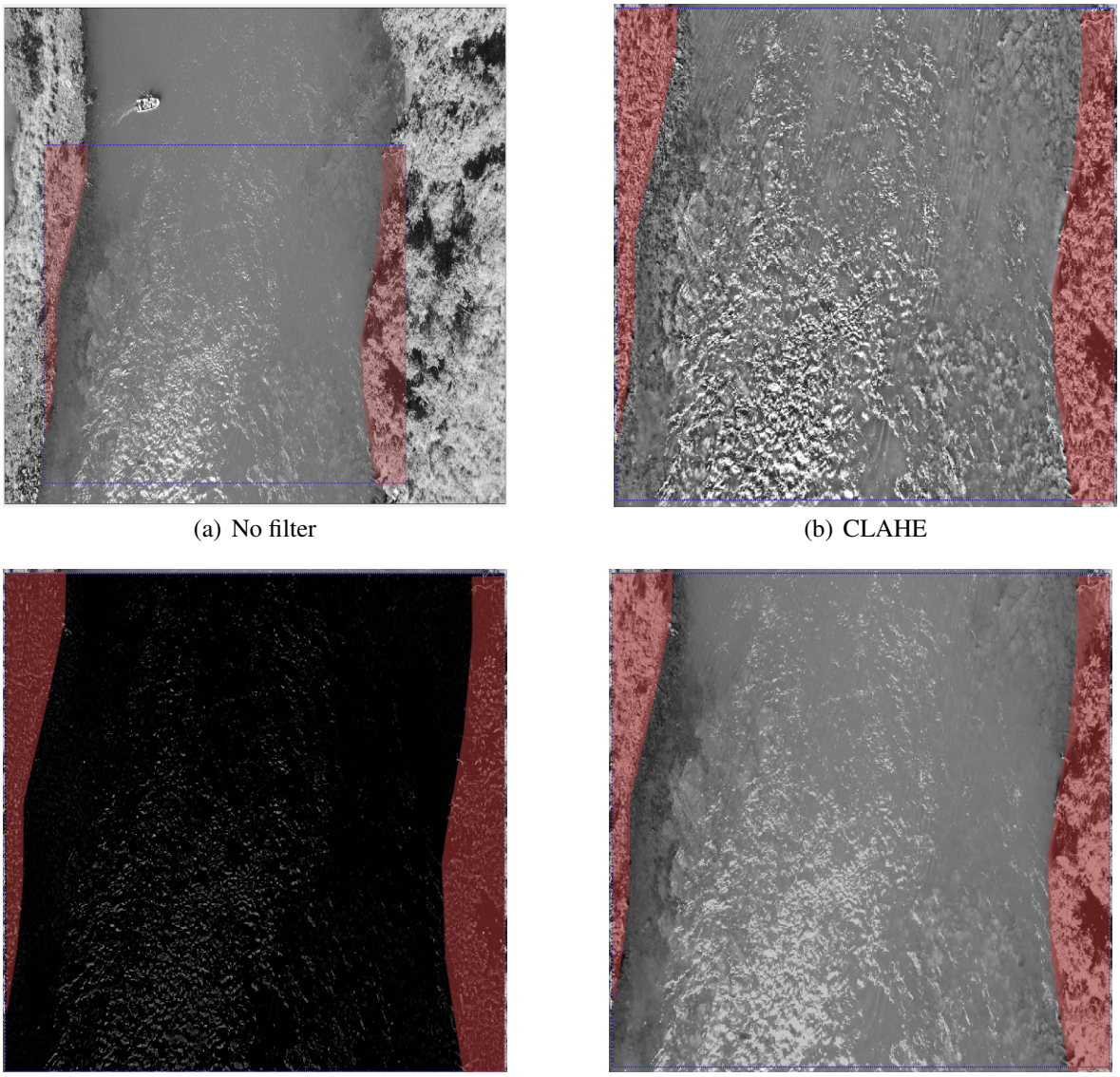

(a) No filter (b) CLAHE

(c) Highpass (d) Capping

Figure 2.14 – The effect of several pre-processing techniques

The following steps from the processing phase are the most sensitive part of the analysis. Now with the filters applied to the frames is necessary to set the interrogation area in the defined ROI. Interrogation areas are small sub-images, where a pair of frames are cross-correlated to derive the most probable particle displacement in the interrogation area. In essence, cross-correlation is a statistical pattern matching technique that tries to find the particle pattern from interrogation area A in interrogation area B, [5]. This statistical technique is implemented with the discrete cross-correlation function, see equation 2.2

$$C(m,n) = \sum_{i} \sum_{j} A(i,j)B(i-m, j-n) \tag{2.2}$$

Where A and B are corresponding to the interrogation areas from frame A and frame B.

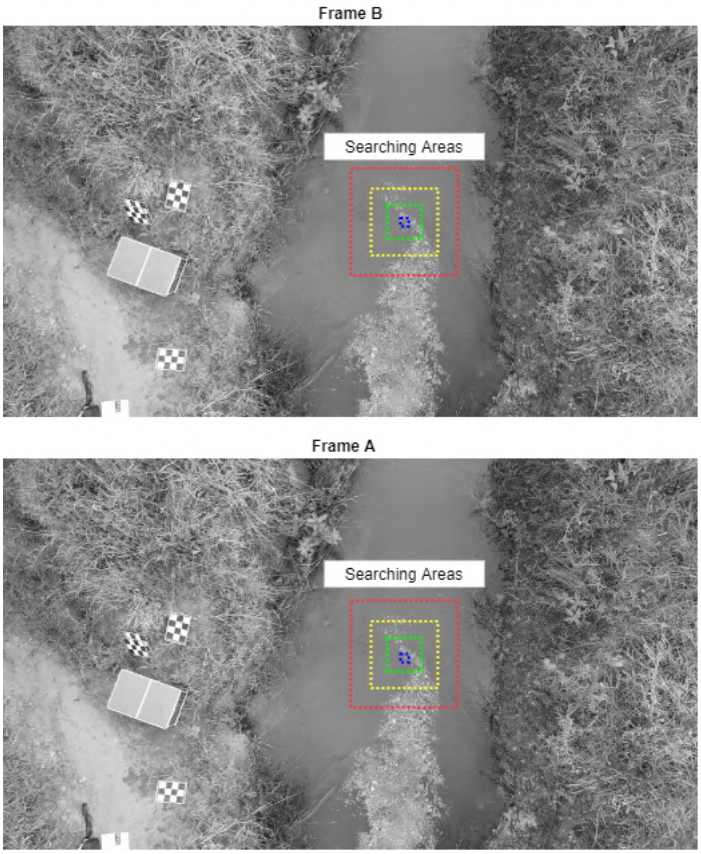

Figure 2.15 – Example of Searching Area at frames obtained by a LSPIV analyse at the Rodeador Channel locate at Brazlândia, Federal District

The interrogation areas are inside searching areas, grid box that decreases in size proportionally, see Figure 2.15. The idea is to characterize the pixel inside these boxes, calling this characterize pixel of interrogation point, and search for this same pattern in the next frame of the image pair [46].

There are two common approaches to solve equation 2.2. The most straightforward approach is to compute the correlation matrix in the spatial domain, this approach is called direct cross-correlation (DCC). The other approach is to compute the correlation matrix in the frequency domain and is called Discrete Fourier Transformation (DFT). Both options are available at PIVLab, and both have their advantages and disadvantages, see Figure 2.16.

The DCC computes the correlation matrix in the spatial domain. Interrogation areas A and B can have two different sizes. When B is chosen twice as large as A, a particle displacement of up to half the size of A will not result in any loss of information and provide a reliable correlation matrix with low background noise. DCC has been shown to create more accurate results than a standard DFT approach. The disadvantage of DCC is the increased computational cost concerning a standard DFT approach see Figure 2.17, especially with large interrogation areas [5].

The correlation matrix can also be calculated at the frequency domain. By doing this, the

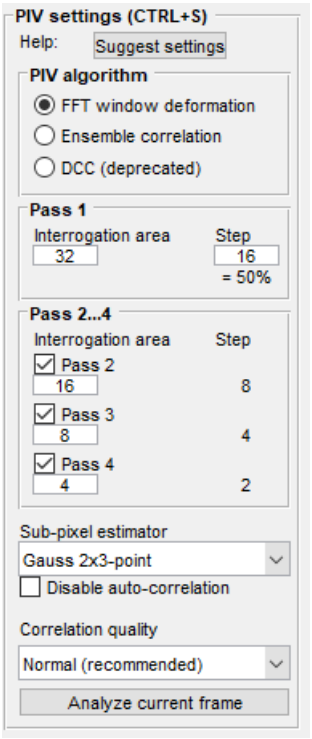

Figure 2.16 – PIVLab interface of the PIV settings

computational cost can be solved. This solution is called the Discrete Fourier Transformation (DFT). This approach uses interrogation areas of identical size. Therefore every particle displacement induces some loss of information, which can be noticed by the increasing amount of background noise in the correlation matrix. This background noise complicates the detection of the intensity peak and decreases accuracy. It is therefore advisable to reduce the displacement to about one-quarter of the interrogation area, to keep the background noise in the correlation matrix low [5]. These disadvantages can be offset by running several passes of the DFT on the same dataset.

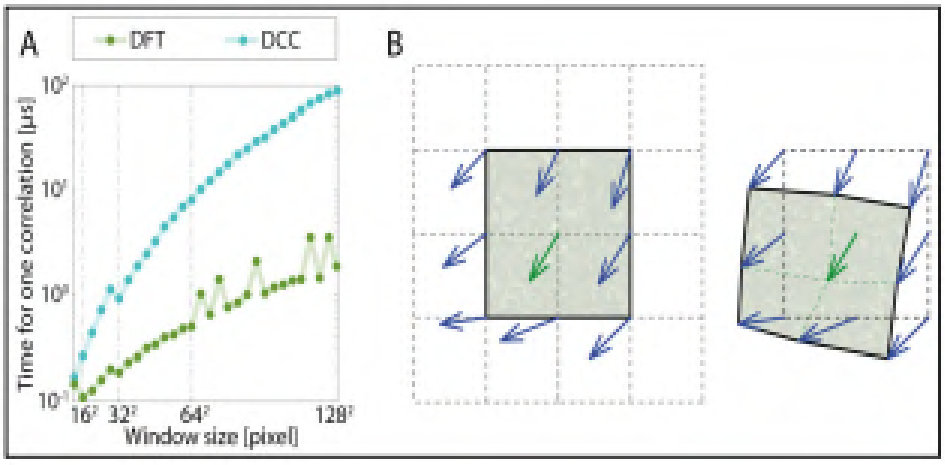

Figure 2.17 – Speed of DCC in comparison with DFT and the principle of window transformation [5]

The DFT option was preferred to perform in PIVLab and it follows this sequence. The first pass yields displacement information at the center of each interrogation area. When the areas overlap one another by e. g. 50%, there is additional displacement information at the borders and corners of each interrogation area, see Figure 2.17. This information is used to calculate displacement information at every pixel of the interrogation areas via bilinear interpolation [5]. Next, interrogation area B is deformed according to this displacement information using either bilinear interpolation (faster) or spline interpolation (higher precision, but slower). The next interrogation pass correlates the original interrogation area A with the deformed area B. The remaining displacement information of each pass is accumulated, see Figure 2.18. After a few passes, the displacement has been determined with high accuracy. Between the passes, but not after the final pass, the velocity information is smoothed and validated, and missing information is interpolated.

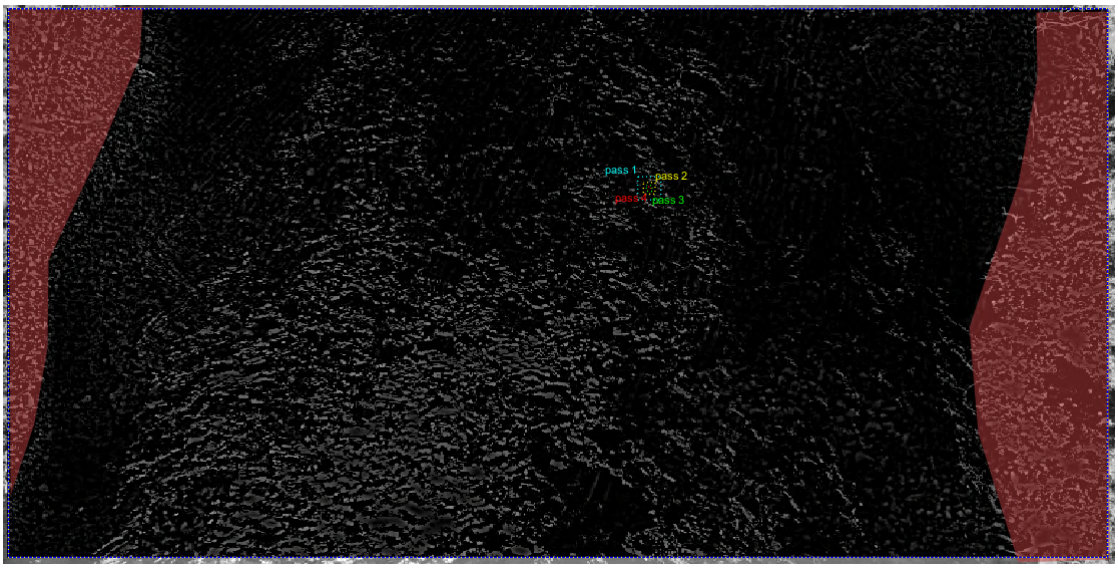

Figure 2.18 – Example of interrogation area and the 4 pass for the LSPIV analyse at PIVLab environment

The integer displacement of two interrogation areas can be determined straightforwardly from the location of the intensity peak of the correlation matrix. A sub-pixel analyse can be performed to refined this location. The typical procedure is to fit a Gaussian function to the integer intensity distribution. Fitting a one-dimensional Gaussian function, solid line to the integer intensity distribution of the correlation matrix, dots for both axes independently, see Figure 2.19. It is sufficient to use only the directly adjacent vertical and horizontal pixels (two times a 3-point fit = 2·3-point fit) and to evaluate the x and y-axis separately [5]. The peak of the fitted function is used to determine the particle displacement with sub-pixel precision.

With all the frames evaluate and the displacement between frames calculated, the final part of the PIV analyses is to calibrate the frames with a measured from the site location. Previously in the explanation the importance off a ground control point (GCP) was men-

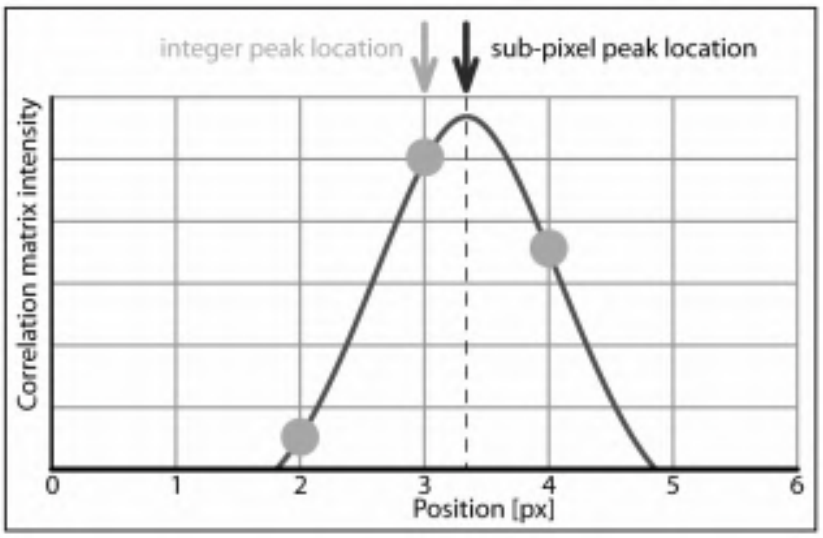

Figure 2.19 – Principle of the Gaussian 2.3 point fit from [5]

tioned to performed this calibration. As mentioned the GCP can be any thing presented at the record that is possible to know the real size of it. The calibration window from PIVLab, see Figure 2.20 is a point click option to set the distance that was measured at the site and then input the real valor in mm, also is required the time step between each frame that was obtained in the frame extraction at the RIVeR pogram.

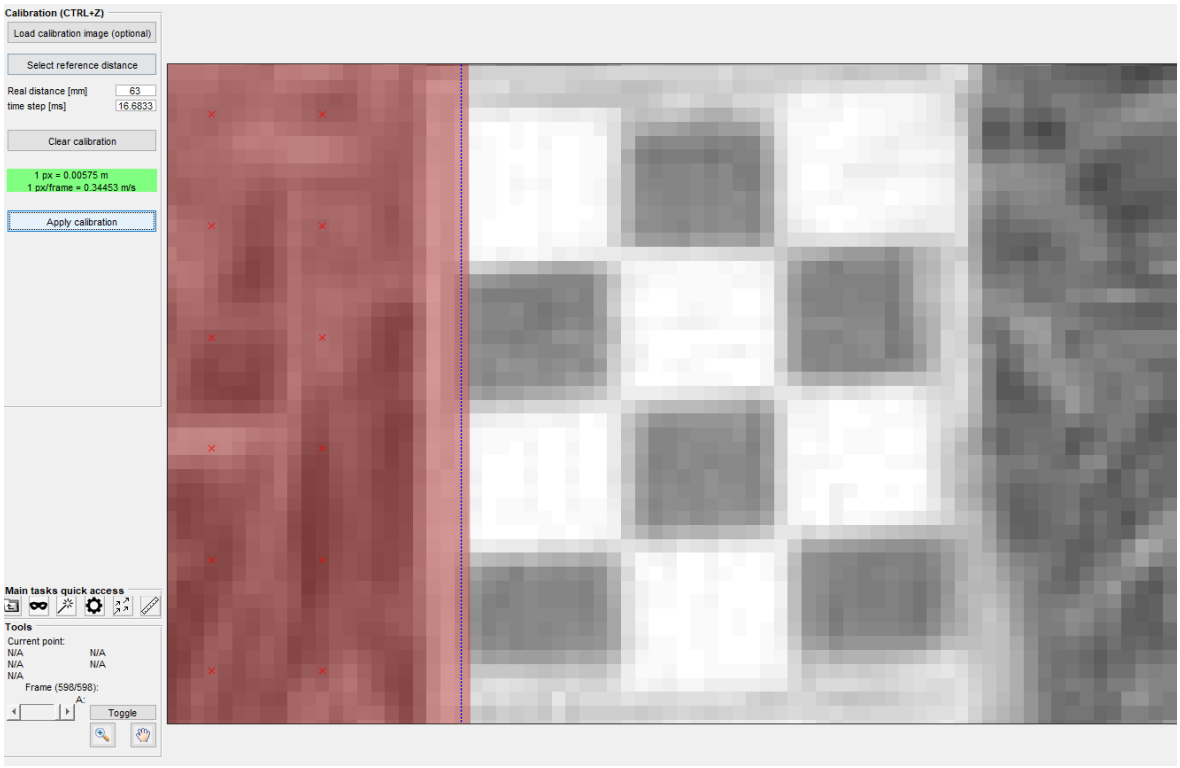

Figure 2.20 – Calibration example at the PIVLab interface using a GCP

Now the velocity vector fields calculated by PIVLab have units of $meters/second$ and

the final extraction of the analyses can be performed. The idea is to analyze velocity in different cross-sections from the Region of Interest defined so it's possible to compare with measurements made by ADCP equipment. So from the vector fields, 3 sections were extracts to be compared, see Figure 2.21. It was chosen to perform 3 extractions to analyzed the first extraction at the bottom of the region on interest, then the middle, and finally on top, always in the direction of the river flow.

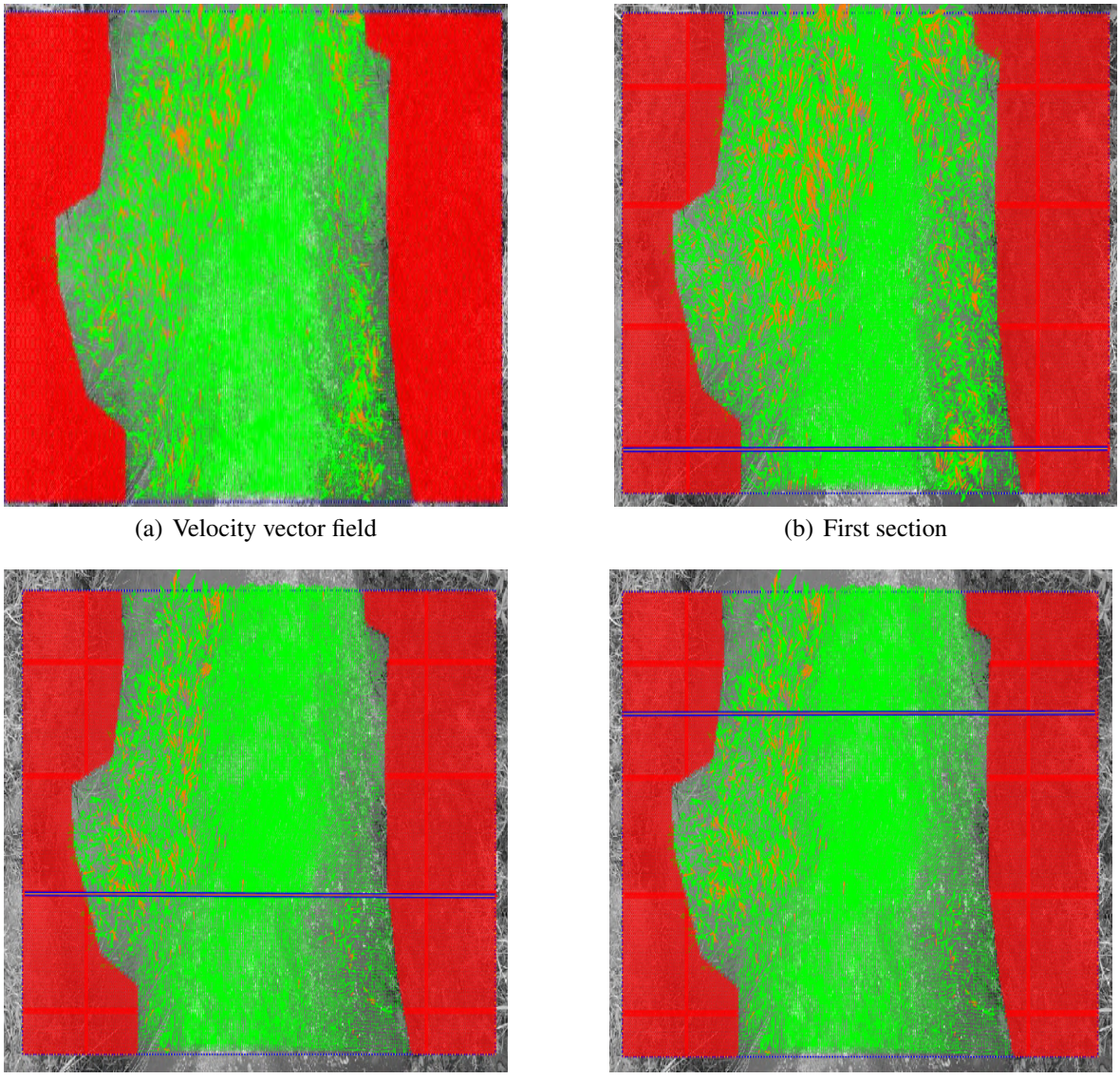

(a) Velocity vector field

(b) First section

(c) Second section

(d) Third section

Figure 2.21 – Vector field from the Rodeador Channel and each section that had the velocity extract

Each pair of frames analyzed results in one $.txt$ format file extract with the location and the velocity at several points equally spaced between them through the cross-section. So from each section, 600 text files are extracted with the location and velocity information disposable at it. With all the files extracted, a script in python language was written to read

and generate graphics with the mean velocity from each point calculated from the 600 files. An overall sequence from the methodology with the fundamental points is presented, see Figure 2.22.

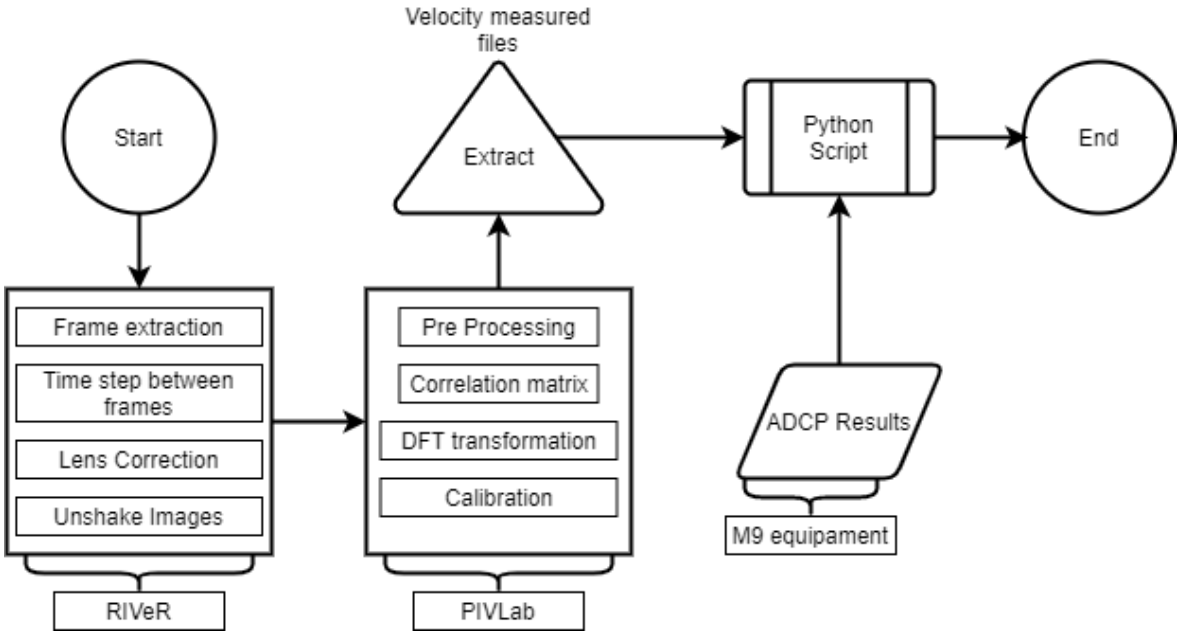

Figure 2.22 – LSPIV methodology

2.3 ACOUSTIC DOPPLER CURRENT PROFILER

Acoustic Doppler Current Profiler has become extensively used for discharge measurements in field conditions, capitalizing on operational efficiency and rugged configuration [4]. The ADCP equipment used in field measurement was the RIVERSURVEYOR M9 from Sontek company, see Figure 2.23. It's a multi-band, vertical acoustic beam sensor that internally computed discharge and secure data. Preventing lost data from communication dropouts. The specifications are present at table 2.2.

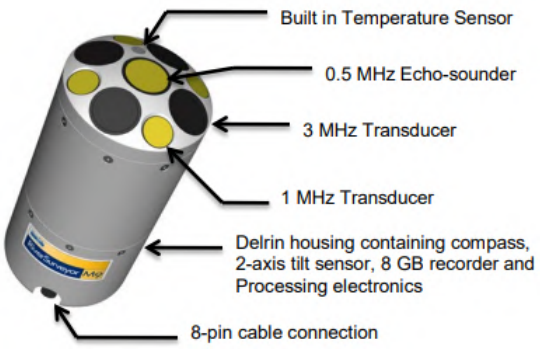

Figure 2.23 – M9 ADCP Features by [6]

RiverSurveyor® M9 Specification	
Profile Range	
Distance Velocity	0.06 to 40 m $\pm$20 m/s
Velocity	
Accuracy Resolution	$\pm$0.25% of measured velocity $\pm$0.2 cm/s 0.001 m/s
Number of Cells	Up to 128
Depth	
Range Accuracy Resolution	0.20 to 80 m 1% 0.001 m
Discharge Measurement	
Range - Bottom Track RTK GPS	0.3 to 40 m 0.3 to 80 m
Computation	Internal

Table 2.2 – River M9 specification adapt from Sontek [6]

The most important thing to perform a good measurement with ADCP is to select a good site that the basic assumptions from the equipment are achieved. The goal is to be able to measure velocities that are representative of the mean channel velocity. Ideally, there will be a straight section of the channel of appropriate length that is free from flow disturbance caused by bends in the channel, obstacles in the water, inflows, outflows [7].

ADCP transmits sounds pulses at a fixed frequency in the column of water and listens to the returning echoes from small suspended particles moving in the acoustic beam [7]. With acoustics, measuring length or distance is different than a measure by a ruler for example. To measure velocity, the main focus is on the change in frequency (Doppler Shift) of the acoustic sound. Because an acoustic ping is a wave sound it obeys Snell's Law, see Equation 2.3. So is possible to calculate the change in the speed and the direction of a wave when it travels from a medium of one density into a medium of another.

$$\frac{\sin\theta_1}{C_1} = \frac{\sin\theta_2}{C_2} \tag{2.3}$$

Where θ_1 and θ_2 are the angles of the acoustic beam in two adjacent density layers and C_1 and C_2 are the sound speeds in each layer. If there are multiple layers with different sound speeds, it needs to be applied this equation between each layer.

Now using Equation 2.4, the change in frequency is calculated for each layer, D_1 and D_2

$$D_1 = \frac{-2U_1F\sin\theta_1}{C_2} \quad \text{and} \quad D_2 = \frac{-2U_2F\sin\theta_2}{C_1} \tag{2.4}$$

Then applying Snell's Law by substitution into Equation 2.4 and rearrange to calculate the velocity:

$$U_2 = \frac{-D_2 C_1}{2F \sin \theta_1} \tag{2.5}$$

Measuring accurate water velocities anywhere in the water column is purely a function of the frequency of the transducer F, the angle of the transducer θ, and the speed of sound C [7]. The velocity in layer 2 is calculated using the speed of sound from layer 1, see Figure 2.24.

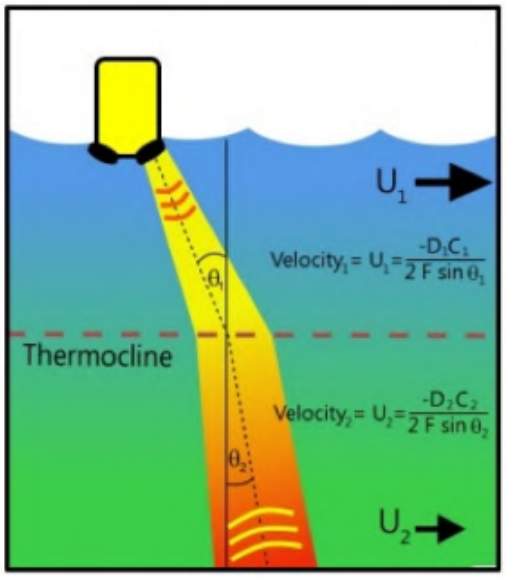

Figure 2.24 – Velocity measurement in each layer from [7]

The M9 equipment is a robust and highly accurate Acoustic Doppler Current Profiler (ADCP) system specifically designed to measure river discharge, 3-Dimensional water currents, depths, and bathymetry from a moving or stationary vessel. Knowing how the equipment works, the procedure on the field will be present.

The equipment works integrate with an RTK GPS, which allows measuring minimum stream widths consistently to less than 1 meter, see Figure 2.25. The RTK Base Station consists of an RTK GPS receiver with an external, high-gain GPS antenna, a Spread Spectrum radio modem for communication with the PCM (Power and Communications Module) see Figure 2.26, an external, high gain antenna, and a mounting tripod.

(a) Mounting mast (b) RTK Base Station

Figure 2.25 – RTK GPS mounted at field site

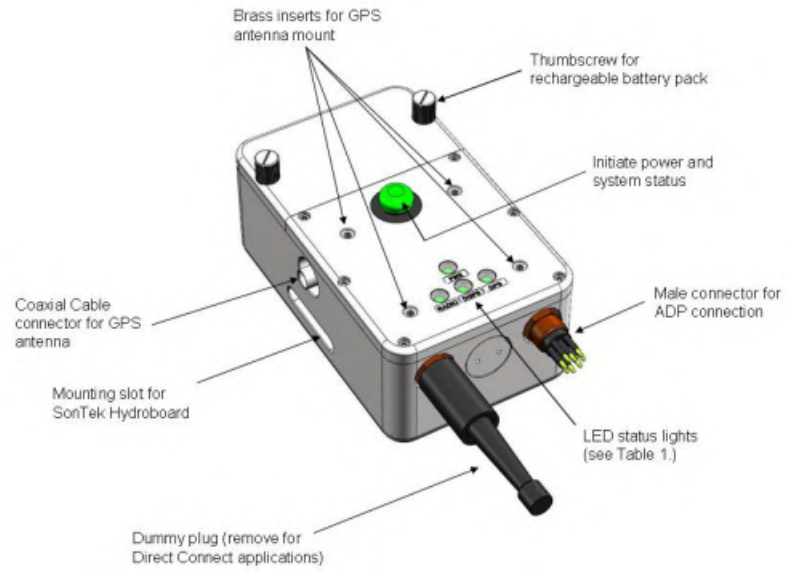

Figure 2.26 – PCM Setup by [7]

There are four different configuration options to mount the M9 system: A direct connection with M9, Bluetooth connection, Spread Spectrum Communications, and RTK GPS connection. For this work, the RTK GPS option was used. The setup for this configuration follow these steps:

- Connect the GPS high gain antenna to the aluminium mast by screwing the male threads on the mast into the antenna receiver.
- Connect the mounting bracket for the antenna mount to the ADP by inserting the four thumb screws located on the mounting bracket into the four brass holes on the ADP.

- Connect the coaxial cable to the PCM and the GPS antenna by connecting the female connectors on the coaxial cable to the male connectors in the PCM and GPS antenna.
- Turn the system on by pressing the power button on the PCM.
- RTK quality data requires that the RTK Base Station be installed within 2 kilometers of the PCM.

A general setup from the ADCP field procedure is present in Figure 2.27.

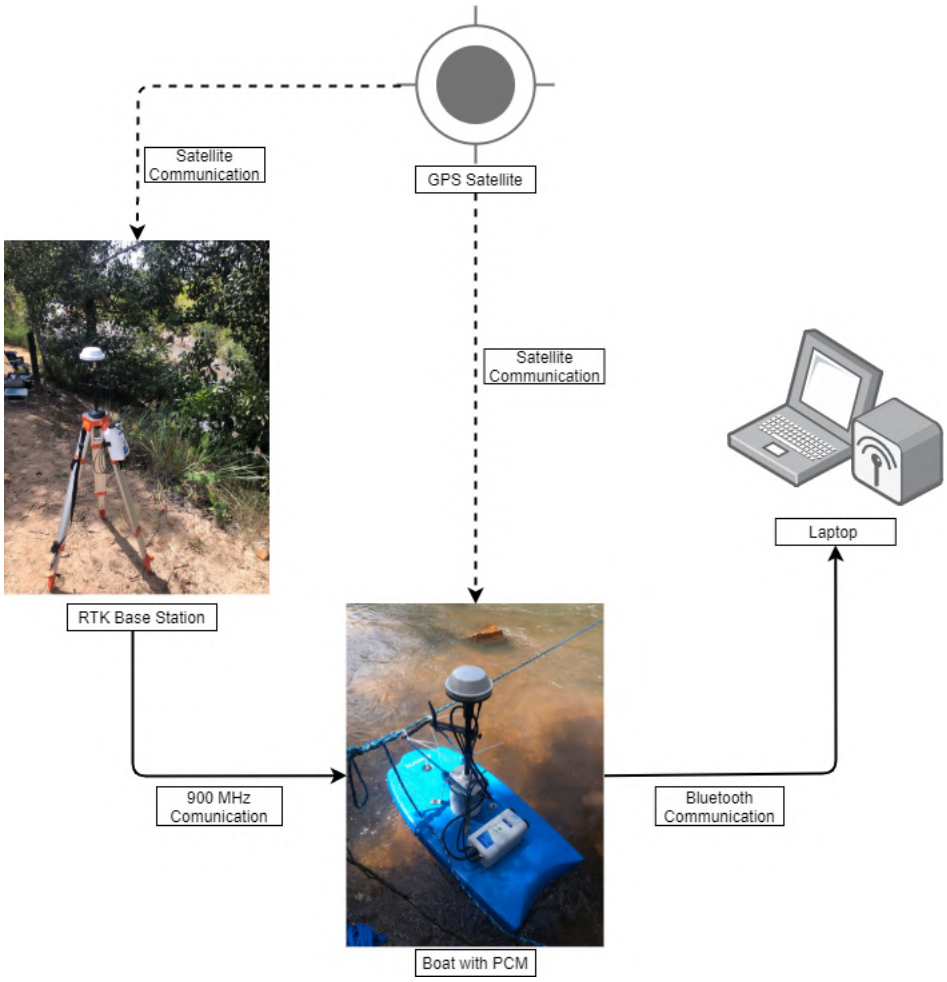

Figure 2.27 – Setup and communications of the M9 equipment

Two boats were developed for field measurement. One is a board design, see Figure 2.28 (a), to perform measurement using a rope to conduct the M9 through the define section, see figure 2.28 (b). The other one is a manually piloted boat, 62 pieces printed in a 3D printer and glued with glass resin, see Figure 2.28 (c) that was built to measure long river section, see Figure 2.28 (d).

(a) Board with M9

(b) Measuring ADP with rope

(c) Manually pilot boat

(d) Manually pilot boat at the Paranoá Lake

Figure 2.28 – Boats create to assemble the M9

The measurements were performed inside the region of interest defined for the LSPIV technique. The M9 operates through three sections. First assembling the bathymetry of the section and then collecting the velocity and discharge of the same at the transect. With the setup ready at the location, RTK base station connect, PCM ready, and connect to the laptop with the RiverSurveyor Live for PC software ready to start. The procedure to measure, attend this sequence.

- Starting the system: After the system is configured, start the system collecting data.
- Collecting Star Edge data: Position the vessel for the starting edge position and begin collecting edge data with the vessel as stationary as possible. It is recommended that a minimum of 10 profiles/samples are collected to perform the edge discharge

calculation. Enter the edge distance and shape.

- Collecting Transect Data: After collecting the start edge data, proceed to move the vessel across the channel. Keep the vessel speed and direction as constant as possible.
- Collecting End Edge Data: After moving across the channel and arriving at an end edge location, enter the end edge distance and shape. Collect at least 10 samples/profiles with the vessel as stationary as possible.

The M9 ADCP has limitations on the areas from the cross-section that it can measure, see Figure 2.29. Only the Measured Area is measured by the M9. The Start and End Edge are calculated from a mean velocity profile that is developed by maintaining a fixed position at the edge. The discharge calculation at the edge is based on the selection of a constant sloped bank or vertical wall and uses a combination of mean depth and velocity profile at the edge.

Top, Bottom, and Shore estimates are calculated by a technique known as Velocity Profile Extrapolation. This theoretical approach, to modeling the velocities within the water column, allows all velocities and therefore the discharge to be computed.

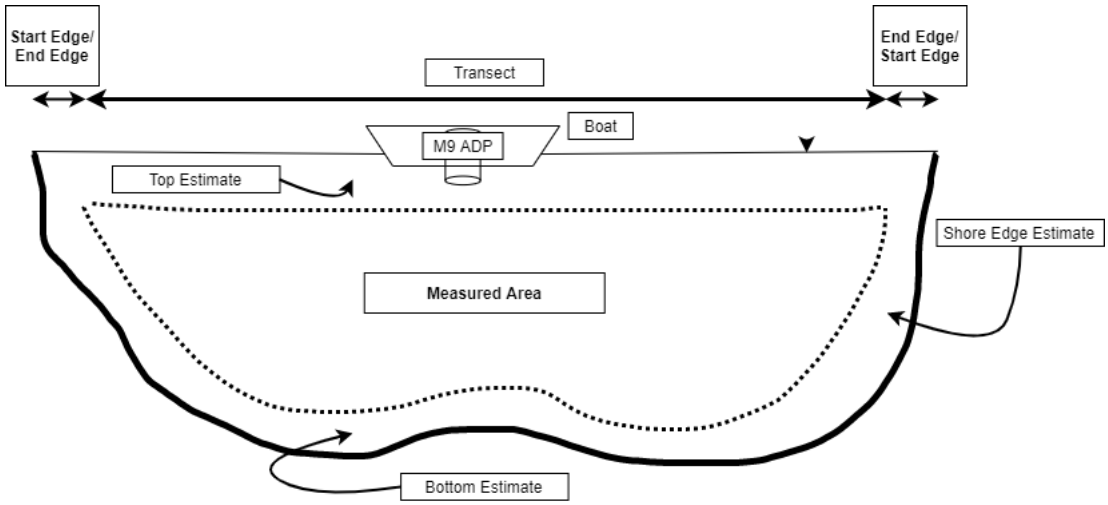

Figure 2.29 – M9 ADCP measure at a River Section

Velocity Profile Extrapolation uses a power-law velocity, see Equation 2.6 profile proposed by Simpson and Oltamann (2004), to calculate velocities above and below the Measured Area.

$$\frac{u}{u_*} = 9.5 \times \left(\frac{z}{z_0}\right)^b \tag{2.6}$$

Where u is the velocity at height z measured from the river bottom, u_* is the bottom shear velocity, z_0 is the bottom roughness height, and b is a constant, equal to 1/6. This equation assumes the current in the profile is traveling in approximately the same direction.

Carrying out the ADCP measurements involved multiple people. For all the evaluate made in the field, at least 3 people were participating. Carrying the equipment, like boat, rope, mounting vast, laptop requires logistics and organization to properly conduct a field data compilation. Also, all measurements were performed right after an LSPIV recorded had happened.

An example of an output from the RiverSurveyor Live for PC software for a measurement execute at the Rodeador Channel at Brazlândia, Federal District in each section from the Region of Interest is presented in Figure 2.30.

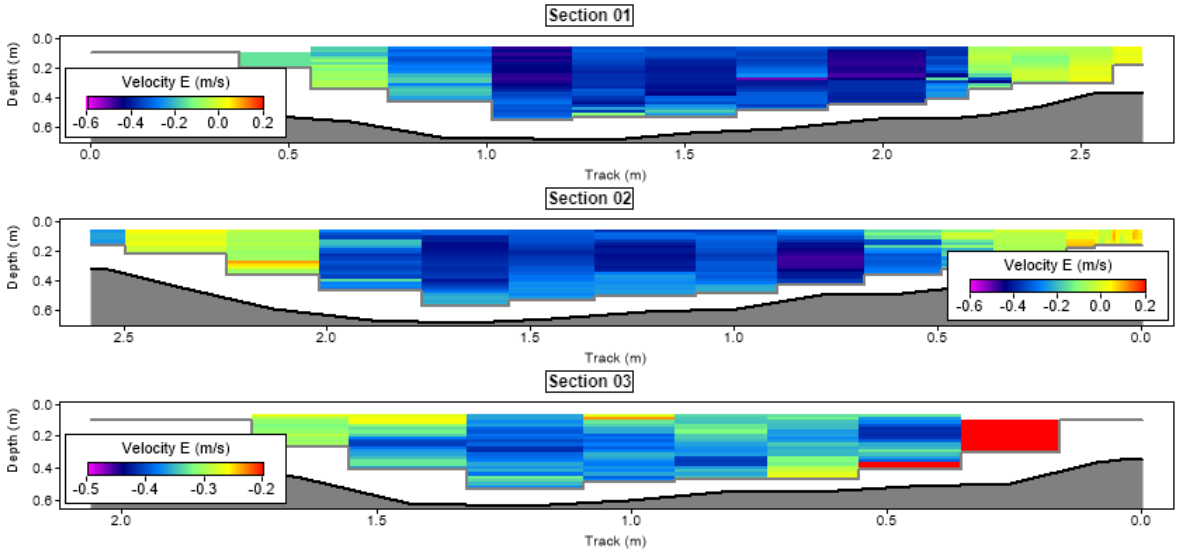

Figure 2.30 – Bathymetry and Velocity profile from the section measured at the Rodeador Channel

2.4 HYDROKINETIC POTENTIAL

This section will bring a brief and summarize explanation on how to measure the energy potential from rivers by knowing their velocities. The main focus of this work is to perform A LSPIV measurement in rivers. However, it also intends to propose a non-intrusive methodology to determine hydrokinetic potential from rivers.

As mentioned before, hydrokinetic energy is defined as associated with the movement of water in rivers, coastal areas, and oceans. Recalling the Equation 1.2, the potential amount of energy is a direct correlate to the velocity that is passing through the turbines. The velocity and depth of rivers is a parameter that allows the dimensioning of the rotor diameter in a

hydrokinetic turbine design [47].

$$P_{hk} = \frac{1}{2} C_p \rho A V^3 \tag{1.2}$$

Also, this potential depends on the C_p which is the machine power coefficient. To a better comprehension about how to utilize this hydrokinetic potential, a direct and summarized explanation of how the velocities decay in a river column and types of hydrokinetic turbines will be present. According to Kumar and Sarkar (2016) and Yuce and Muratoglu (2015), the maximum efficiency that an ideal turbine can attain is known as the Betz limit. Betz's law proposes that the theoretical maximum power coefficient for a rotating turbine in fluid flow is 0.593 [49]. However, according to Vermaak, Kusakana, and Koko (2014), the small turbines in rivers have their own losses, reducing the power coefficient to 0.25.

The velocity profile in rivers and channel decay, see Figure 2.31, in a form that can be calculated by a logarithmic law, see Equation 2.7. Knowing the depth and the bed roughness of the river is possible to calculate the whole profile from the section. Ideally knowing the superficial velocity of the river is possible to calculate the velocity profile for each depth. Equation 2.7 has been consolidated in literature by several authors [51].

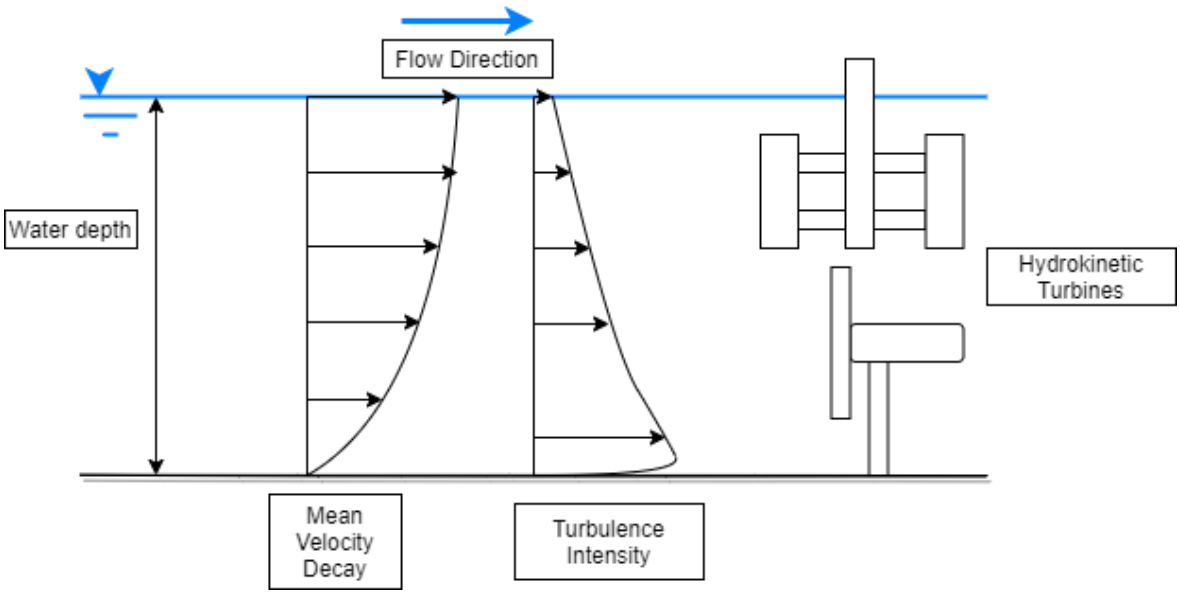

Figure 2.31 – Velocity and turbulence typical behavior at a water column

$$\frac{u}{u_*} = \frac{1}{k} \ln \frac{y}{y_0} \tag{2.7}$$

In Equation 2.7, u is the velocity measured at the normal distance y from the bed, u_* is the shear velocity, y_0 is the boundary distance of the wall and k is the Von-Kárman constant.

The shear velocity is calculated by Equation 2.8 and y_0 is calculated by Equation 2.9.

$$u_* = \sqrt{\frac{\tau_0}{\rho}} \tag{2.8}$$

$$y_0 = k_s e^{kA} \tag{2.9}$$

Where τ_0 is the shear stress limit, ρ is the specific mass of water, k_s is the equivalent sand roughness height of Nikuradse = $2d_{50}$, d_{50} is the diameter of the bed material and A is the integration constant = 8.5 for a fully developed flow [52].

There is also for an uniform equilibrium flows in a wide open channel, the power law that can calculated the velocity profile and can be expressed in the following form, see Equation 2.10.

$$\frac{u}{u_{Max}} = \left(\frac{y}{h}\right)^{\frac{1}{m}} \tag{2.10}$$

Where u is the stream-wise, time-mean flow velocity, u_{max} is the maximum flow velocity taken at the free surface ($y = h$), y is the bed-normal distance measured upwards from the profile datum, h is the flow depth, and $1/m$ is referred as the power-lax exponent or index [53]. In using the power law for the representation of velocity profile measurements, many m-values have been reported in the literature including studies concerning boundary layer, pipe and channel flows. One of well-cited examples is the classical case due to Prandtl, who suggested that the one-seventh power law (m = 7) can be used for turbulent flows over a smooth boundary to approximate the velocity profiles in boundary layer flows for low Reynolds numbers [54].

So for the calculation of the hydrokinetic potential fo the velocities gather by the LSPIV method, the power-law was used and the power-law exponent equal to 7 (m=7) for all the measurements realized. This method was chosen due to simplified and generalize the analysis of the potential for all the fields site and to have an estimation of the watt/meters² that each cross-section evaluation can produce. The mean velocity u that will be assume to calculate the power density for each section will be estimate using the adapt Equation 2.11.

$$u = u_{lspiv}\left(\frac{D/2}{h}\right)^{\frac{1}{7}} \tag{2.11}$$

Where D is equal to the turbine diameter and u and h are the same values previously define. The u_{lspiv} is calculated by gathering the mean values of the superficial velocities that correspond to 75% of the total length of the cross-sectional. Both edges velocities were

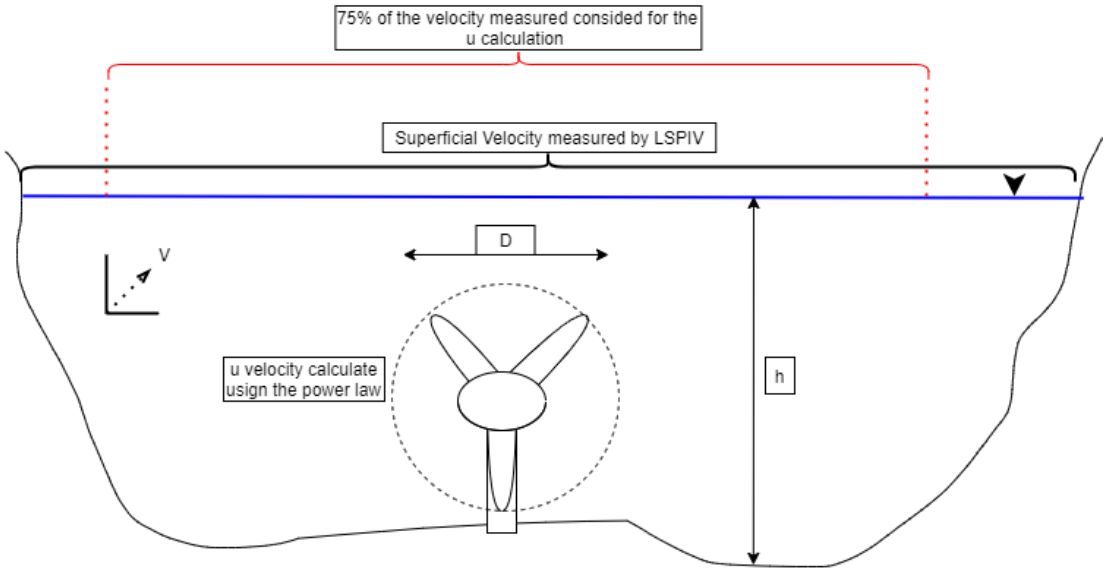

Figure 2.32 – Diagram of the u estimation for the calculation of the hydrokinetic potential

excluded from the analysis due to the impossibility to install a hydrokinetic turbine in the margin of channels and rivers that are too shallow, see Figure 2.32. For each cross-section the diameter of the fictional turbine was calculate based on a simplification that is equal to 2/3 of the maximum depth (h) of the section.

Current energy conversion technologies are a class of marine and hydrokinetic (MHK) technologies that convert the kinetic energy of river, tidal or ocean to generate electricity [34]. To convert kinetic energy to electricity is needed a turbine. There are different forms to characterize a turbine. It can be for the presence or absence of rotor confinement in the fairing. Can be as to the type of axle: horizontal, vertical, or horizontal transverse. Finally can also be for the type of installation: floating, at the bottom, in a pillar, and at bridges or anchors.

The cross-section define could be filled with a set of turbines, in such a way composing a hydrokinetic park that take advantage of the quantified resource. Some important restriction, operational and practical, must be observed [55]:

- For practical reasons, turbines cannot be installed near the banks or close to the bottom, for safety and operation criteria. The minimum distance from a turbine to the bottom and the edges are limited to 1-2D;
- For the assembly of parks, turbine lines must have a distance between axes of 2.3D machines;
- Other lines of machines can compose the arrangement of the park, suggesting a longitudinal distance of the arrangement in 1.5 - 2.0D, for the second line in an offset arrangement. A third line can be foreseen, as long as the energy recovery by the slope of the reservoir allows it;
- Hydrokinetic turbines have adequate operating levels for current velocity greater than 1 m/s. Below this value, the entire process of converting from hydrodynamics to electromechanical systems becomes ineffective;
- Limiting criteria for local navigability and for the safety of the downstream reservoir should be considered in hydrokinetic park projects;

Most of these technologies are still at early stages of development compared to other renewable technologies, such as wind turbines. However, there are already available option in the market of turbines with different sizes and models [56] [57] [58], see Figure 2.33.

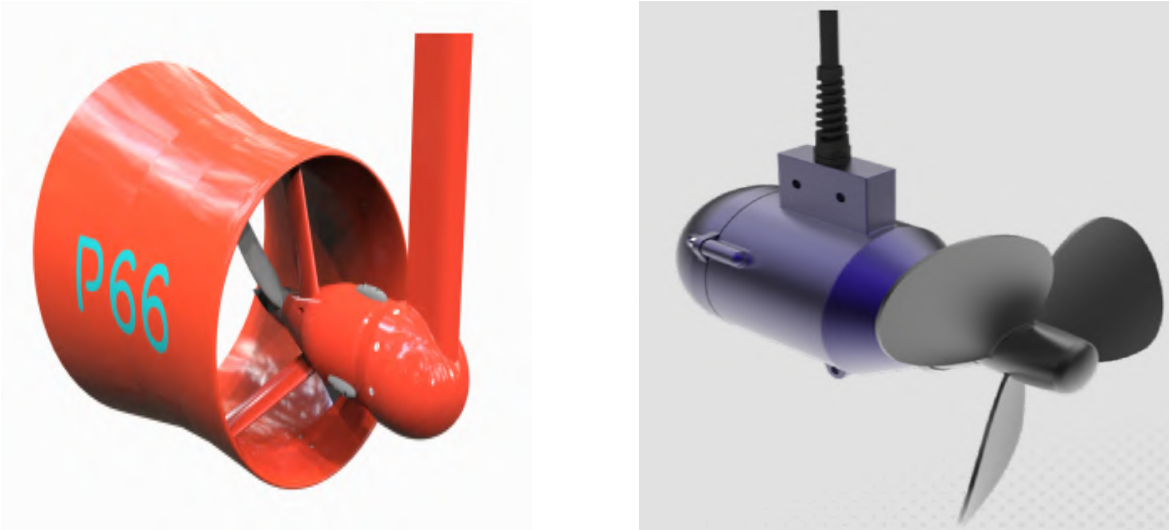

(a) P66 Turbine by [57]

(b) Seamap Aquair Q100 by [58]

Figure 2.33 – Example of hydro turbine available at the market

3 FIELD MEASUREMENTS AND RESULTS

In this chapter, the field experiments conducted with the LSPIV and ADCP techniques will be present. Three sites were explored, with different sizes, discharge, and water use. Two of them are located in Federal District, Brazil's capital. The third is located at Catalão, a city from the state of Goiás.

3.1 RODEADOR CHANNEL

The Rodeador channel where the experiment occurred, is an irrigation channel made between 1966 and 1973, which is located in the administrative region of Brazlândia, a rural zone from Federal District [59]. It's the largest irrigation channel in Federal District, there are 18km of the main channel and 25 km if counting the ramifications. It serves approximately 102 farms of rural producers, who mostly produce vegetables in the form of subsistence agronomy. The channel was created by barring the Rodeador stream, which is the main tributary of the Descoberto Lake, and through a floodgate, see Figure 3.1, regulated by ADASA (Water, Energy and Basic Sanitation Regulatory Agency of the Federal District), the flow pass to the channel.

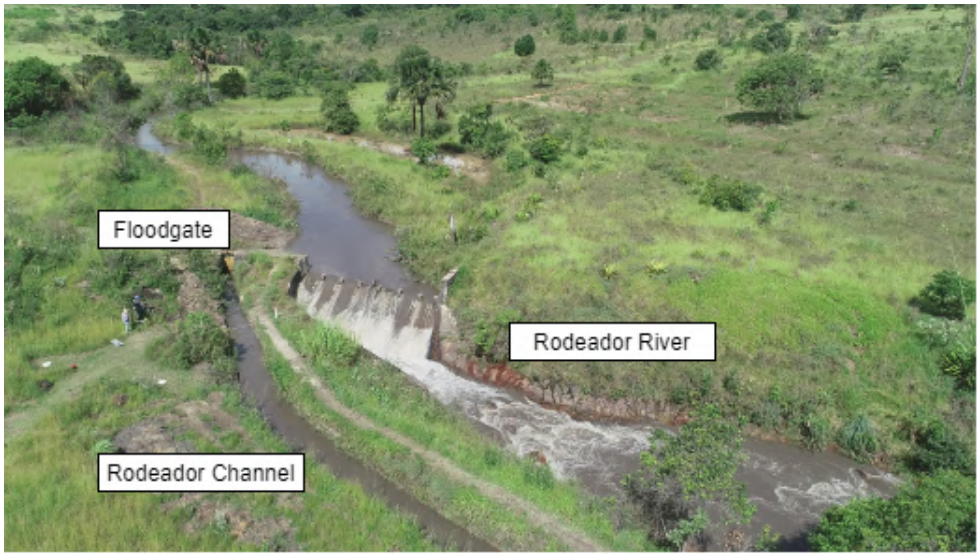

Figure 3.1 – Rodeador site: Drone photo from the Rodeador river and channel

Two experiments were conducted at the Rodeador channel. One comparing the measurements made by the M9 with the LSPIV technique, with and without sawdust. The other, by invitation from ADASA, an experiment comparing the LSPIV with their flow measurement

equipment, Flowtracker.

3.1.1 LSPIV & ADCP M9

This experiment was conducted by 3 operators. All of them have been instructed on how to operate the M9 equipment and how the LSPIV works. The first step was to decide the Region of Interest (ROI) that it would execute the experiment at the channel, see Figure 3.2. The region must have easy access from both sides. So is possible to pass the rope that would be carrying the board with the M9. Also with as little vegetation around the water flow as possible to not compromise the LSPIV analysis. The region has approximately three meters wide and has a maximum depth of 0.6 meters.

Figure 3.2 – Setting up the measurement area

The second step was to take off the drone, taking the necessary security procedure, and stabilize it on top of the ROI. Two ground control points were spread in the field, so it could act as a calibration after. The Drone was flying at an altitude of 8 meters above ground level. This altitude was set because was a height that the drone's propellers did not interfere in the water motion.

Two records were made, both 30 seconds long. One adding a natural tracer to the channel, see Figure 3.3 (a) and the other without, see Figure 3.3 (b). The second record only started after all the natural tracer has gone. The natural tracer added to the channel was sawdust, which is biodegradable, and won't cause any problem in the water quality. Its dispersion tried to be as heterogeneous as possible, with one person on each side of the channel throwing randomly to the water flow.

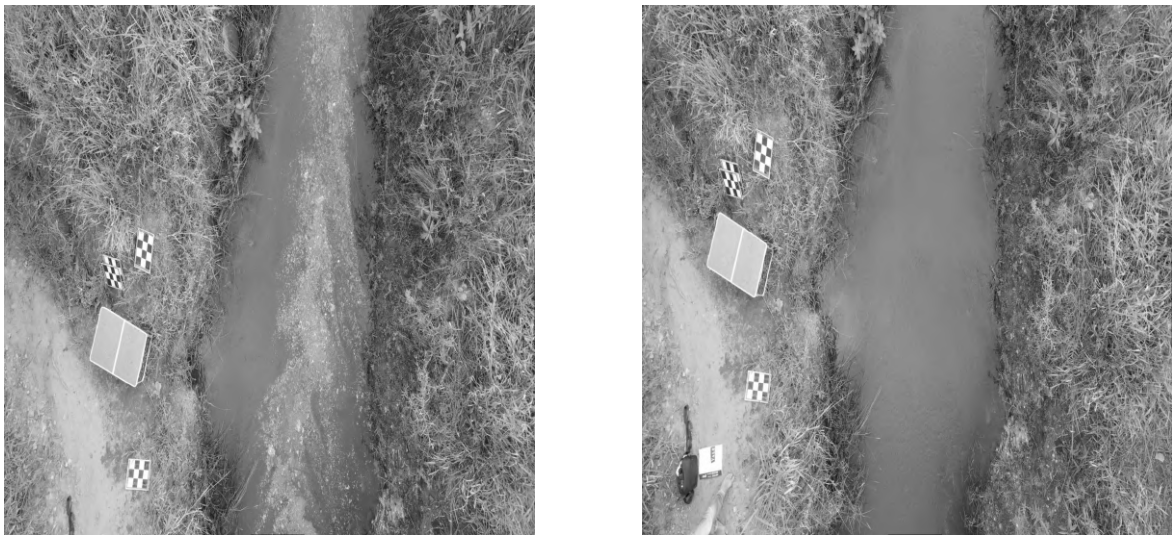

(a) Rodeador Channel with sawdust (b) Rodeador Channel without sawdust

Figure 3.3 – Images extract from the videos made at the Rodeador Channel

Then with the videos recorded, the rope was pass and the M9 board was inserted in the channel. Three cross-sections inside the ROI were measured. In each section, the M9 repeats the act four times. Doing all the procedures list in the Methodology chapter. Starting Edge, then the Transect, and finally the End Edge.

With all the measures and bathymetry from each section complete. The next step was to extract the frames from the videos, apply the LSPIV technique, and finally compare them with the M9 results. The extraction happened at the same section where the M9 passed through, see Figure 3.4.

Following the methodology, procedure to extract the frames from the videos and to process them with the RIVeR and PIVLab tools. All this data were treated using a programming language named Python. Now the results from this treatment are presented. Each blue line in Figure 3.5 (b,c,d) is a extraction of superficial velocity vector extract from the LSPIV analyse. A total of 600 frames were analyzed in sequence, so 600 files gathering 600 velocity information from each section were pull off at each evaluation. The extraction gathers velocity information point to point through that line. The ΔS from each point extract is $0.005m$.

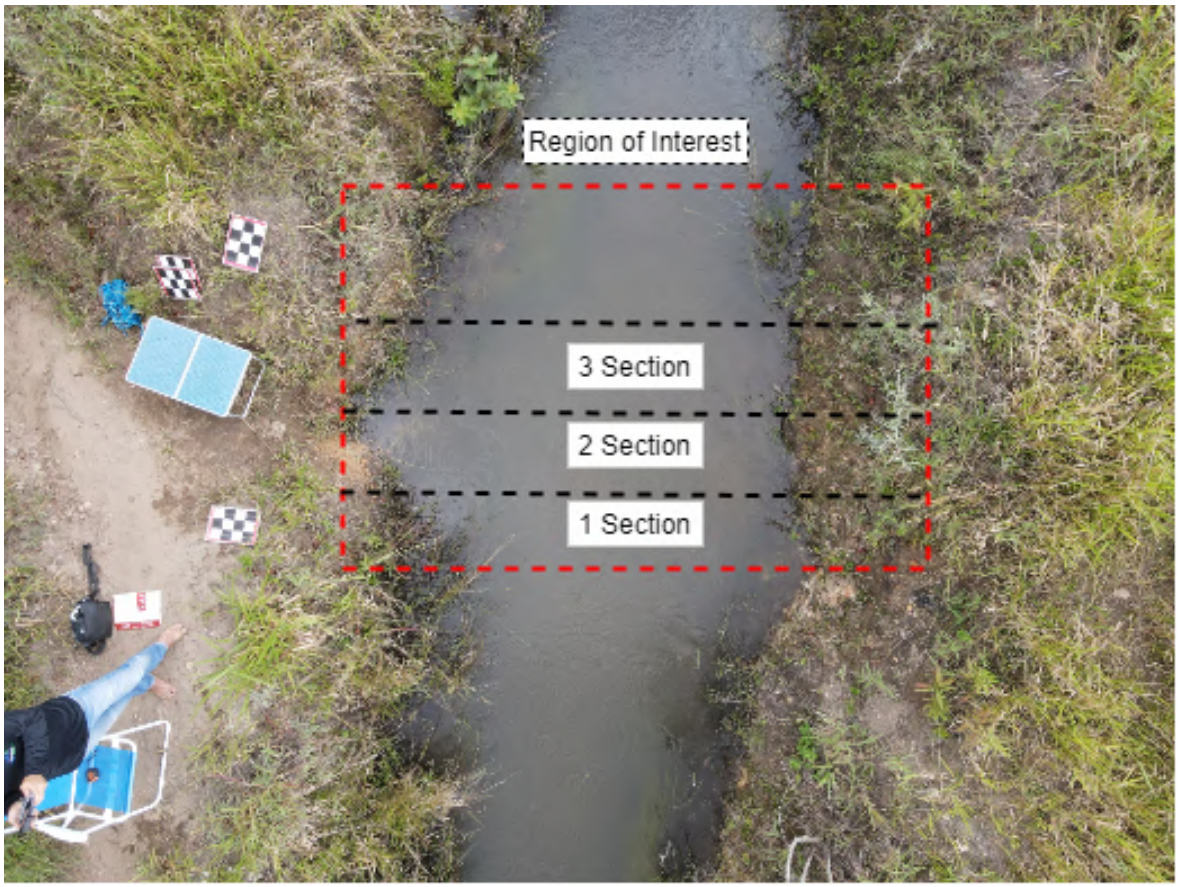

Figure 3.4 – ROI and each section analyse from it

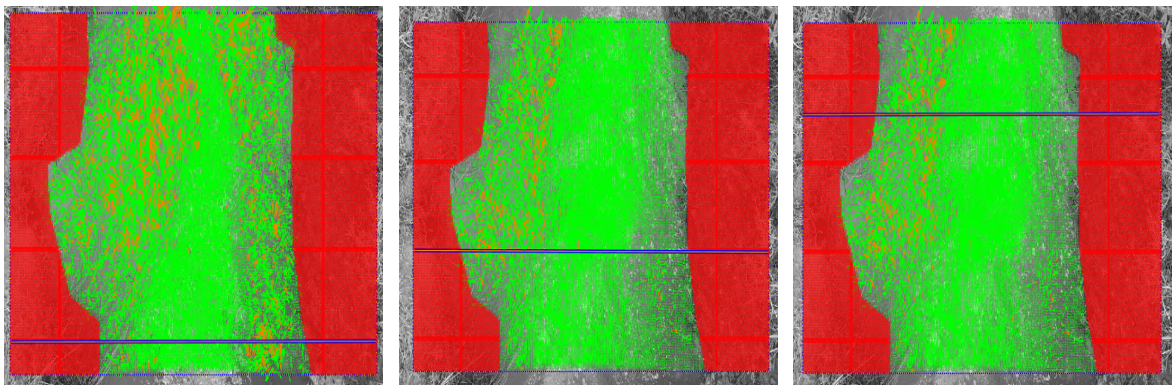

(a) First section (b) Second Section (c) Third Section

Figure 3.5 – Section define and Velocity vector field from LSPIV analyse

A histogram, Figure 3.6 (a) and a boxplot, Figure 3.6 (b), from section one is plot to better understand of the velocity distribution and behavior through the section. Each point extract from the section has 600 velocity information obtained from the LSPIV. The boxplot graph represents all this data gathered in one graph through the section.

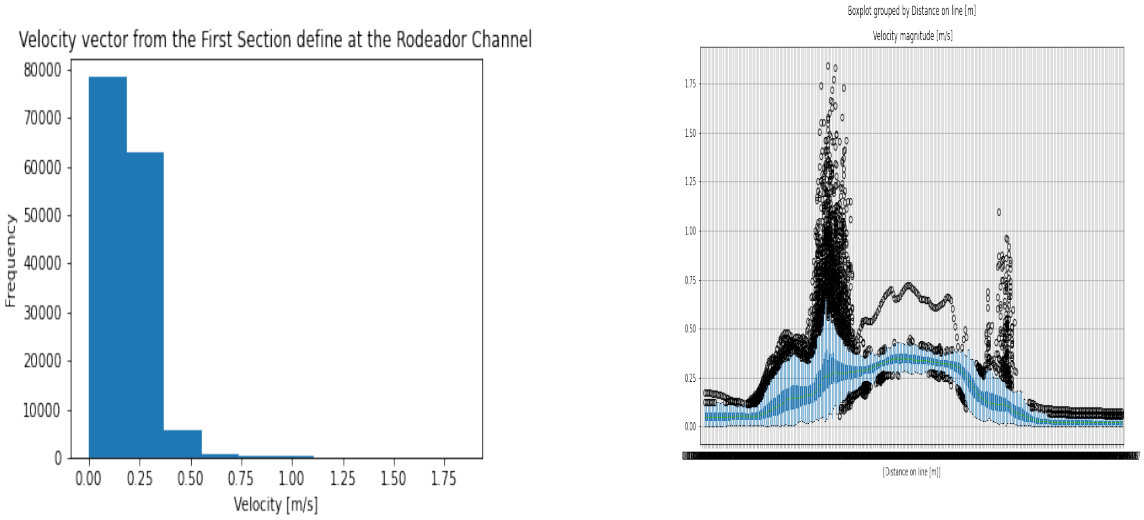

(a) (b)

Figure 3.6 – Histogram and Boxplot from section one with sawdust

To ensure our sample of 600 analyzed frames is representative, a convergence test of the mean and the standard deviation was performed for each section, see Figure 3.7. This convergence test was calculated using Equations 3.1

$$\sum_{N}\left(\frac{\bar{U}_N - \bar{U}_{N-1}}{N}\right) \text{ and } \sum_{N}\left(\frac{\sigma_N - \sigma_{N-1}}{N}\right) \tag{3.1}$$

Here $\bar{U}, \sigma$ and N represents the velocity mean, the standard deviation and the sample size respectively.

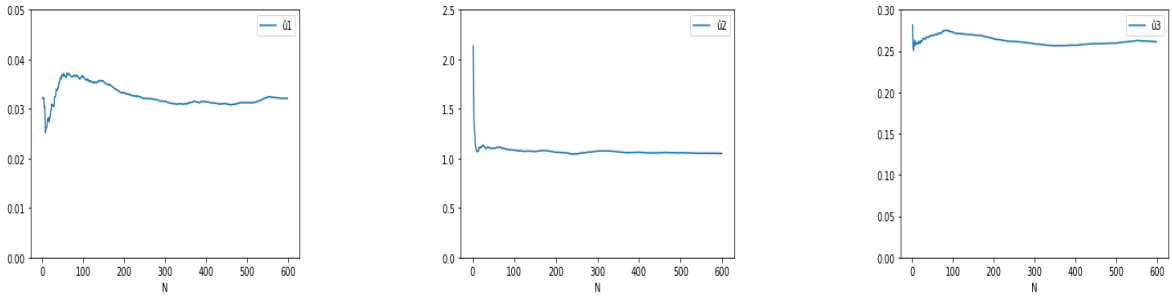

(a) (b) (c)

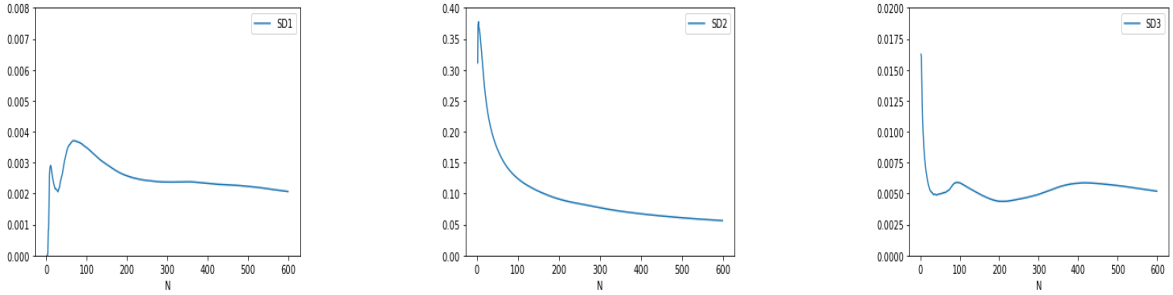

(d) (e) (f)

Figure 3.7 – Convergence test from the mean and the Standard Deviation from the velocity vector measure from the Rodeador Channel adding sawdust

With our sample being representative the next step is to analyze the mean velocity from each point. First, the result from the channel with sawdust added will be present, then the results without, and finally the results from the ADCP.

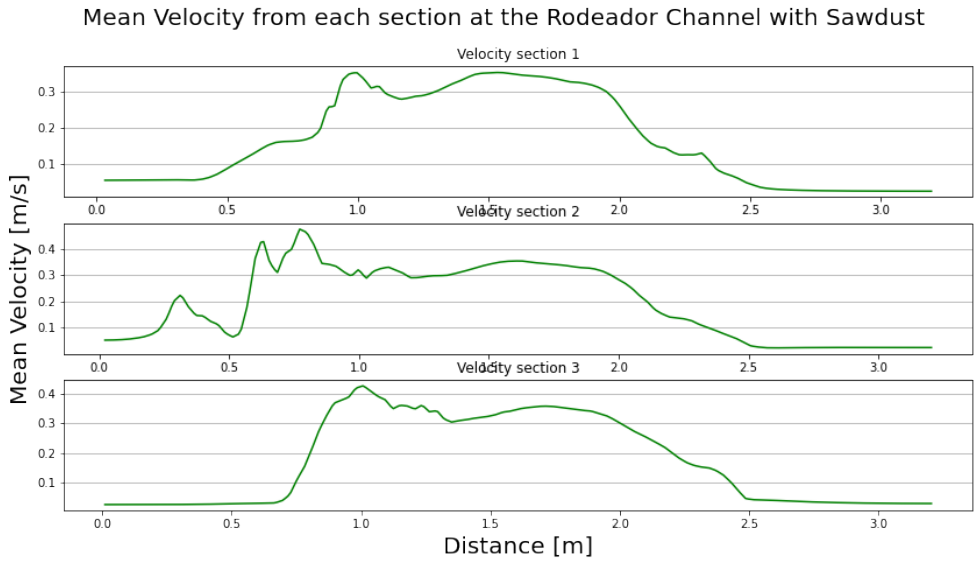

Figure 3.8 – Mean velocity from Rodeador Channel with sawdust

The behavior of the line from Figure 3.8 is expected. Normally rivers and channels are faster in the middle and slower in the edge, basically because of the friction with the wall.

Now the mean velocity from each section extract with the LSPIV without adding sawdust is present, see Figure 3.9.

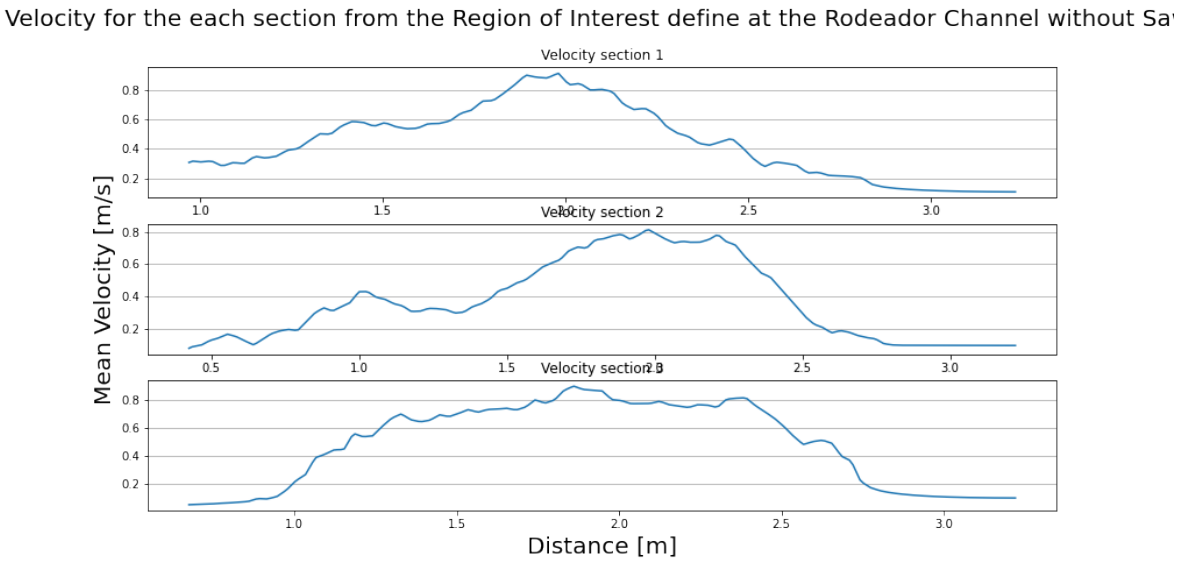

Figure 3.9 – Mean velocity from Rodeador Channel without sawdust

All sections from the channel, with and without sawdust, have the same line behavior but the magnitude of the velocity almost doubled between methods. Now with the ADCP results, see Figure 3.10, to serve as a parameter it will clarify if the sawdust added to the river improves the LSPIV technique.

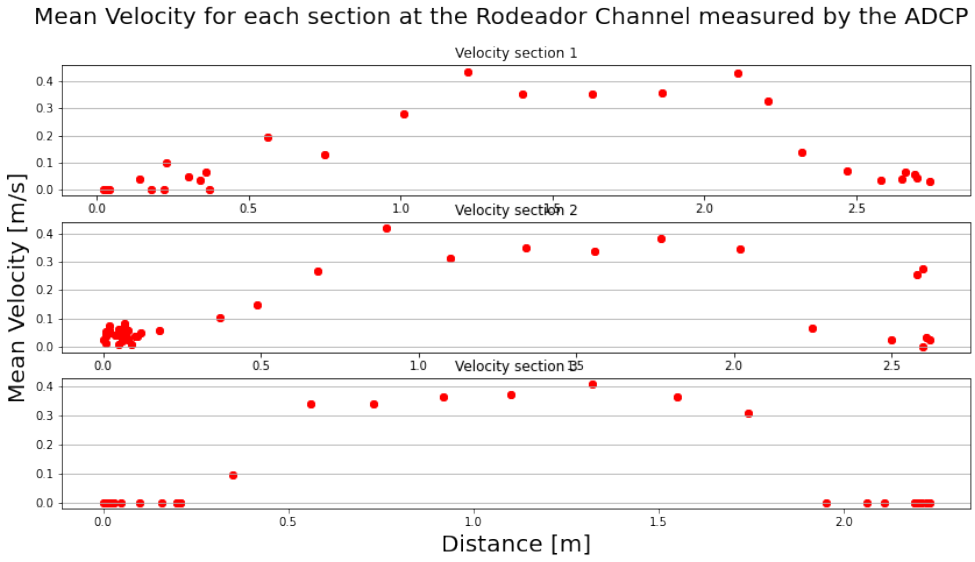

Figure 3.10 – ADCP M9 Results from Rodeador Channel

Each red dot from Figure 3.10 represents the mean velocity from the water column that the equipment measured. The presence of more red dots at the edges is part of the measure

standard procedure requires from the equipment to achieve good data.

The complete data extract from the M9 equipment is present in Figure 3.11. Here the velocity profile from all the sections is showed and also the bathymetry from each section of the channel.

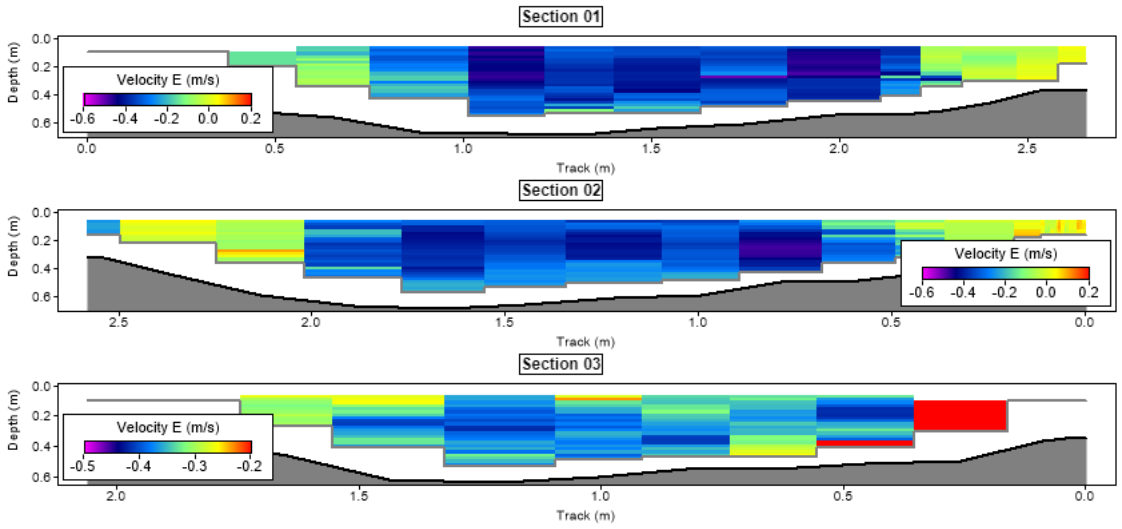

Figure 3.11 – Bathymetry and Velocity profile from Rodeador Channel

To a better visualization of the results, each method is overlaid in Figure 3.12 at each section.

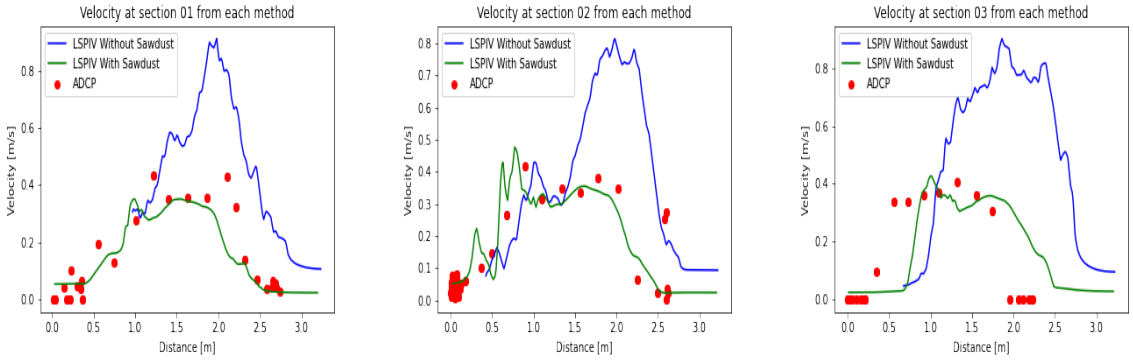

(a) (b) (c)

Figure 3.12 – Velocity extraction from each section overlap to comparison

It's clear from Figure 3.12 that the LSPIV method with sawdust achieves similar results with the ADCP M9. The mean velocity from each section is present in Figure 3.13 (a). Also using the area section calculate with the M9 the discharge from each section was calculate and compare, see Figure 3.13 (b).

The final analysis is the power density for each section between the methods. As mentioned early the diameter of the fictional turbine is equal to $2/3$ of the maximum depth of the

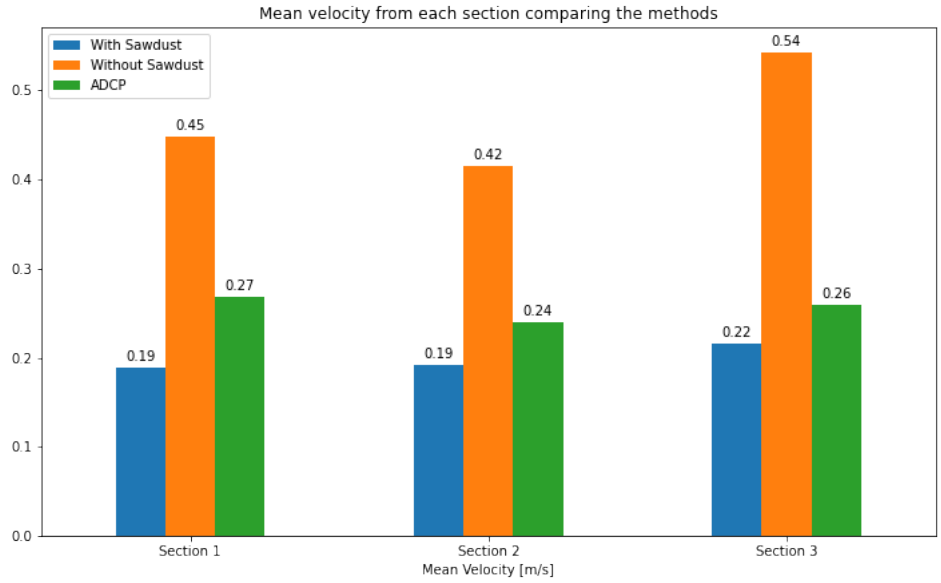

(a) Velocity mean

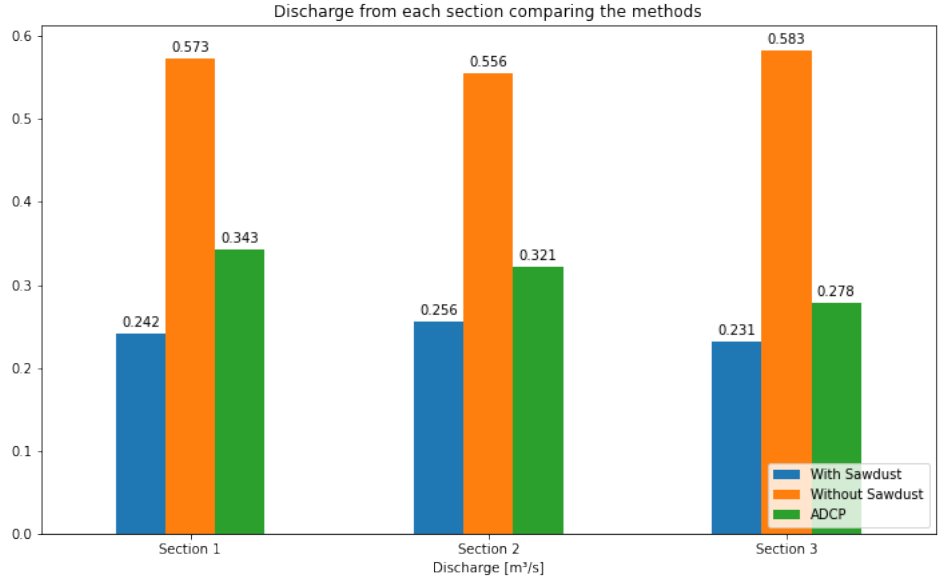

(b) Discharge

Figure 3.13 – Velocity and Discharge from each section comparing the method at the Rodeador Channel

Rodeador Channel				
Method	Section	Max. Depth	Diameter	u Power law
LSPIV with sawdust	1	0.600	0.400	0.277
	2	0.600	0.400	0.275
	3	0.600	0.400	0.296
LSPIV without sawdust	1	0.600	0.400	0.513
	2	0.600	0.400	0.590
	3	0.600	0.400	0.655
ADCP	1	0.600	0.400	0.270
	2	0.600	0.400	0.240
	3	0.600	0.400	0.260

Table 3.1 – Specification for the power density calculation at the Rodeador Channel

section and the local velocity at the turbine was calculate with the power law, see Equation 2.10. Table 3.1 present the value for each section at the Rodeador channel that were used to estimate the power density e_{hk}.

The total power density calculate in W/m² for each section is presented in Figure 3.14.

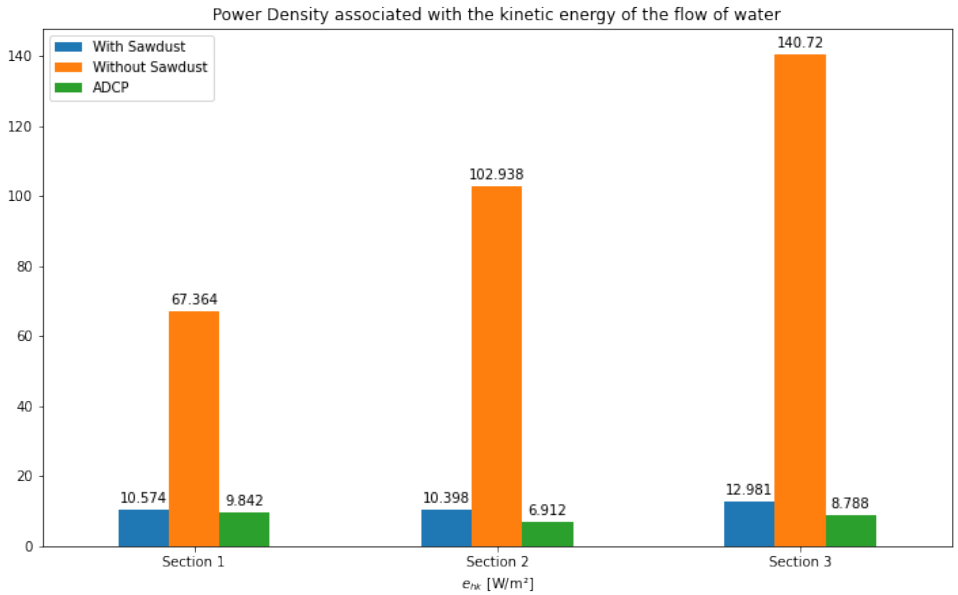

Figure 3.14 – Power density e_{hk} for the Rodeador Channel

3.1.2 LSPIV & ADV Flowtracker

Another field measurement was performed at the Rodeador channel. It's ADASA's responsibility to ensure that the Channel Discharge is respecting the endowment given by them. So every mouth an inspection team measures the discharge with an ADV (Acoustic Doppler Velocimeter) equipment, the Flowtracker.

The LSPIV method was applied with two different cameras. One fixed camera, GoPro Hero 3, positioned beside the channel and a Drone, DJI Phantom 4. More details about, how the ADV works and how the orthorectification from the images of the fixed camera performed can be found at [46]. Here only the main results will be present, to illustrate the work and to maximize the discussion if adding a natural tracer improves the LSPIV analysis.

Two measures were performed with the Flowtracker, see Figures 3.15 and 3.16. This happened because the floodgate that controls the flow, needed to release more flow to comply with the endowment.

So in each measure, two records were made, one from the fixed camera and the other from the drone. Also from each record, two videos were extracted from each camera. One with sawdust and the other without.

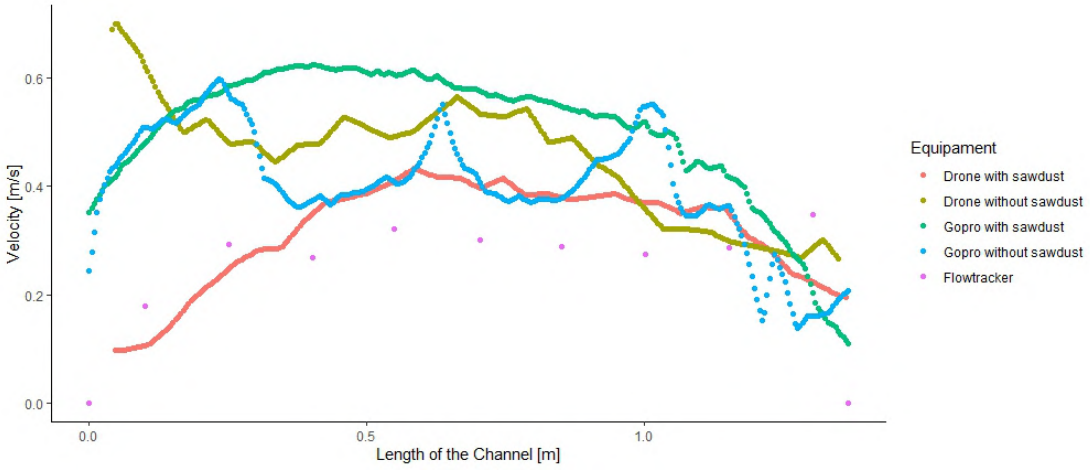

Figure 3.15 – Velocity through the Rodeador Channel from the first measurement

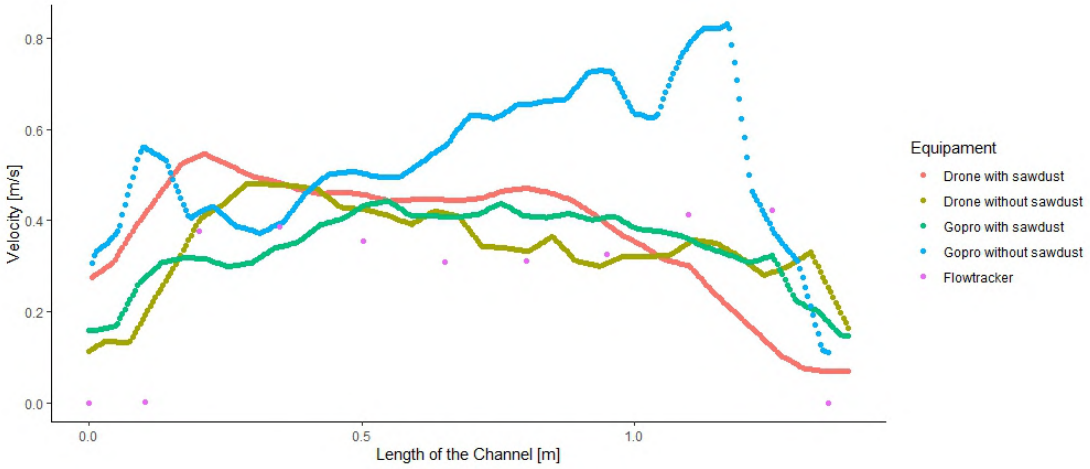

Figure 3.16 – Velocity through the Rodeador Channel from the second measurement

The flowtracker make an estimation of the area from the section. From that the discharge from each measurement was calculate and compare, see Figures 3.17 and 3.18.

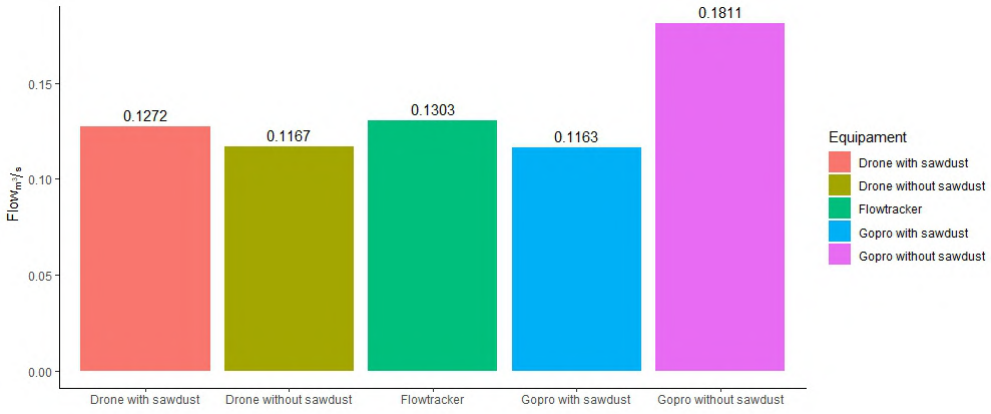

Figure 3.17 – Discharge through the Rodeador Channel from each method

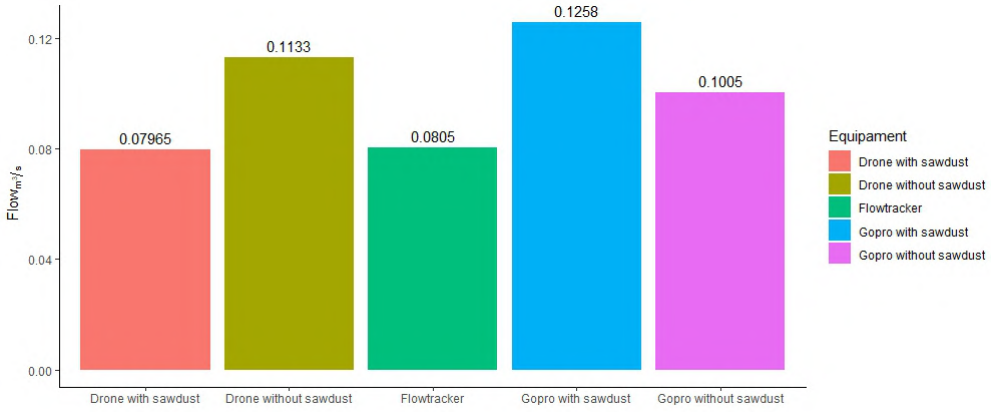

Figure 3.18 – Discharge through the Rodeador Channel from each method

This experiment results in two papers present in the 18th Brazilian Congress of Thermal Sciences and Engineering (ENCIT 2020) and XV Simpósio de Recursos Hídricos do Nordeste (SRHINE 2020), in both articles, can be found more information and detail of the experiment went through.

3.2 RODEADOR RIVER

The experiment was conducted at the Rodeador River, which is located in the Federal District, capital of Brazil. The River is in the administrative region of Brazlândia, a predominantly rural region. The Rodeador River is the main tributary of the Descoberto reservoir, the primary water reservoir in the Federal District.

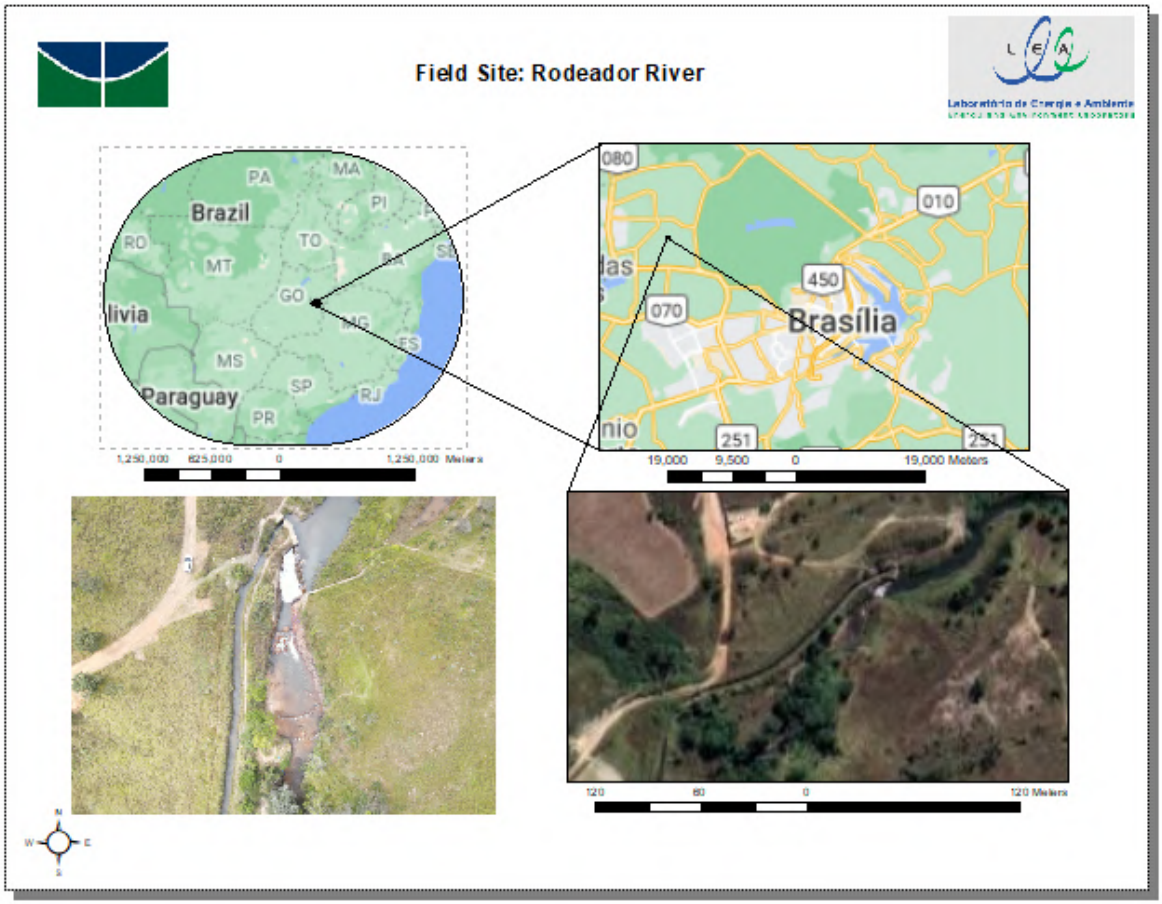

Figure 3.19 – Location site

The same board design to carry the M9 equipment used at the Rodeador Channel, was used to traveled through a Region of Interest to collect information on both the river's bathymetry and velocity profiles, see Figure 3.20. With this information gathered the flow of the river was calculate and compared with the flow measured by the LSPIV.

Figure 3.20 – ROI from the Rodeador River

The drone took off in a flat region away from any type of vegetation and was manually driven to the area of interest, previously measured by the M9 sensor. It was positioned 6 meters above the water level and with its camera positioned orthogonally to the direction of the river's flow. Sawdust was added to the flow to work as a natural tracer.

The M9 Sensor collected data from the region of interest determined, see Figure 3.20. From this area three cross-sections were extracted from the LSPIV method, see Figure 3.21, and from the ADCP equipment to compare the velocity and discharge results that were obtained, which are represented by the dashed lines.

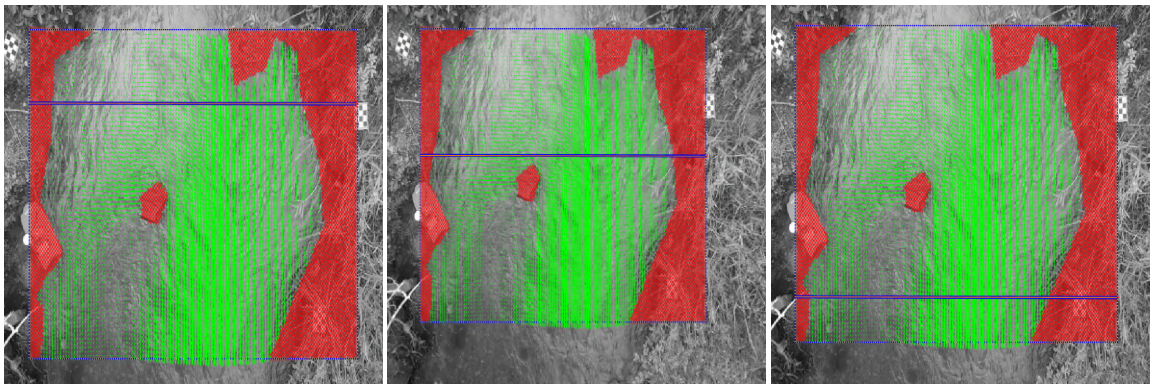

(a) Velocity vector section 1 (b) Velocity vector section 2 (c) Velocity vector section 3

Figure 3.21 – Velocity extraction from each section from the LSPIV method

Some parts of the area analysis were too shallow for the M9 sensor to be able to collect information, therefore some pieces of the section went unmeasured. The bathymetry and the velocity profile from the section are shown in Figure 3.22.

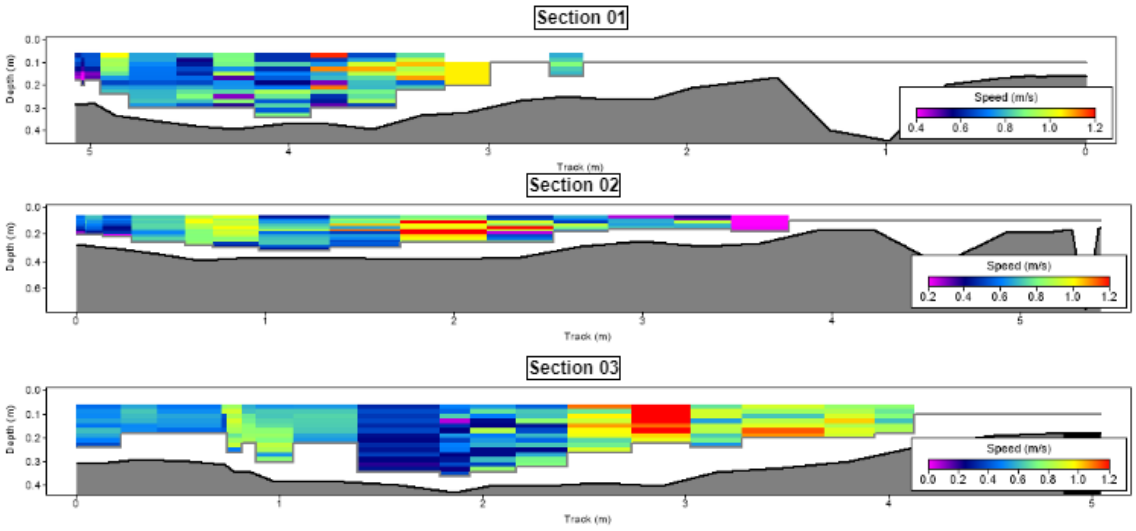

Figure 3.22 – Bathymetry and Velocity profile from the Rodeador River

The analyse from the LSPIV without sawdust is present in Figure 3.23.

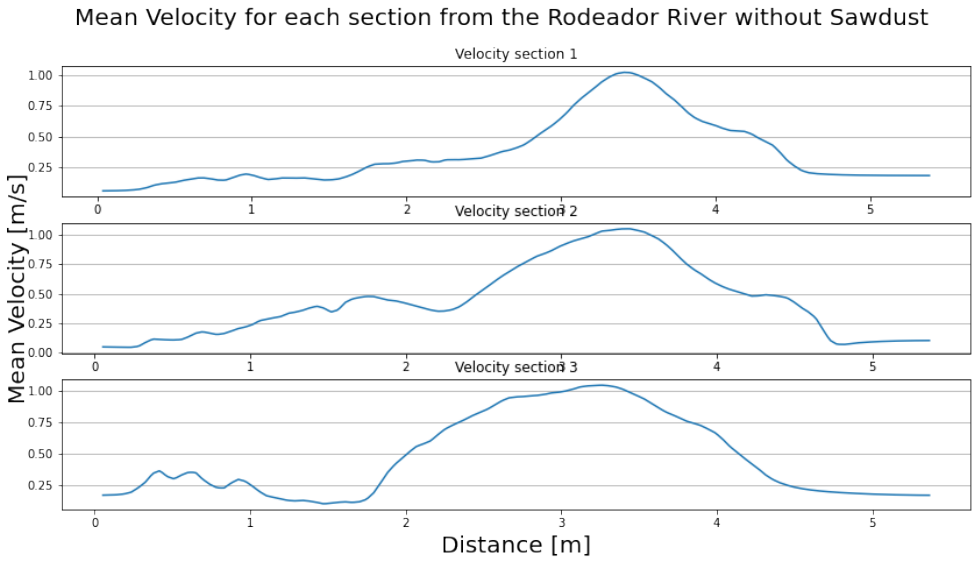

Figure 3.23 – Velocity mean from each section of the Rodeador River

The analyse from the LSPIV with sawdust is present in Figure 3.24.

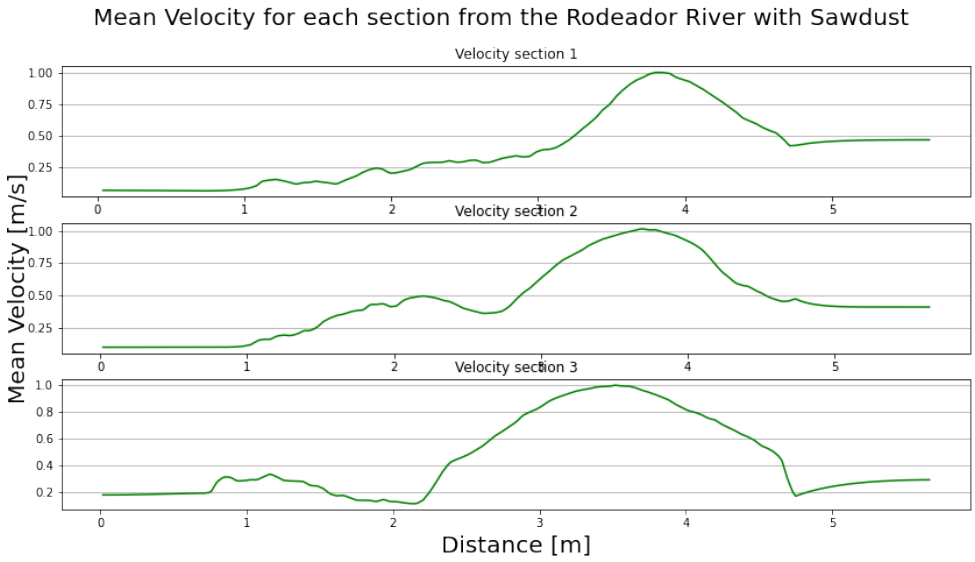

Figure 3.24 – Velocity mean from each section of the Rodeador River with sawdust added

The behavior and the magnitude from the superficial velocity didn't change a lot from the addition of sawdust, see Figure 3.25

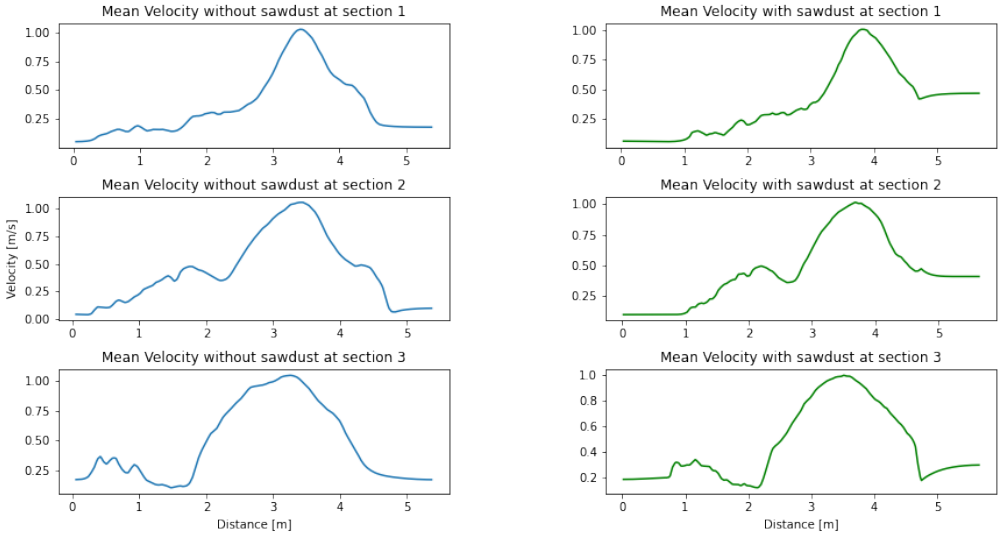

Figure 3.25 – Velocity mean from the LSPIV method comparing the addition of sawdust

Even though it was possible to measure the select site with the M9. The location area did not follow the recommendation for a good place to perform the analysis. The water level was too shallow and the riverbed had a lot of rocks. The ideal place is where the condition of a uniform flow can be applied. The ideal place is away from any sources of flow disturbance so that there is sufficient linear distance for any turbulence, eddies, up-welling, backwater effects to settle out to a uniform, steady flow. The results from the M9 equipment are demonstrated in Figure 3.26.

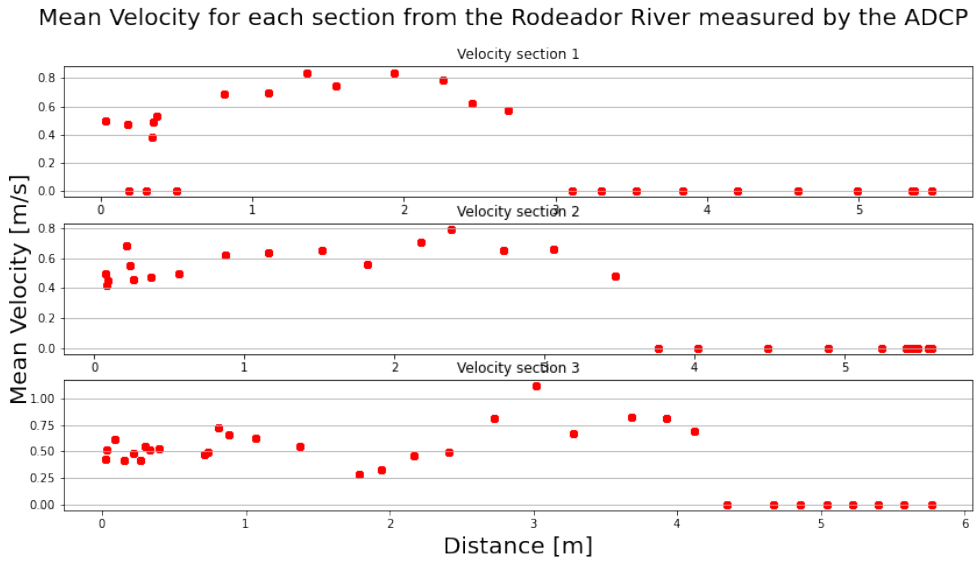

Figure 3.26 – Velocity in each cross section of the Rodeador River

Now all the methods perform at the river are plotted together, see Figure 3.27. Is clear how the M9 results are different from the LSPIV analysis. Upstream from the ROI there was

a small change in level from the river and cause a lot of turbulence. This turbulence causes a foam that worked as a natural tracer that improves the LSPIV analysis that the results with sawdust and without are similar but the shallow water and these non-uniform conditions for the flow interfere in the M9 results.

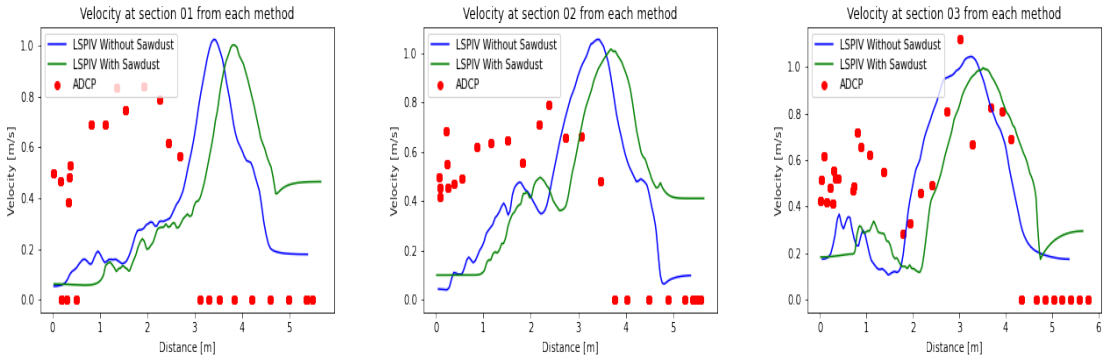

(a) (b) (c)

Figure 3.27 – Velocity extraction from each section overlap to comparison

The mean velocity from each section and method was calculated and plotted to evaluation, see Figure 3.28

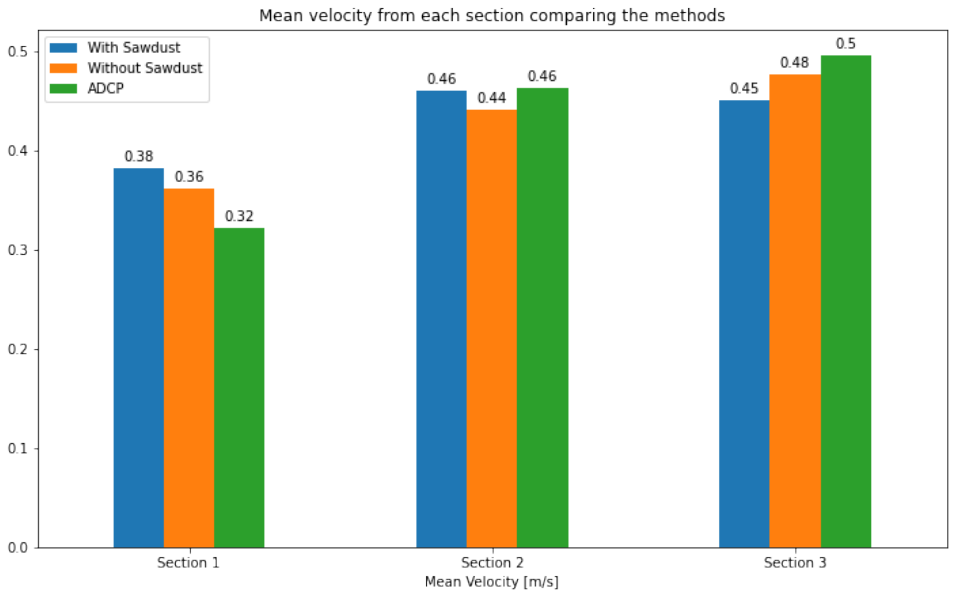

Figure 3.28 – Mean velocity from each section and method

The discharge was calculate using the mean area measured by the M9 sensor, see Figure 3.29. The value from the areas are show below and they units are in m^2, see table 3.2. More information about this experiment can be found at the paper present on the congress COBEM

Rodeador River				
Method	Section	Max. Depth	Diameter	u Power law
LSPIV with sawdust	1	0.4	0.27	0.41
	2	0.6	0.40	0.49
	3	0.4	0.27	0.61
LSPIV without sawdust	1	0.4	0.27	0.45
	2	0.6	0.40	0.54
	3	0.4	0.27	0.68
ADCP	1	0.4	0.27	0.32
	2	0.6	0.40	0.46
	3	0.4	0.27	0.50

Table 3.3 – Specification for the power density calculation at the Rodeador River 2021 [60].

Section 1	Section 2	Section 3
1.568	1.542	1.369

Table 3.2 – Section Areas [m^2]

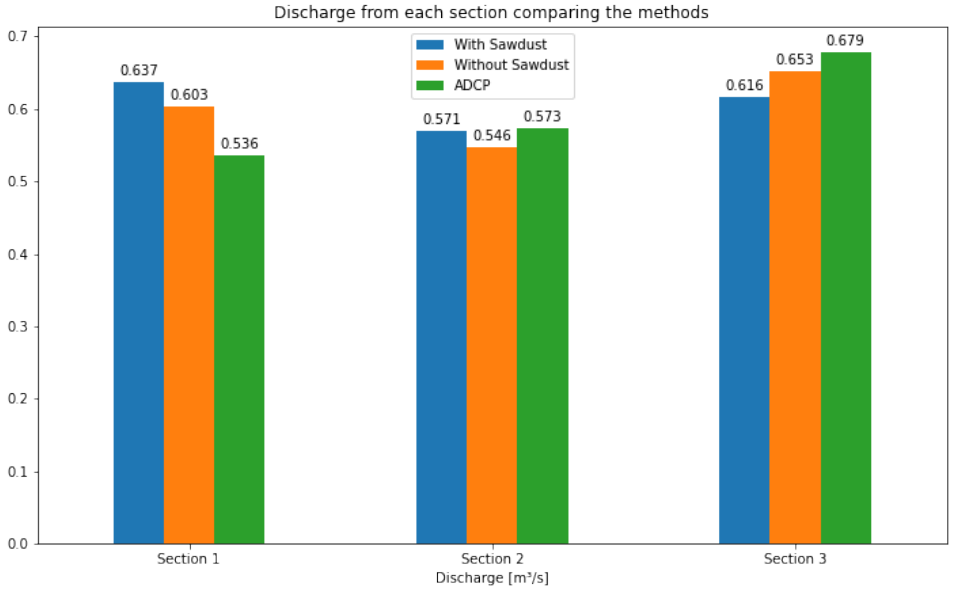

Figure 3.29 – Discharge measured at the Rodeador River

The power density analysis follow the same procedure from the Rodeador channel. The maximun depth for each section was verify with the batymetry measured with the ADCP equipment and the diameter of the turbine was calculate. Then using the power law the u velocity was estimate to finally calculate the e_{hk}, see table 3.3.

The total power density calculate in W/m² for each section is presented in Figure 3.30.

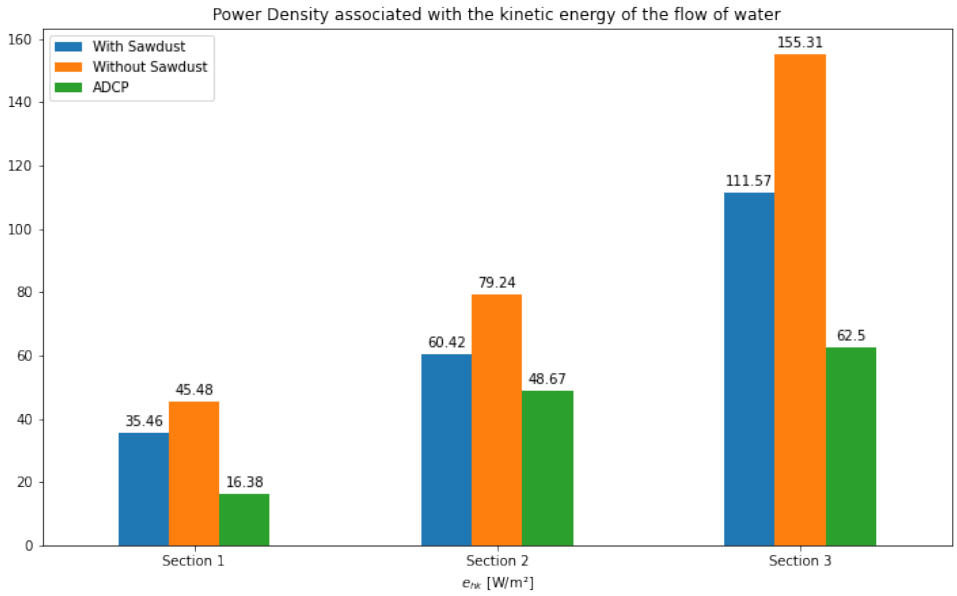

Figure 3.30 – Power density e_{hk} for the Rodeador River

3.3 SÃO MARCOS RIVER

The São Marcos River is located downstream from the Serra do Facão Hydroelectric Power Plant, between the municipalities of Davinópolis and Catalão from the State of Goiás, see Figure 3.31. The Power Plant has an installed capacity of 212.58 MW, enough to supply the energy demand of a city with 1.2 million inhabitants. The construction started in February 2007 and the plant opened in October 2010 [61].

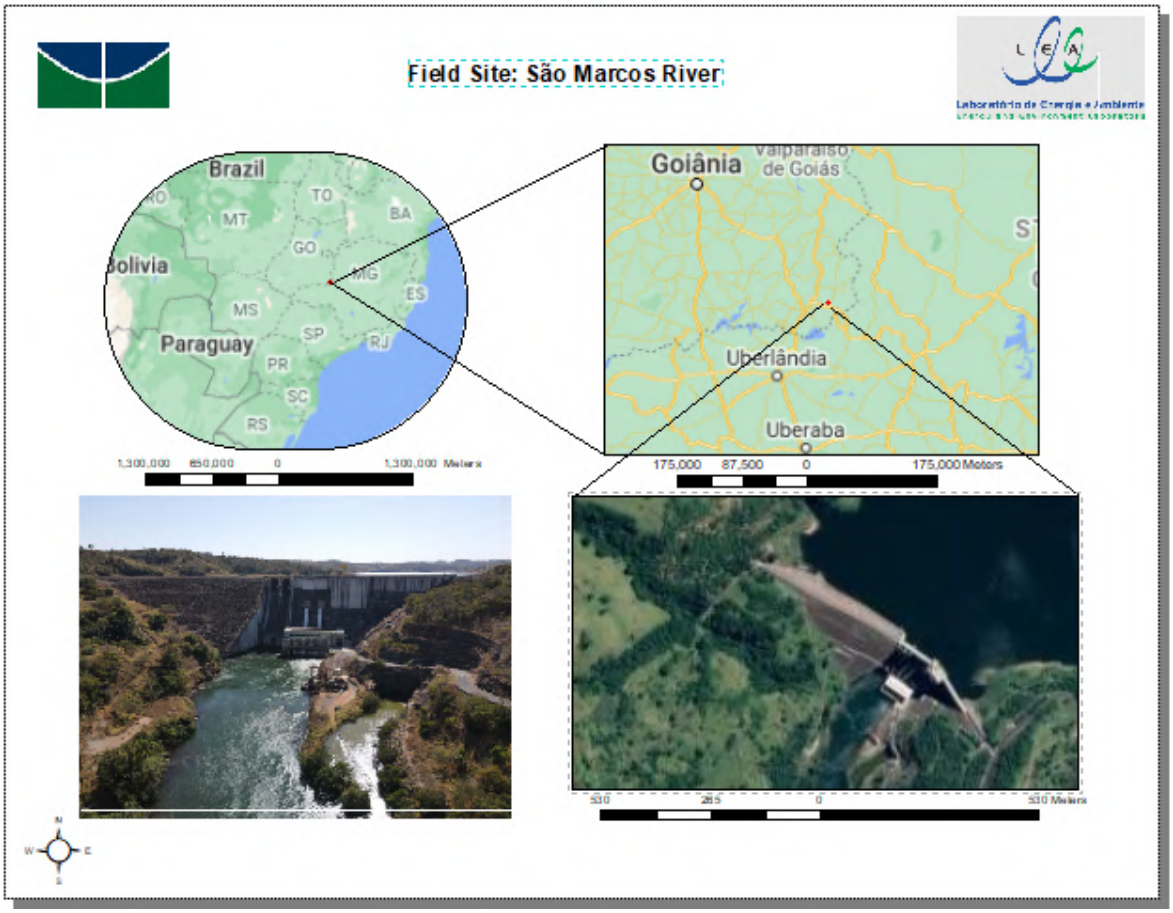

Figure 3.31 – Location site: São Marcos River

In this field experiment, it was not added sawdust to the water flow. However, this measurement in addition to the ADCP measure will also have the plant's discharge value.

The sequence of the data assemblage follows the descriptions explained in the Methodology Chapter. First, the field team mounted the RTK GPS bass, see Figure 3.32(a), then with the support from the crew of the power plant and with a boat the ADCP M9 equipment was able to perform the analysis, see Figure 3.32(b).

(a) RTK GPS Base (b) Crew seeting up the M9 boat

Figure 3.32 – Field preparation to collect the velocity data

The area measured by the M9 and recorded by the drone camera is present in Figure 3.33. The idea of three sections to compare the method was maintain and the results will be present next. The bathymetry and velocity profile collect by the M9 are present in Figure 3.34. The width measure by the M9 is different from the LSPIV technique because the water level was so low at the margin of the river that was not safe to measure with the boat due to the number of rocks that were there.

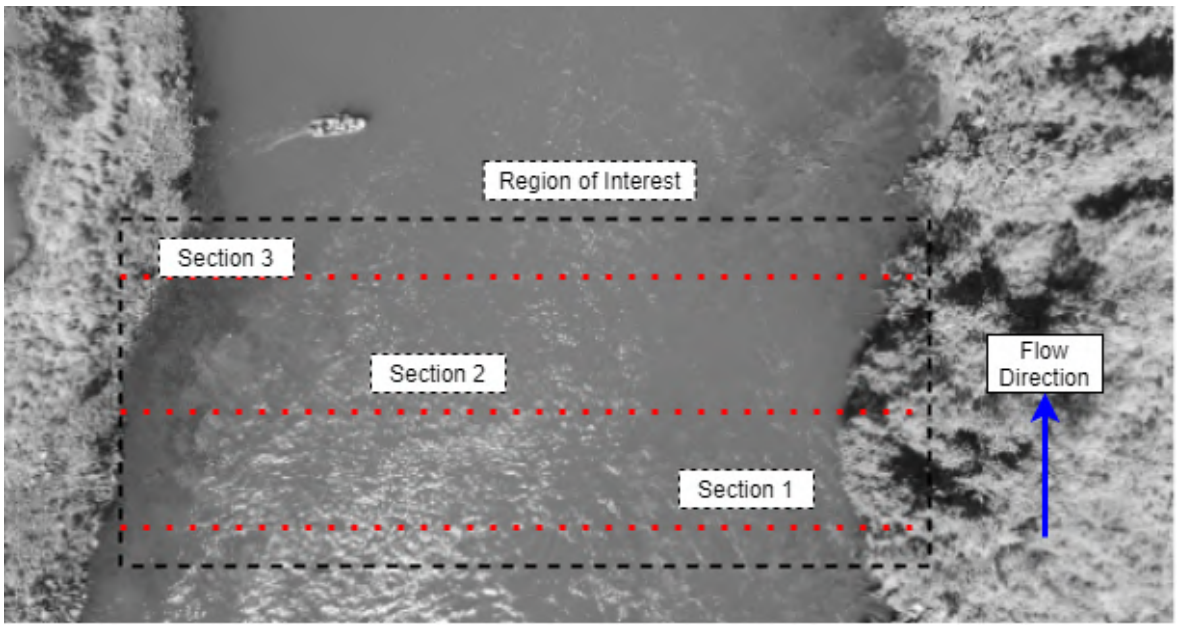

Figure 3.33 – Region on Interest from São Marcos River

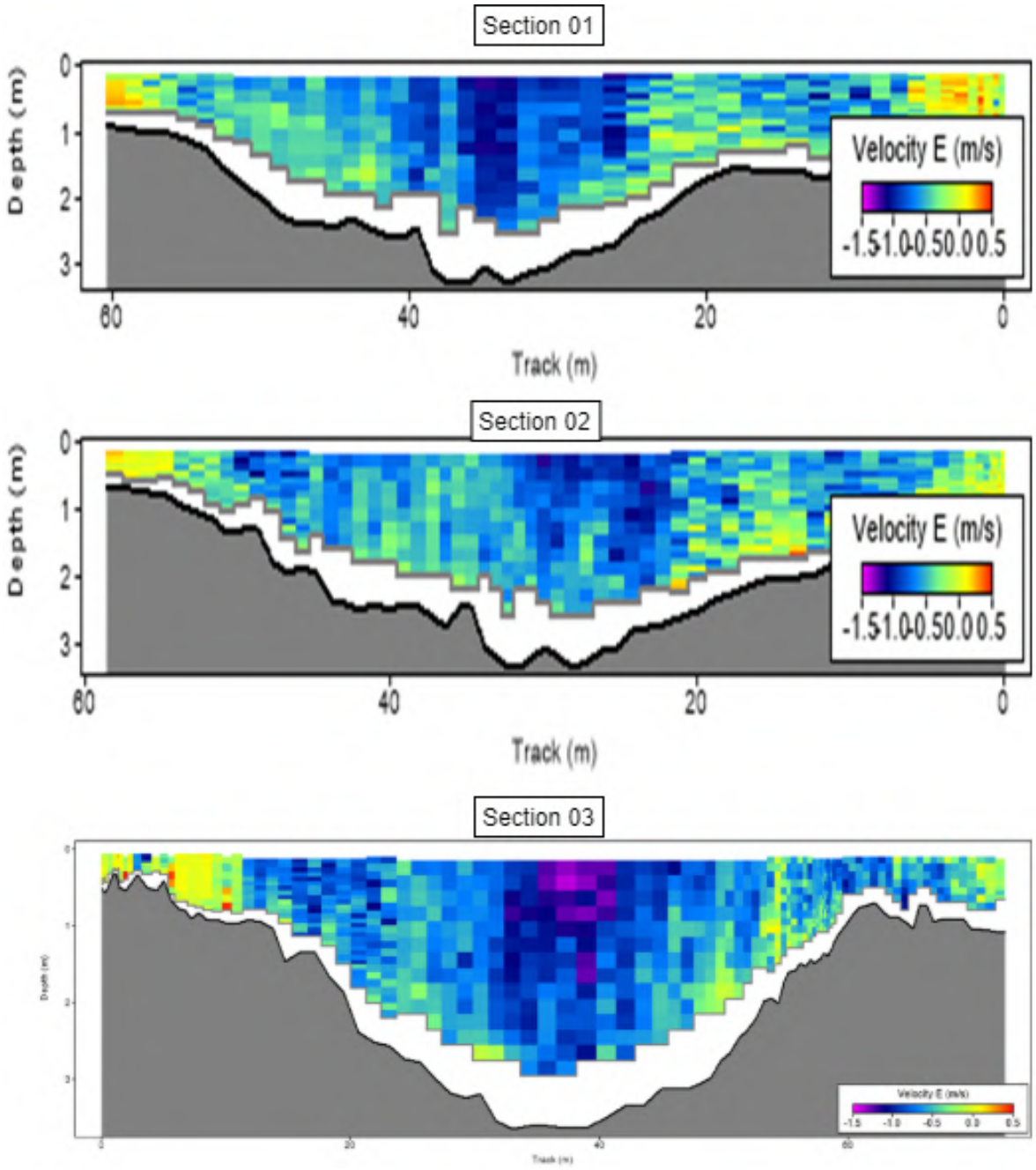

Figure 3.34 – Bathymetry and Velocity profile from the São Marcos River

Three-section were extracted from the vector field and plotted to compare with the M9 results. The superficial velocity vector field measured by the LSPIV technique is shown in Figure 3.35. As mentioned, in this experiment it was not possible to add a tracer to the river, so only a comparison from the LSPIV technique without any added tracer with the ADCP results will be present. The velocity through each cross-section defined is present in Figure 3.36.

The results through the cross-section from each section from the M9 sensor are present in Figure 3.37. As explained previously the M9 couldn't measure all the river sections due

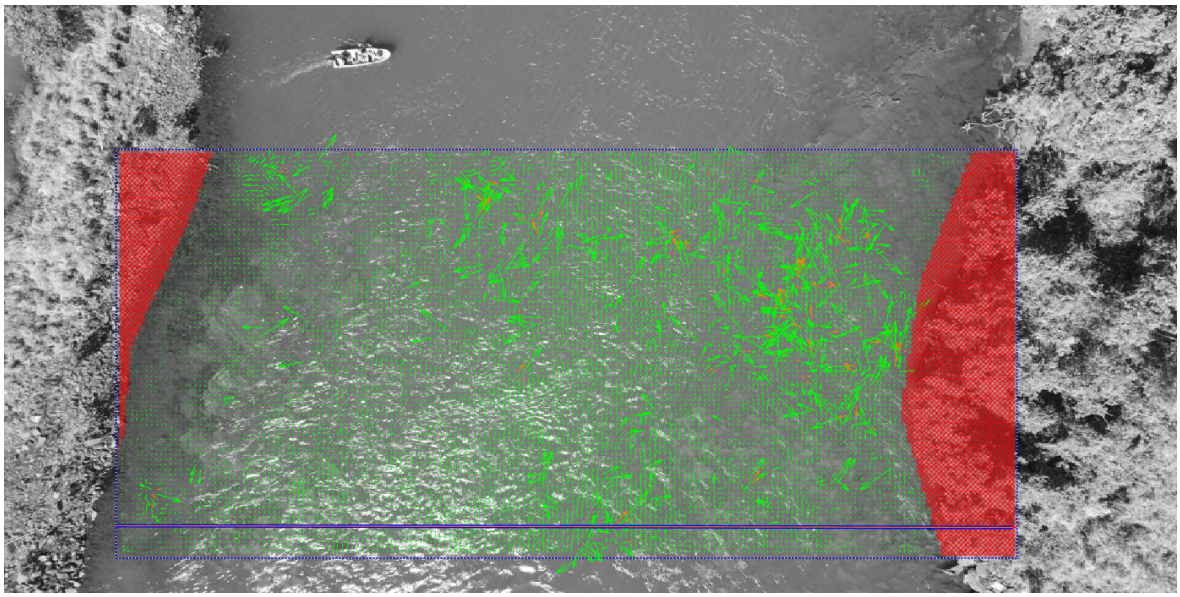

Figure 3.35 – Velocity field from the LSPIV technique

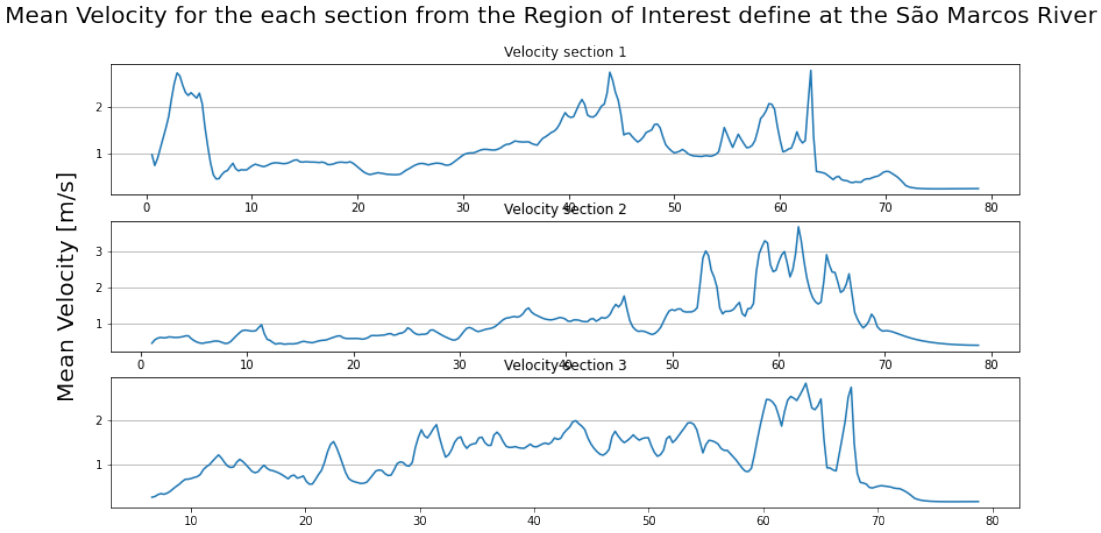

Figure 3.36 – Velocity through each section at the São Marcos River

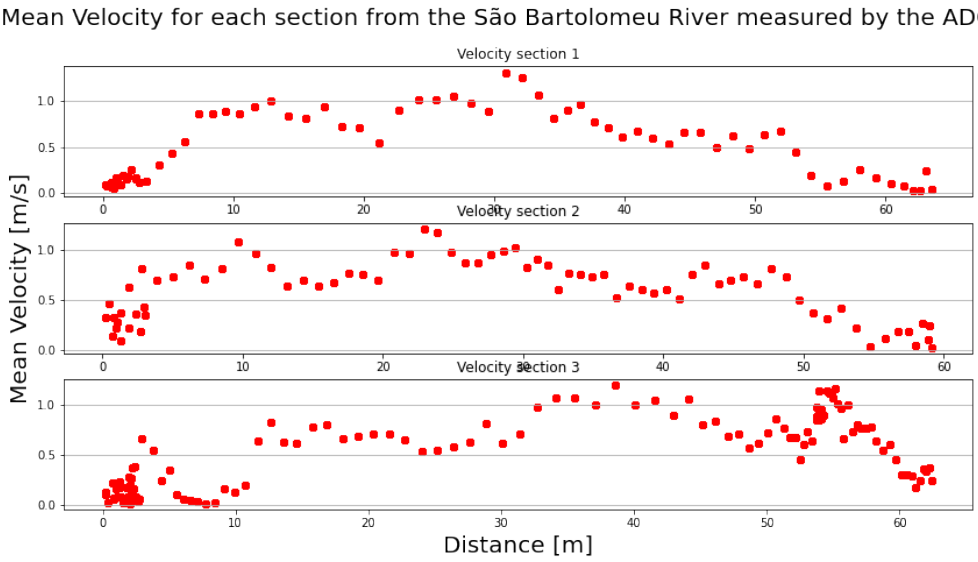

Figure 3.37 – Velocity in each cross-section of the São Marcos River

to the water level to navigate with the boat. It was added to the program manually the total distance that the margin was from the last point measured.

All results were plotted together so it would be easy to visualize the results through each section, see Figure 3.38. The results were not as good as those obtained in other experiments. The size of the river influence the size of the region of interest that was analyzed. Unfortunately, it was not possible to add sawdust to perform an analysis with a natural tracer, which would bring better results compared to the M9. Yet in sections 1 and 3 the velocity behavior from both methods was similar.

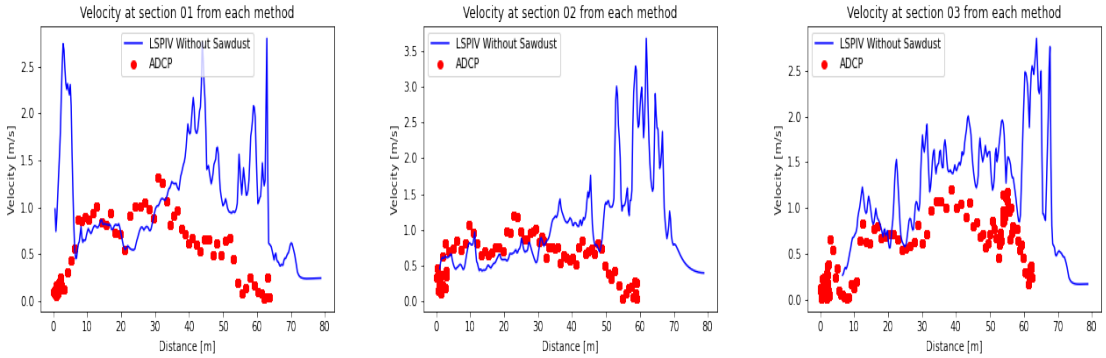

(a) (b) (c)

Figure 3.38 – Velocity extraction from each section overlap to comparison

The mean velocity from each section and method was calculated and plotted to evaluation, see Figure 3.39.

With the bathymetry measure, the area from each section was calculated and is present

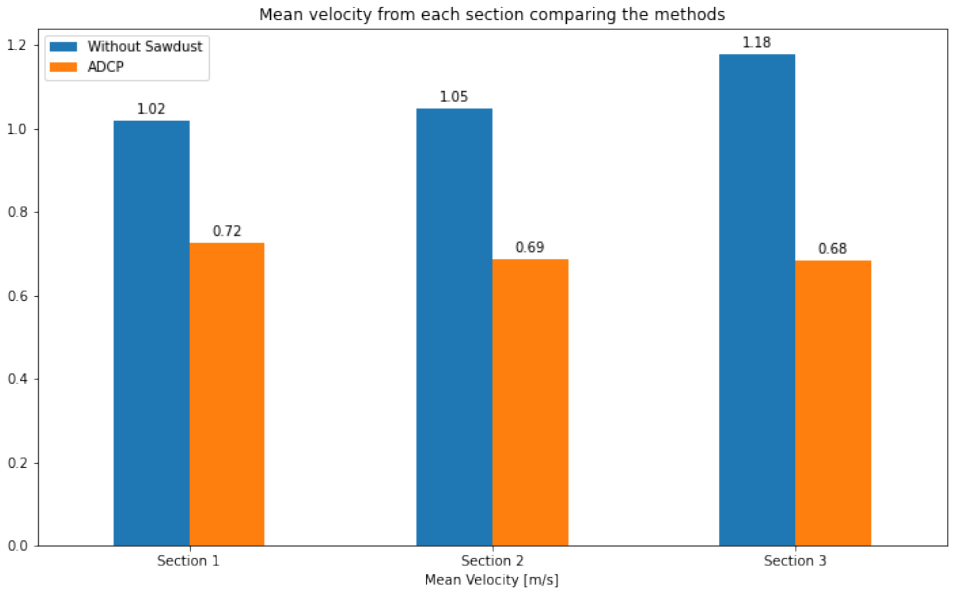

Figure 3.39 – Mean velocity from each section and method

at table 3.4. Using the area and the mean velocity from each section the discharge was calculated. The São Marcos River is downstream of a hydroelectric dam, having the discharge controlled by the turbines operations. So it was possible to compare the discharge measured by the LSPIV and the ADCP with the one from the hydroelectric Sefac, see Figure 3.40. The results obtained from the M9 equipment are remarkable, living up to the reputation of reliable and accurate equipment.

Section 1	Section 2	Section 3
128.96	129.54	129.38

Table 3.4 – Section Areas [m^2]

Finally the power density is estimate using the values presented at table 3.5 and the values for each section are presented in Figure 3.41.

SEFAC				
Method	Section	Max. Depth	Diameter	u Power law
LSPIV without sawdust	1	3	2	0.88
	2	3	2	0.90
	3	3	2	1.01
ADCP	1	3	2	0.72
	2	3	2	0.69
	3	3	2	0.68

Table 3.5 – Specification for the power density calculation at the São Marcos River

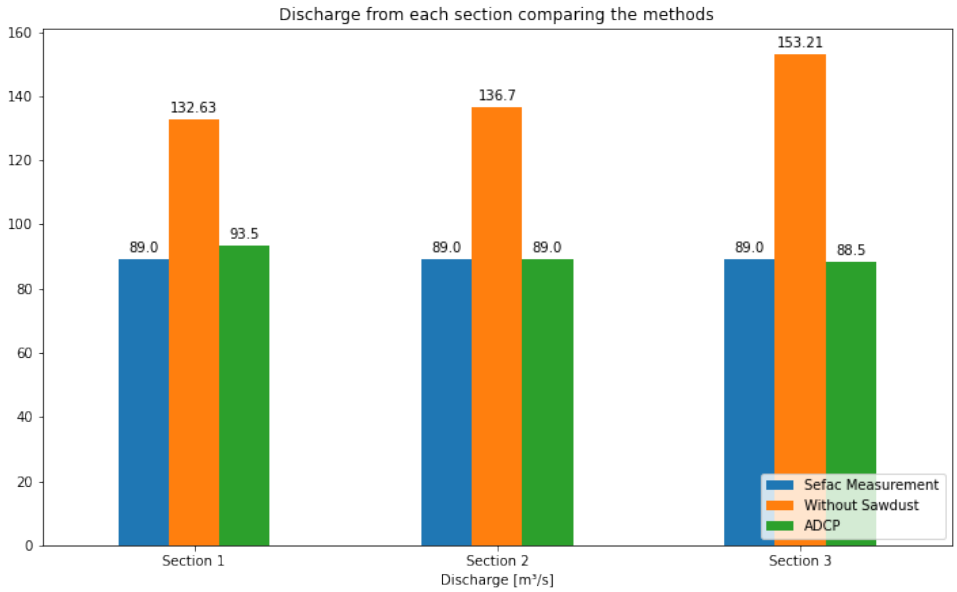

Figure 3.40 – Discharge measured at the São Marcos River

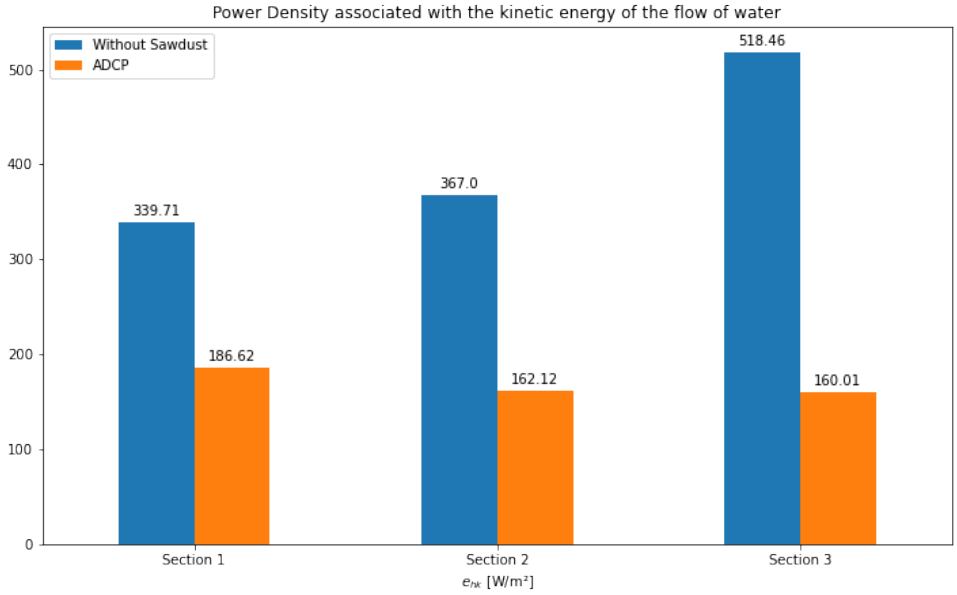

Figure 3.41 – Power density e_{hk} for the São Marcos River

3.4 RESULTS AND DISCUSSION

A discussion of the results gathered from each site experiment is necessary. Especially to bring attention to some points. The LSPIV method measures the superficial velocity from water flows. Waves, wind, or anything that cause some kind of turbulence on top of the river can impact the results. The M9 equipment was used as a parameter to know if the results

obtain from the LSPIV were satisfactory.

The M9 calculates the mean velocity from the water column profile. It's recognized that the data about velocity profile from rivers from the M9 is more complete and accurate. However, the idea here is to propose a non-intrusive equipment, that can easily register river flows and bring important information from that inspection.

In most of the experiments, the behavior from the velocity from the cross-section was equal from both methods. The magnitude of the velocity was not equal but that was not supposed to be.

Knowing the depth and bottom roughness is possible to determine the current velocity with the superficial velocity. So for an initial evaluation of possible areas for an installation of a hydrokinetic plant, the LSPIV method can be very useful.

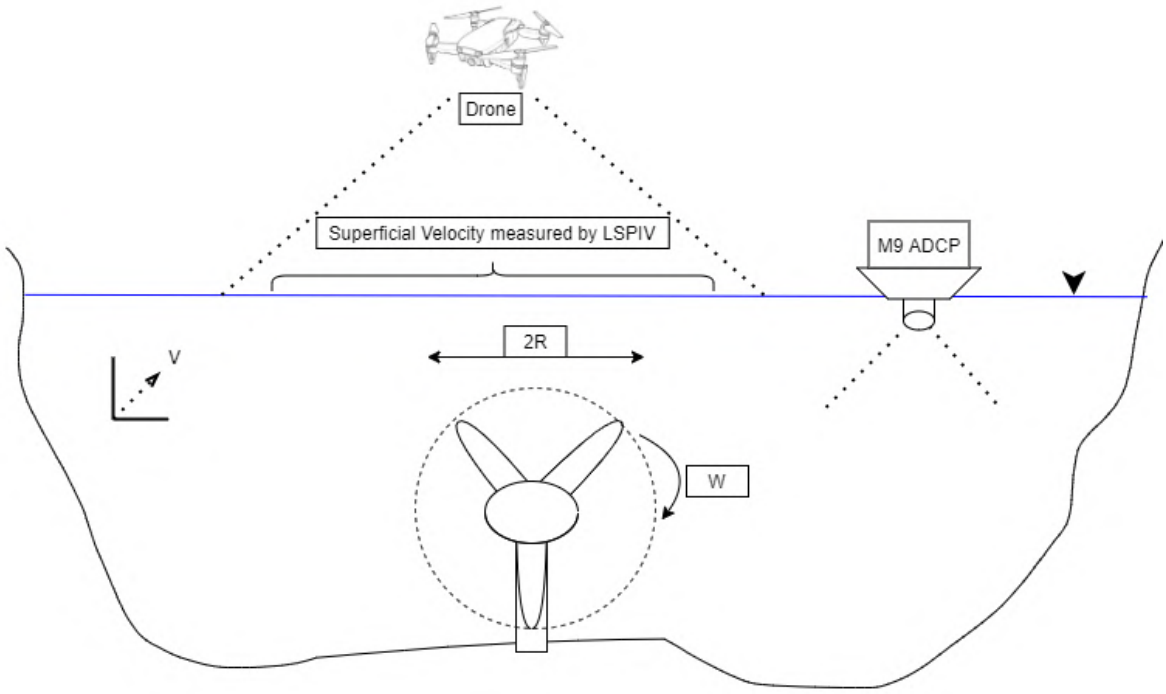

Figure 3.42 – illustration of speed measurement techniques with a hydrokinetic turbine. Not in scale

The field sites were a very good example to explained the technique in different environments. The Rodeador Channel is an artificial channel, with controlled discharge and is the perfect location for an ADCP measure because the consideration of uniform flow is adequate to the flow and has a sufficient depth. The riverbed is made of concrete and even that it has some sediment on the ground the only problem was the vegetation on the edge that in some experiments cause a shadow on the records.

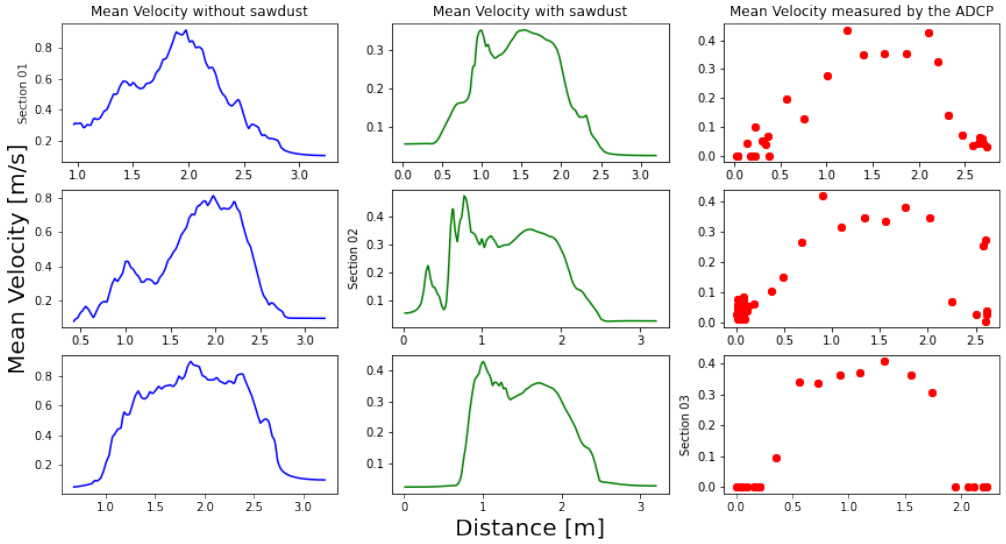

Figure 3.43 – Velocity from the Rodeador Channel

The Rodeador River exposed some difficulties for the M9. The only available area that could pass the rope to drive the board through the channel was too shallow and with a riverbed full of rocks, which cause a lot of turbulence in the measured area. It was still possible to analyze with the ADCP equipment and the LSPIV method indicates that when the river has a natural tracer in it, like foam, adding a natural tracer maintain reasonable results since the river had already a perceptual tracer, see Figure 3.44.

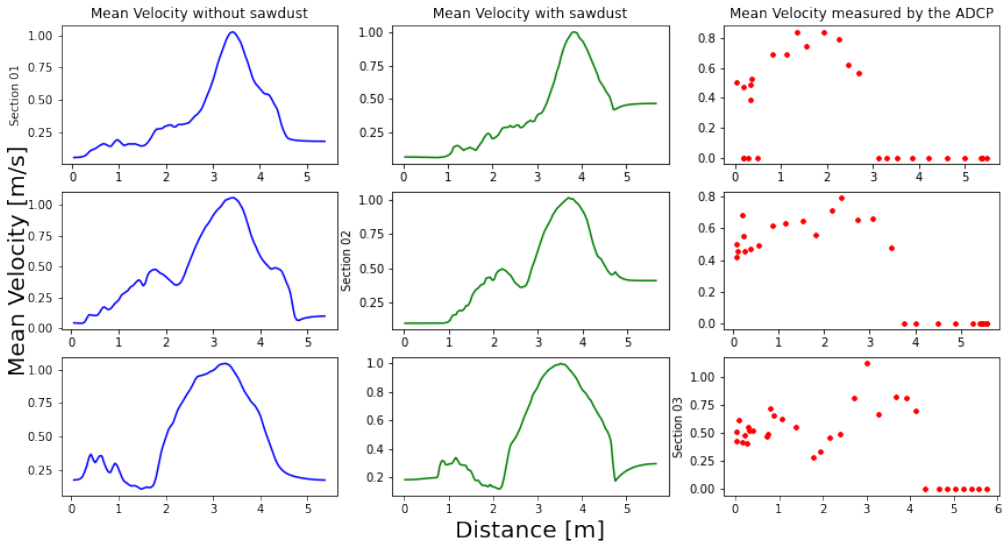

Figure 3.44 – Velocity from the Rodeador River

The Rodeador River have an installed telemeter, regulated and managed by CAESB (Federal District Environmental Sanitation Company), unfortunately, due to the COVID-19 Pandemic the maintenance on the equipment has been postponed and it doesn't have a register

of the discharge measure on the day that our crew was measuring the River.

The São Marcos River is downstream of a hydroelectric dam. It's the best possible place to exemplify the method presented in this work. A river with a great length wide that only with a boat to perform any type of measure and also needing to assemble a crew to do it. With the LSPIV method, only one person is necessary to take off the Drone and overfly the river mapping hydrokinetic potential.

Figure 3.45 – Process image from the Hydroelectric Dam at São Marcos River

The results from the LSPIV comparing to the M9 from the São Marcos River achieve satisfactory results. However, is necessary to repeat the experiment to add an artificial tracer to compare the results. The results from each section are plotted in Figure 3.46.

The power density value present in the previous section reinforces the importance to find a precise velocity at the location that the turbine will be installed. The velocity variable is power to the third, so each minimum difference between the real and the measured value has an important weight in the estimation.

The bar-plots for the power density did not follows the behaviour from the mean velocity graphs. This happened, as explained in the methodology chapter, because the velocity measured for each section by the LSPIV were calculate by the u velocity using the power law. The ADCP equipment used the mean velocity calculate from it, without removing any velocity, since it has it own velocity measurements estimation and it indicate the mean value for all the section profile. Table 3.6 present a summary of the velocity measured and calculate for the work. All power density values are present on table 3.7.

It is worth mentioning that in addition to recording the river flow keeping a satisfactory

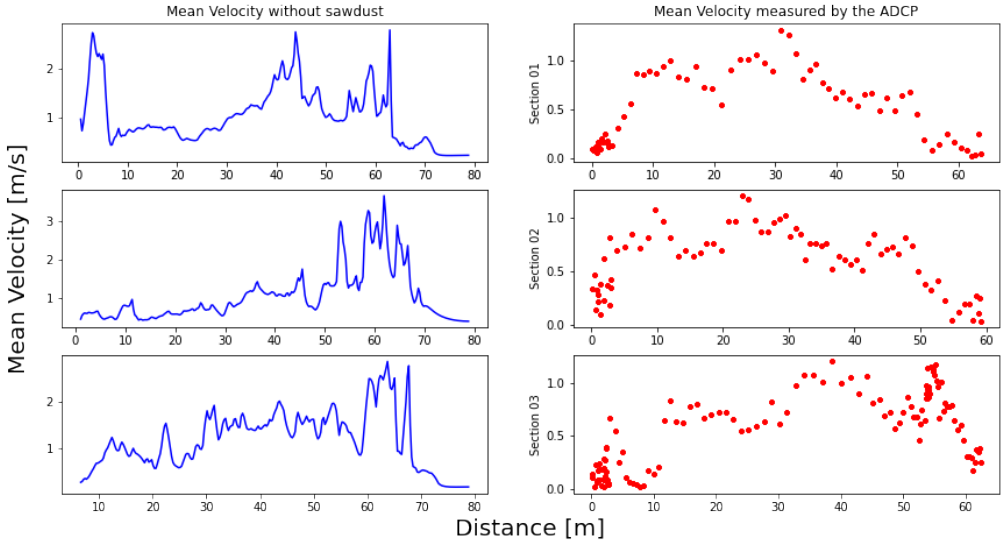

Figure 3.46 – Velocity from São Marcos River

	Method	Section	Mean Velocity	U measure [75%]	u Power law
Rodeador Channel	LSPIV with sawdust	1	0.19	0.324	0.277
		2	0.19	0.322	0.275
		3	0.22	0.346	0.296
	LSPIV without sawdust	1	0.45	0.600	0.513
		2	0.42	0.691	0.590
		3	0.54	0.767	0.655
	ADCP	1	0.27	0.270	0.270
		2	0.24	0.240	0.240
		3	0.26	0.260	0.260
Rodeador River	**Method**	**Section**	**Mean Velocity**	**U measure [75%]**	**u Power law**
	LSPIV with sawdust	1	0.38	0.48	0.41
		2	0.46	0.58	0.49
		3	0.45	0.71	0.61
	LSPIV without sawdust	1	0.36	0.53	0.45
		2	0.44	0.63	0.54
		3	0.48	0.79	0.68
	ADCP	1	0.32	0.32	0.32
		2	0.46	0.46	0.46
		3	0.50	0.50	0.50
São Marcos River	**Method**	**Section**	**Mean Velocity**	**U measure [75%]**	**u Power law**
	LSPIV without sawdust	1	1.02	1.03	0.88
		2	1.05	1.06	0.90
		3	1.18	1.18	1.01
	ADCP	1	0.72	0.72	0.72
		2	0.69	0.69	0.69
		3	0.68	0.68	0.68

Table 3.6 – Velocity Summary

stability the Drone also can be used for other measurements. Just to illustrate the potential of this equipment an orthomosaic photo, see Figure 3.47 (a), and a digital superficial model, see Figure 3.47 (b), from the hydroelectric site was generate using photos capture at the field site [43]. Is an impressive tool that has multiple uses.

	Power Density e_{hk} [w/m²]								
	Rodeador Channel			Rodeador River			São Marcos River		
	1	2	3	1	2	3	1	2	3
LSPIV with sawdust	10.57	10.40	12.98	35.46	60.42	111.57	####	####	####
LSPIV without sawdust	67.36	102.94	140.72	45.48	79.24	155.31	339.71	367.00	518.46
ADCP	9.84	6.91	8.79	16.38	48.67	62.50	186.62	162.12	160.01

Table 3.7 – Power Density Values e_{hk}

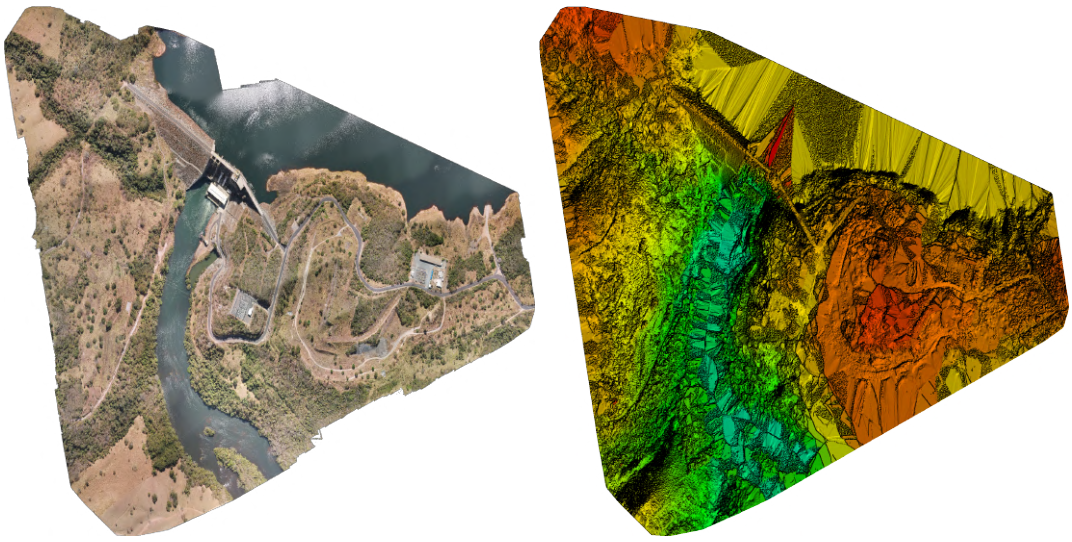

(a) Orthomosaic (b) Digital superficial model

Figure 3.47 – Result from the drone processing

The LSPIV method accomplishes its objective to measure superficial velocity in rivers and obtain excellent results using the M9 equipment as a parameter. The LSPIV proves itself a faster, cheaper, and reliable method to measure superficial velocities, see Table 3.8. Also, the M9 proves itself reliable and accurate equipment achieving exceptional results of discharge measurements compared to the discharge informed by the hydroelectric staff from the São Marcos river. Determine hydrokinetic potential only using the LSPIV method is not recommend, as was explained the velocity variable in the potential characterization has a influence power to the third, so an accurate number has to be measure to insure the potential of the area.

Average Price	
Mavic air 2 by DJI	R$ 12.000,00
M9 ADCP by Sontek	R$ 300.000,00

Table 3.8 – Equipment's Price

4 CONCLUSION

In IEA (International Energy Agency) report to achieve Net Zero by 2050 [10] is clear that the world will need to focus its electricity mix on renewable. Most of them will be in charge of solar and wind energy.

A simplification of the calculus for the energy generation by wind power plant can be done to compare with the hydrokinetic power plant. Focusing on the density, ρ, of the fluid. Hydrokinetic plants are underwater so it ρ compared to the air is 1000 times bigger, needing much less area to produce energy.

Hydrokinetic become even more attractive when researching in a country like Brazil, which has the majority of its electricity mix from hydroelectric. The opportunity for hydroelectric plants to generate more energy is attractive for any business.

Also the hydrokinetic energy can provide a renewable energy source for isolate communities in Brazil. Riverside and low-income population can have access to a electrical energy in a form that improves their life quality.

The LSPIV proves itself a reliable, safe, and simple methodology to characterize the superficial velocity from rivers. The non-intrusive method has been applied all around the world, France, United States, Japan, and now applied in different rivers from Brazil. The approach to correlate the technique to hydrokinetic potential is audacious. However, the results prove that is possible to use in an initial field investigation to analyze possible areas to implement an enterprise involving kinetic energy.

The power density calculation proves the importance of the velocity characterization. Enhancing the relevance of new methods to measure velocity in river sites. Further experiments and analysis have to be done, to assure that the LSPIV can determine hydrokinetic potential. The technique has the capability to define regions on a transect or area that the has a higher potential. Combining the LSPIV with the ADCP is efficient and accurate methodology to determine the potential.

Adding a natural tracer improves the results when the river doesn't have a noticeable tracer of its own. The method is a matching pattern technique, so adding a tracer to it, improves and facilitate the identification of pixel in the cross-correlation analysis.

An experiment work is susceptible to human error. This work was implemented in the outdoor field. With less control of illumination, flow, and types of equipment. Field measures always have to account for human error that is why this work applied the LSPIV method in three different sites and compared the results in three different sections applying the M9 ADCP equipment as a parameter to our measures. The results present in chapter three are

a compilation of several field trips because the necessities do redo the M9 measurement. A trained and prepared crew is extremely necessary and important for measurement success.

Is necessary to remain exploring the LSPIV method and to perform more field measurement to compare with other methodologies, like ADCP. Also, is important to recreate the field environment in a laboratory, so a more controlled and precise analysis could be performed. This could lead to a better understanding of the method and some important parts of it, like the calibration part and the influence of turbulence and wind on superficial velocity.

Further experiments most be accomplish to determine if the altitude of the drone flying impact the results. Also, analysis how the pixel identification is correlating with the addition of a natural tracer. If it depend on the illumination, the amount of particle per area of the flow, and the type of tracer used.

To conclude, the LSPIV combined with the GUI software, PIVLab, and RIVeR is a powerful method. The work achieves its main and secondary objectives. In addition to the measurement, it expects that this dissertation also serves as a manual to field measurement applying the LSPIV methodology.

BIBLIOGRAPHY

1 OVERVIEW of the Energy brazilian market. ://www.metronlab.com/blog/overview-brazilian-market.

2 STATISTICAL Review of World Energy. 2021. <https://www.bp.com/en/global/corporate/energy-economics/statistical-review-of-world-energy/downloads.html>. Accessed: 2021-08-25.

3 BARKER, D. B.; FOURNEY, M. E. Measuring fluid velocities with speckle patterns. *Optics Letters*, v. 1, n. 4, p. 135, 1977. ISSN 0146-9592.

4 MUSTE, M.; YU, K.; SPASOJEVIC, M. Practical aspects of ADCP data use for quantification of mean river flow characteristics; Part I: Moving-vessel measurements. *Flow Measurement and Instrumentation*, v. 15, n. 1, p. 1–16, 2004.

5 THIELICKE, W.; STAMHUIS, E. J. PIVlab – Towards User-friendly, Affordable and Accurate Digital Particle Image Velocimetry in MATLAB. *Journal of Open Research Software*, v. 2, 2014.

6 ADCP Site Selection Guide. 2021. <https://info.xylem.com/rs/240-UTB-146/images/ADCP20Site20Selection20Guide.pdf>. Accessed: 2021-05-30.

7 RANGE, Velocity, Sound Speed, and Snell's Law. 2021. <https://www.sontek.com/media/pdfs/velocity-range-and-snells-law.pdf>. Accessed: 2021-05-30.

8 MAVIC air 2 - Especificações. 2021. <https://www.dji.com/br/mavic-air-2/specs>. Accessed: 2021-02-15.

9 GATES, B. *How to avoid a climate disaster*: The solutions we have and the breakthroughs we need. [S.l.]: Alfred A. Knopf, New York, 2021.

10 IEA. *Net Zero by 2050*. 2021. Disponível em: <https://www.iea.org/reports/net-zero-by-2050>.

11 ACESSO à energia com fontes renováveis em regiões remotas no Brasil. 2020. <https://www.wwf.org.br/?76422/Acesso-a-energia-com-fontes-renovaveis-em-regioes-remotas-no-brasil>. Accessed: 2021-09-16.

12 YUCE, A. M. M. Hydrokinetic energy conversion systems: A technology status review. *Renewable and Sustainable Energy Reviews*, v. 43, p. 72–82, 2015.

13 SOOD, S. K. S. M. Development of hydrokinetic energy technology: A review. *International Journal of Energy Research*, v. 43.

14 TSUBAKI, R.; FUJITA, I.; TSUTSUMI, S. Measurement of the flood discharge of a small-sized river using an existing digital video recording system. *Journal of Hydro-Environment Research*, v. 5, n. 4, p. 313–321, 2011. ISSN 15706443.

15 CREUTIN, J. D. et al. River gauging using PIV techniques: A proof of concept experiment on the Iowa River. *Journal of Hydrology*, v. 277, n. 3-4, p. 182–194, 2003. ISSN 00221694.

16 JODEAU, M. et al. Application and evaluation of LS-PIV technique for the monitoring of river surface velocities in high flow conditions. *Flow Measurement and Instrumentation*, v. 19, n. 2, p. 117–127, 2008. ISSN 09555986.

17 SUN, X. et al. Discharge estimation in small irregular river using LSPIV. *Proceedings of the Institution of Civil Engineers: Water Management*, v. 163, n. 5, p. 247–254, 2010. ISSN 17417589.

18 FINCHAM, A. M.; SPEDDING, G. R. Low cost, high resolution DPIV for measurement of turbulent fluid flow. *Experiments in Fluids*, v. 23, n. 6, p. 449–462, 1997. ISSN 07234864.

19 MUSTE, M.; FUJITA, I.; HAUET, A. Large-scale particle image velocimetry for measurements in riverine environments. *Water Resources Research*, v. 44, n. 4, p. 1–14, apr 2008. ISSN 00431397. Disponível em: <http://doi.wiley.com/10.1029/2008WR006950>.

20 MEYNART, R. Flow Velocity Measurement By A Speckle Method. In: GROSMANN, M. H.; MEYRUEIS, P. (Ed.). *2nd European Congress on Optics Applied to Metrology*. [s.n.], 1980. v. 0210, n. May 1980, p. 25–28. Disponível em: <http://proceedings.spiedigitallibrary.org/proceeding.aspx?articleid=1229496>.

21 ADRIAN, R. J. Twenty years of particle image velocimetry. *Experiments in Fluids*, v. 39, n. 2, p. 159–169, 2005. ISSN 07234864.

22 ADRIAN, R. J. Scattering particle characteristics and their effect on pulsed laser measurements of fluid flow: speckle velocimetry vs particle image velocimetry. *Optical Society of America.*, v. 23, p. 1690–1691, 1984. Disponível em: <https://osapublishing.ez54.periodicos.capes.gov.br/view{_}article.cfm?gotourl=https{\%}3A{\%}2F{\%}2Fwww.osapublishing.org{\%}2FDirectPDFAccess{\%}2F261FD6B3-C3FA-A817-2BF3719DF58D9B2C{_}165106{\%}2Fao-23-11-1690.pdf{\%}3Fda{\%}3D1{\%}26id{\%}3D165106{}.>

23 PICKERING, C. J. D.; HALLIWELL, N. A. Laser speckle photography and particle image velocimetry: photographic film noise. *Applied Optics*, v. 23, n. 17, p. 2961, 1984. ISSN 0003-6935.

24 SANTINELLO, M. *Estimativa de velocidades superficiais e vazão em canais usando velocimetria por imagem.* 2019. 99 p.

25 FUJITA, I.; KOMURA, S. Application of Video Image Analysis for Measurements of River-Surface Flows. *Proceedings of Hydraulic Engineering*, v. 38, p. 733–738, 1994. ISSN 0916-7374.

26 AYA, S.; FUJITA, I.; YAGYU, M. Field-Observation of Flood in a River by Video Image Analysis. *Proceedings of Hydraulic Engineering*, v. 39, p. 447–452, 1995. ISSN 0916-7374.

27 FUJITA, I.; MUSTE, M.; KRUGER, A. Large-scale particle image velocimetry for flow analysis in hydraulic engineering applications. *Journal of Hydraulic Research*, v. 36, n. 3, p. 397–414, 1998. ISSN 00221686.

28 FUJITA, I.; HINO, T. Unseeded and Seeded PIV Measurements of River Flows Videotaped from a Helicopter. *Journal of Visualization*, v. 6, n. 3, p. 245–252, 2003. ISSN 13438875.

29 KANTOUSH, S. A. et al. Flow field investigation in a rectangular shallow reservoir using UVP, LSPIV and numerical modelling. *Flow Measurement and Instrumentation*, v. 19, n. 3-4, p. 139–144, 2008. ISSN 09555986.

30 Le Coz, J. et al. Performance of image-based velocimetry (LSPIV) applied to flash-flood discharge measurements in Mediterranean rivers. *Journal of Hydrology*, Elsevier B.V., v. 394, n. 1-2, p. 42–52, 2010. ISSN 00221694. Disponível em: <http://dx.doi.org/10.1016/j.jhydrol.2010.05.049>.

31 MUSTE, M.; HO, H. C.; KIM, D. Considerations on direct stream flow measurements using video imagery: Outlook and research needs. *Journal of Hydro-Environment Research*, v. 5, n. 4, p. 289–300, 2011. ISSN 15706443.

32 DRAMAIS, G. et al. Advantages of a mobile LSPIV method for measuring flood discharges and improving stage-discharge curves. *Journal of Hydro-Environment Research*, v. 5, n. 4, p. 301–312, 2011. ISSN 15706443.

33 KANTOUSH, S. A. et al. LSPIV implementation for environmental flow in various laboratory and field cases. *Journal of Hydro-Environment Research*, Elsevier B.V, v. 5, n. 4, p. 263–276, 2011. ISSN 15706443. Disponível em: <http://dx.doi.org/10.1016/j.jher.2011.07.002>.

34 THE application of LS-PIV to a small irregular river for inbank and overbank flows. Elsevier Ltd, v. 24, p. 1–12, 2012. ISSN 09555986. Disponível em: <http://dx.doi.org/10.1016/j.flowmeasinst.2012.02.001>.

35 TAURO, F. et al. Large-Scale Particle Image Velocimetry from an Unmanned Aerial Vehicle. *IEEE/ASME Transactions on Mechatronics*, v. 20, n. 6, p. 3269–3275, 2015. ISSN 10834435.

36 BECHLE, A. J. et al. Development and application of an automated river-estuary discharge imaging system. *Journal of Hydraulic Engineering*, v. 138, n. 4, p. 327–339, 2012. ISSN 07339429.

37 HUANG, W. C.; YOUNG, C. C.; LIU, W. C. Application of an automated discharge imaging system and LSPIV during typhoon events in Taiwan. *Water (Switzerland)*, v. 10, n. 3, 2018. ISSN 20734441.

38 Le Boursicaud, R. et al. Gauging extreme floods on YouTube: Application of LSPIV to home movies for the post-event determination of stream discharges. *Hydrological Processes*, v. 30, n. 1, p. 90–105, 2016. ISSN 10991085.

39 GUILLÉN, N. F. et al. Use of LSPIV in assessing urban flash flood vulnerability. *Natural Hazards*, v. 87, n. 1, p. 383–394, 2017. ISSN 15730840.

40 WILLIAMS, E.; SIMPSON, J. H. Uncertainties in estimates of Reynoldes stress and TKE production rate using the ADCP variance method. *Journal of Atmospheric and Oceanic Technology*, v. 21, n. 2, p. 347–357, 2004. ISSN 07390572.

41 GORDON, B. R. L. Acoustic Measurement of River Discharge. v. 115, n. 7, p. 925–936, 1989.

42 FUJITA, I.; AYA, S. Refinement of LSPIV technique for monitoring river surface flows. *Water Resources 2000*, n. 1, p. 1–9, 2004.

43 CAMARGO, F. *UTILIZAÇÃO DE AERONAVE PILOTADA REMOTAMENTE (RPA) PARA MAPEAMENTO DO ATERRO CONTROLADO DO JOCKEY CLUBE DE BRASÍLIA*. Dissertação (Bachelor's Thesis) — Universidade de Brasília, 2018.

44 PATALANO, A.; GARCÍA, C. M.; RODRÍGUEZ, A. Rectification of Image Velocity Results (RIVeR): A simple and user-friendly toolbox for large scale water surface Particle Image Velocimetry (PIV) and Particle Tracking Velocimetry (PTV). *Computers and Geosciences*, v. 109, p. 323–330, 2017. ISSN 00983004.

45 TABORDA, R.; SILVA, A. COSMOS: a lightweight coastal video monitoring system. *Comput. Geosci.*, 2012.

46 Camargo, F.; Brasil Junior, A.; Castilho Faria Mendes, R. LSPIV from the Rodeador Channel, using an UAV and a fixed camera to compare with an ADCP instrument of measure. In: . [S.l.: s.n.], 2020. v. 2020, n. 1998.

47 PUNYS, P. et al. Riverine hydrokinetic resource assessment. A case study of a lowland river in Lithuania. *Renewable and Sustainable Energy Reviews*, n. 50, p. 643–652, 2015.

48 KUMAR, D.; SARKAR, S. A review on the technology, performance, design optimization, reliability, techno-economics and environmental impacts of hydrokinetic energy conversion systems. *Renewable and Sustainable Energy Reviews*, v. 128, n. 58, p. 796–813, 2016.

49 BETZ, A. Windenergie und ihre Ausnutzung durch Windmühlen. Germany: Ökobuch Verlag. 1926.

50 VERMAAK H. J.AND KUSAKANA, K.; KOKO, S. P. Status of micro-hydrokinetic river technology in rural applications: A review of literature. *Renewable and Sustainable Energy Reviews*, n. 29, p. 625–633, 2014.

51 BABAEYAN-KOOPAEI, K. et al. Uncertainties in estimates of Reynoldes stress and TKE production rate using the ADCP variance method. *Journal of Hydraulic Engineering-Asce*, v. 128, n. 2, p. 891–900, 2002.

52 CRUZ, J. da S.; BLANCO, C. J. C.; JUNIOR, A. C. P. B. Flow-velocity model for hydrokinetic energy availability assessment in the Amazon. *Acta Scientiarum*, p. 15, 2019.

53 CHENG, N.-S. Power-law index for velocity profiles in open channel flows. *Advances in Water Resources*, v. 30, n. 8, p. 1775–1784, 2007. ISSN 0309-1708. Disponível em: <https://www.sciencedirect.com/science/article/pii/S0309170807000152>.

54 SCHLICHTING, K. G. H. *Boundary-layer Theory*. [S.l.]: Springer, 2017. ISBN 978-3-662-52917-1.

55 JUNIOR, J. L. A. B. *hydro-k Sistemas de turbinas hidrocinéticas em arranjo flutuante e modular*. [S.l.: s.n.], 2017.

56 TOCARDO, Run of River Plataform. 2021. <https://www.tocardo.com/solutions/rivers/>. Accessed: 2021-09-17.

57 GUINARD Energies Nouvelles. 2021. <https://www.guinard-energies.bzh/en/our-products/p66-hydrokinetic-turbine-3-5-kw/>. Accessed: 2021-09-17.

58 RENUGEN Renewable Generation. 2021. <https://www.renugen.co.uk/seamap-aquair-q100-12v/>. Accessed: 2021-09-17.

59 ADASA RECEBE PROJETO DE RECUPERAÇÃO DO CANAL DO RODEADOR. 2021. <http://www.adasa.df.gov.br/944-adasa-recebe-projeto-de-recuperacao-do-canal-do-rodeador>. Accessed: 2020-10-17.

60 CAMARGO, F.; NUNES, R. Appling the Large-Scale Particle Image Velocimetry with drone images for determining the hydrokinetic potential in rivers. In: . [S.l.]: COBEM-2021-2278, 2021. p. 10.

61 USINA Serra do Facão - 212.58 MW. 2021. <https://www.furnas.com.br/subsecao/130/usina-serra-do-facao---21258-mw?culture=pt>. Accessed: 2021-08-23.